Comparison of Isotropic vs. Anisotropic PSTM Migrations in the Big Horn Basin, WY

A Thesis

Presented to

the Faculty of the Department of Natural Sciences and Mathematics

University of Houston

In Partial Fulfillment

of the Requirements for the Degree

Master of Science

By

Jonathan Parker

December 2011

Comparison of Isotropic vs. Anisotropic PSTM Migrations in the Big Horn Basin, WY

Jonathan Paul Parker

APPROVED:

Dr. Christopher L. Liner, Committee Chair, Advisor

Dr. Robert Stewart, Committee Member

Dr. Steven Peterson, Outside Committee Member

Dr. Mark A. Smith

Dean, College of Natural Sciences and Mathematics

Acknowledgements

Foremost, I would like to thank my advisor, Christopher L. Liner, and committee members, Robert Stewart and Steven Peterson, for their time and guidance on the preparation of this thesis.

A special mention goes to Allen Brummert, Aaron Girard, Stephen Schneider, Scott Schapper, Ken Steele, and Seann Day for technical discussions, revisions, suggestions, and overall support in the preparation of this thesis.

Most of all I would like to express my loving gratitude to my parents, Dennis and Claudia, and grandparents, Claude, Alice, John and Faye, who instilled the value and importance of education in me. My sisters, Denae and Airica, who have supported me in all that I choose to do and my entire extended family who have always been there for me.

Comparison of Isotropic vs. Anisotropic PSTM Migrations in the Big Horn Basin, WY

An Abstract of a Thesis

Presented to

the Faculty of the Department of Natural Sciences and Mathematics

University of Houston

In Partial Fulfillment

of the Requirements for the Degree

Master of Science

By

Jonathan Parker

December 2011

Abstract

As target zones in Wyoming's mature oil fields become smaller and horizontal drilling becomes more critical the need to extract more information from seismic data becomes increasingly important. Seismic in the Big Horn Basin, located in Northwest Wyoming, is expected to behave in an anisotropic manner since the basin is heavily composed of shales, thin beds containing vertical and horizontal fractures, and a non-uniform stress field due to tectonic compression. To extract additional information and value from a seismic survey within the Big Horn Basin anisotropic time migration was performed instead of the standard isotropic processing flow. Anisotropic migration uses fewer assumptions in order to better represent the subsurface and thus yield higher quality seismic data. Due to the few assumptions anisotropic migration requires additional time, capital, and resources compared to isotropic migration which its benefits must outweigh in order to be justified. An additional product of anisotropic processing is azimuthally varying velocities which can give insight into fracture systems that isotropic processing would be unable to provide. It is shown that performing anisotropic migration instead of isotropic migration produces a higher frequency dataset which has better reflector resolution, increased fault clarity, and more reliable attributes such as amplitude and semblance. These incremental improvements provide better insight into the subsurface for vertical infill wells and horizontal well development in thin zones. This additional value far outweighs the incremental increase in time and money required to perform anisotropic instead of isotropic seismic processing on datasets in the Big Horn Basin.

Table of Contents

1.0 Introduction

The structurally complex oil fields in the Big Horn Basin of Wyoming have been studied since they were first discovered in the early 1900's. The basin has seen several geophysical advancements throughout its history. Two dimensional (2D) seismic was first shot in the basin in the 1970's and 80's followed by an influx of three dimensional (3D) seismic surveys in the early 1990's. Since the 1990's, many advancements in seismic acquisition and processing have been achieved. One of the most beneficial of these advances came in processing when computing power increased, reducing the processing computing cost, making pre-stack migration more economically feasible. This was an important advancement due to the steep dips, large amounts of data that needed to be integrated, and the geologic complexity of the fields in the Big Horn Basin which require pre-stack migration to be properly imaged.

The life of many of the oil fields within the Big Horn Basin have been extended due to technology advances in seismic acquisition, processing and interpretation. Anisotropic migration may be the next key geophysical advancement to optimize field development and further extend the life of a field. With thin zones, previously un-economic, becoming target zones for horizontal drilling development it is critical to optimize the seismic data as much as possible. Performing anisotropic processing instead of isotropic processing is one of the options being explored to see if anisotropic migration can provide a better seismic image to aid in the development of these thin zones. Many of the larger well developed main reservoirs in the basin benefit from waterflooding and enhanced oil

recovery (EOR) methods. The planning, evaluation, and eventual success of a waterflood or EOR programs is dependent upon a good understanding of the reservoirs continuity and fractures. In addition to improved traditional seismic analysis and attributes, anisotropic processing provides azimuthal velocity attributes which can help aid in the determination of fracture and matrix dominated regions of the field. This thesis explores the advantages and drawbacks from an interpretation viewpoint of performing this additional anisotropic processing in the time domain utilizing both descriptive and analytical methods.

2.0 Objective and Methodology

The focus of this study is to identify and evaluate the incremental benefits of performing anisotropic pre-stack time migration (PSTM) instead of the industry standard isotropic PSTM for the Big Horn Basin in Wyoming. The benefits of performing anisotropic migration must outweigh the additional time and resources required compared to isotropic migration in order to be justified.

With thinner target zones becoming economic, higher resolution data is imperative for their successful development. Anisotropic migrations may increase the resolution of the data by better focusing the seismic energy and increasing the bandwidth, thus lowering the thickness of resolution and detection. The true bandwidth of the seismic data can be difficult to discern due to frequency enhancements and shaping which alter the bandwidth. To reduce the effect of possible frequency enhancement differences the raw seismic volumes prior to post-migration frequency enhancement will be used to validate any bandwidth improvements.

Non-imaged small scale faults and incorrectly positioned faults can result in wells being drilled out of zone greatly hindering the success of horizontal wells. The potential improvement in focusing of faults with anisotropic processing could aid in the planning and drilling of horizontal wells compared with isotropic processing alone. Comparison of known fault locations from well information with the isotropic and anisotropic seismic data will be used to validate and to help quantity any improvements in fault imaging.

Processing can have a significant impact on attributes used for reservoir characterization. Anisotropic processing is expected to produce better pre-stack data with flatter gathers and a higher signal-to-noise ratio. These improvements should yield more consistent and reliable seismic attributes including amplitude, coherence, and curvature. Variations in attributes between the isotropic and anisotropic volumes will be investigated both analytically and descriptively as appropriate. The anisotropic processing also yields additional velocity attributes, such as the magnitude and azimuth of the maximum velocity (V_{fast}), the minimum velocity (V_{slow}), and the magnitude difference between the velocity in the maximum and minimum azimuths (V_{fast}-V_{slow}), which may help with fracture prediction.

3.0 Background

3.1 Study Location

The Big Horn Basin is located in the Northwest portion of Wyoming near Yellowstone National Park. The basin is bounded by several Laramide uplifts, including the Pryor Mountains to the north, the Bighorn Mountains to the east, the Owl Creek Mountains to the south, and the Absaroka Volcanic Plateau and Beartooth Mountains to the west (Figure 1).

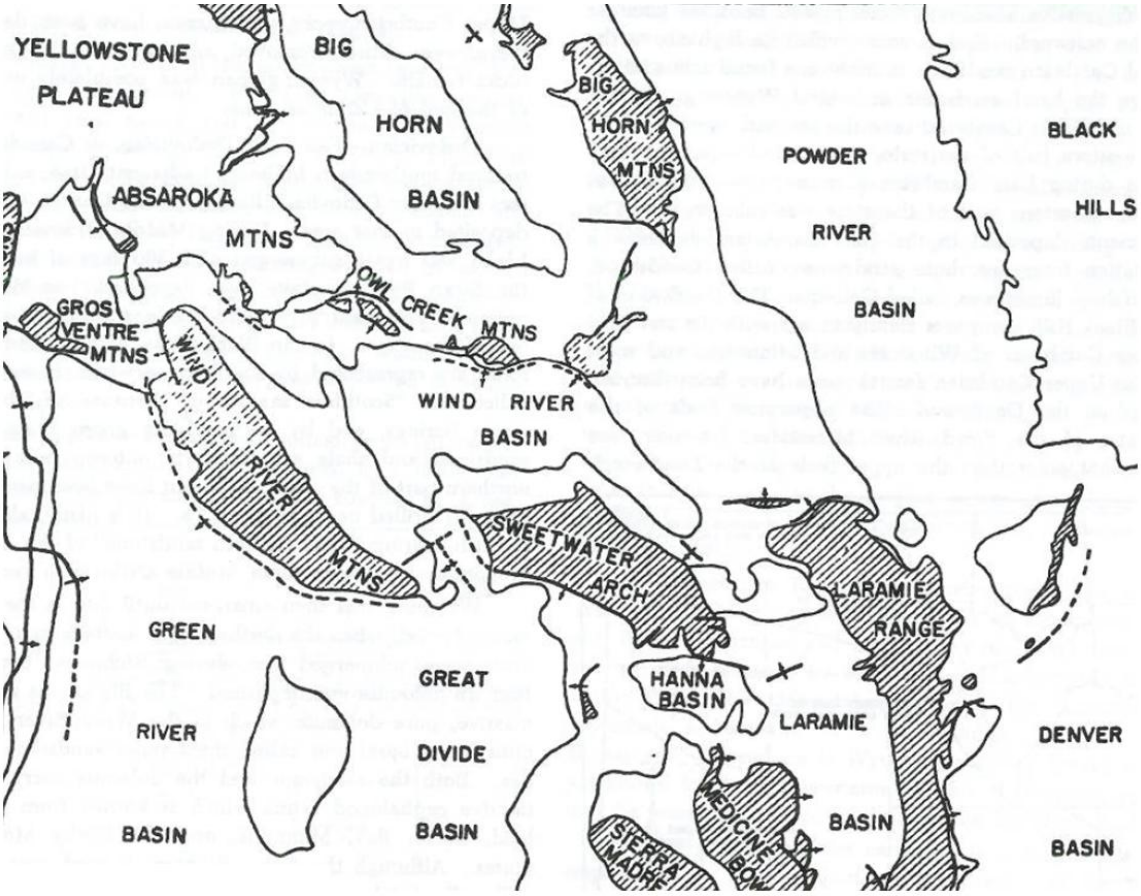

Figure 1: Location of the Big Horn Basin in Wyoming (Thomas, 1957)

3.2 Geologic History

The region which includes the present-day Big Horn Basin in northwest Wyoming has undergone three main phases of structural evolution since the Precambrian. These three phases can be described as the: Passive Margin Phase, Foreland Basin Phase and Laramide Basins Phase.

The first phase, passive margin, began in the Precambrian with the breakup of the supercontinent Rhodinia. The rifting of the supercontinent resulted in a passive margin on the western boundary of North America with a gently dipping ramp in the region of the current day Big Horn Basin, Wyoming. The passive margin phase spanned from the Paleozoic Cambrian until the Mesozoic late-Jurassic. During this period there were multiple transgressions and regressions of the newly formed Pacific Ocean resulting in a thin, continuous stratigraphic package of Phase 1 sediments on the Wyoming shelf (Figure 2). The sediments deposited during this phase account for three to four thousand feet of the Wyoming stratigraphic section. This section contains the major key reservoirs for the Big Horn Basin including the Cambrian Flathead and Gros Ventre, Mississippian Madison, Pennsylvanian Darwin and Tensleep, Permian Phosphoria and Triassic Chugwater (See Figure 3). The Permian Phosphoria is the major hydrocarbon source rock for this section. Hydrocarbons are believed to have migrated from the deeper parts of the Antler foreland in southeastern Idaho and northeastern Utah.

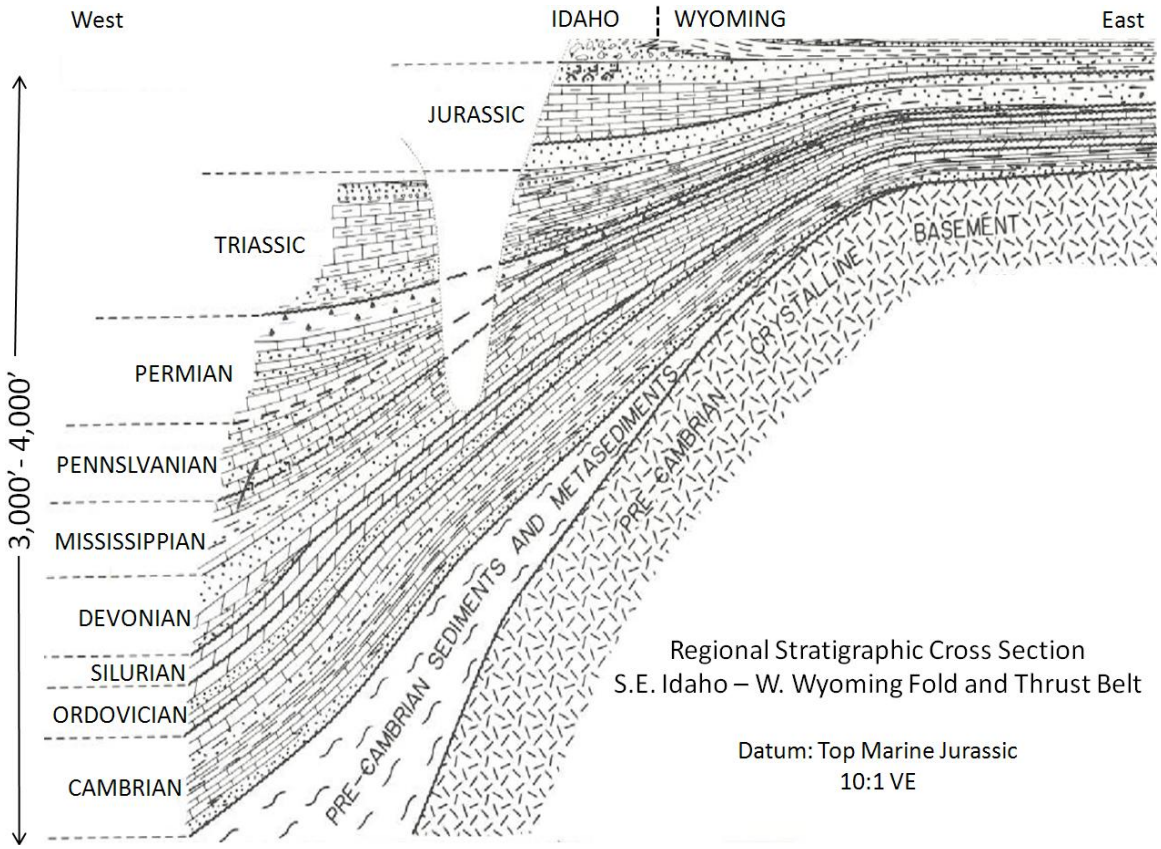

Figure 2: During phase 1 tectonics, Wyoming had multiple transgressions and regressions of the Pacific Ocean depositing sediment on the Wyoming shelf (Modified from Hayes, 1976).

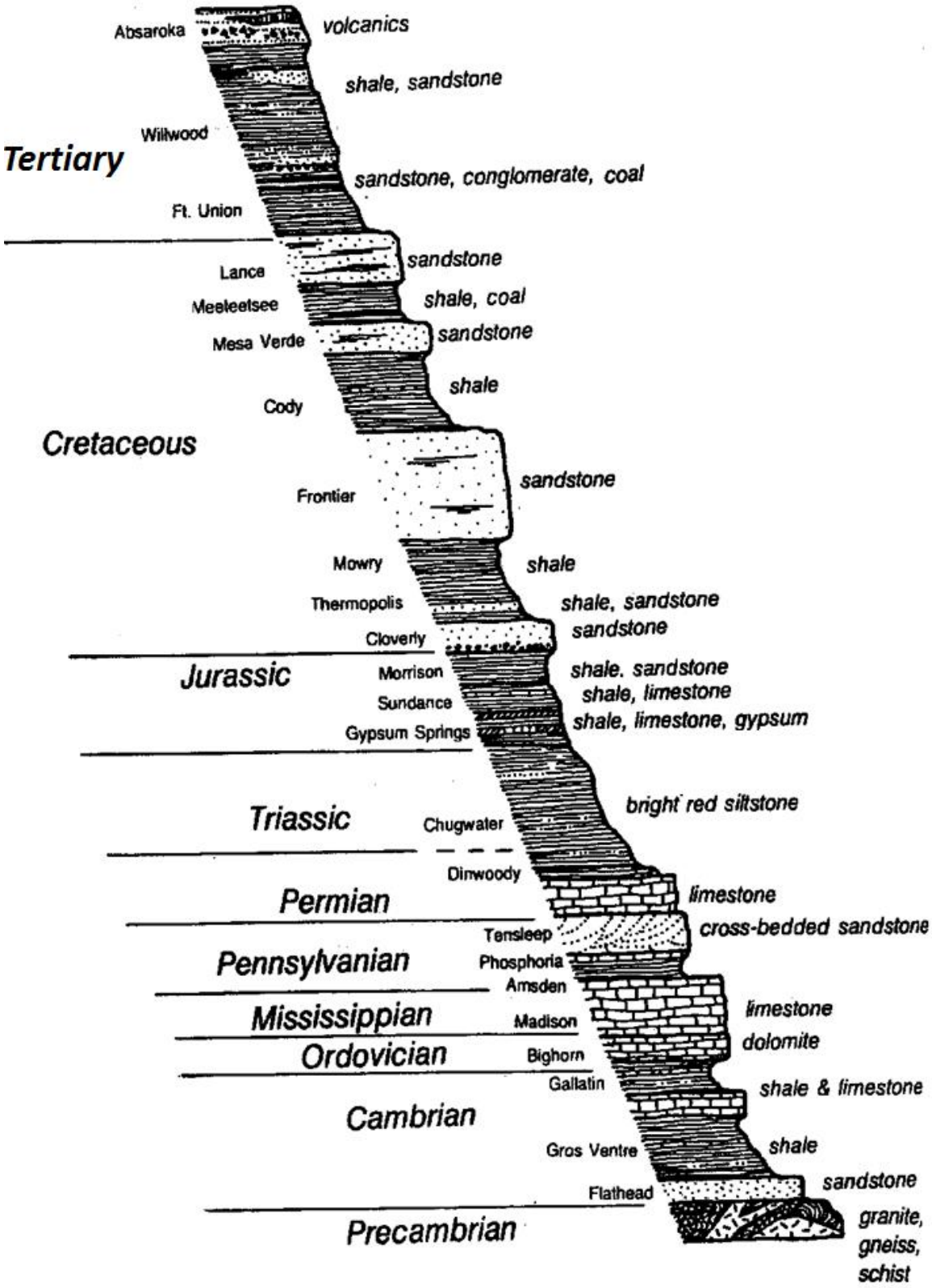

Figure 3: Stratigraphic Column of the Big Horn Basin (Lageson and Spearing, 1988)

The second phase, Foreland Basin, began in the Mesozoic Mid-Jurassic lasting until the end of Mesozoic Cretaceous, spanning about 90 million years. During this period, the former ramp geometry present during the passive margin phase was altered by the Siever Orogeny. The area of the future Bighorn basin was separated from the Pacific Ocean by a continuous chain of mountains on the western edge of North America extending from Alaska to New Mexico. Phase 2 sedimentation shed from these highlands into the Cretaceous Western Interior seaway. During this period some of the shallower reservoirs were deposited, These units include the Cretaceous Lakota, Dakota, Muddy, and Frontier reservoirs, as well as the indigenous source rock, including the organic shales of the Cretaceous Mowry and Thermopolis.

Phase 3, Laramide Basins, began with the Laramide Orogeny and spanned about 70 million years. The Laramide created the mountain ranges which define the Bighorn Basin (Figure 1) and is responsible for the formation of the asymmetric anticlines that are present day oil fields (Figure 4). The post-Laramide history is marked by three sequential events: the mountains erode, the basins fill and the basins erode. The portion of phase 3 stratigraphy is dominated by Paleocene strata (Fort Union, Willwood and an influx of volcanic deposits).

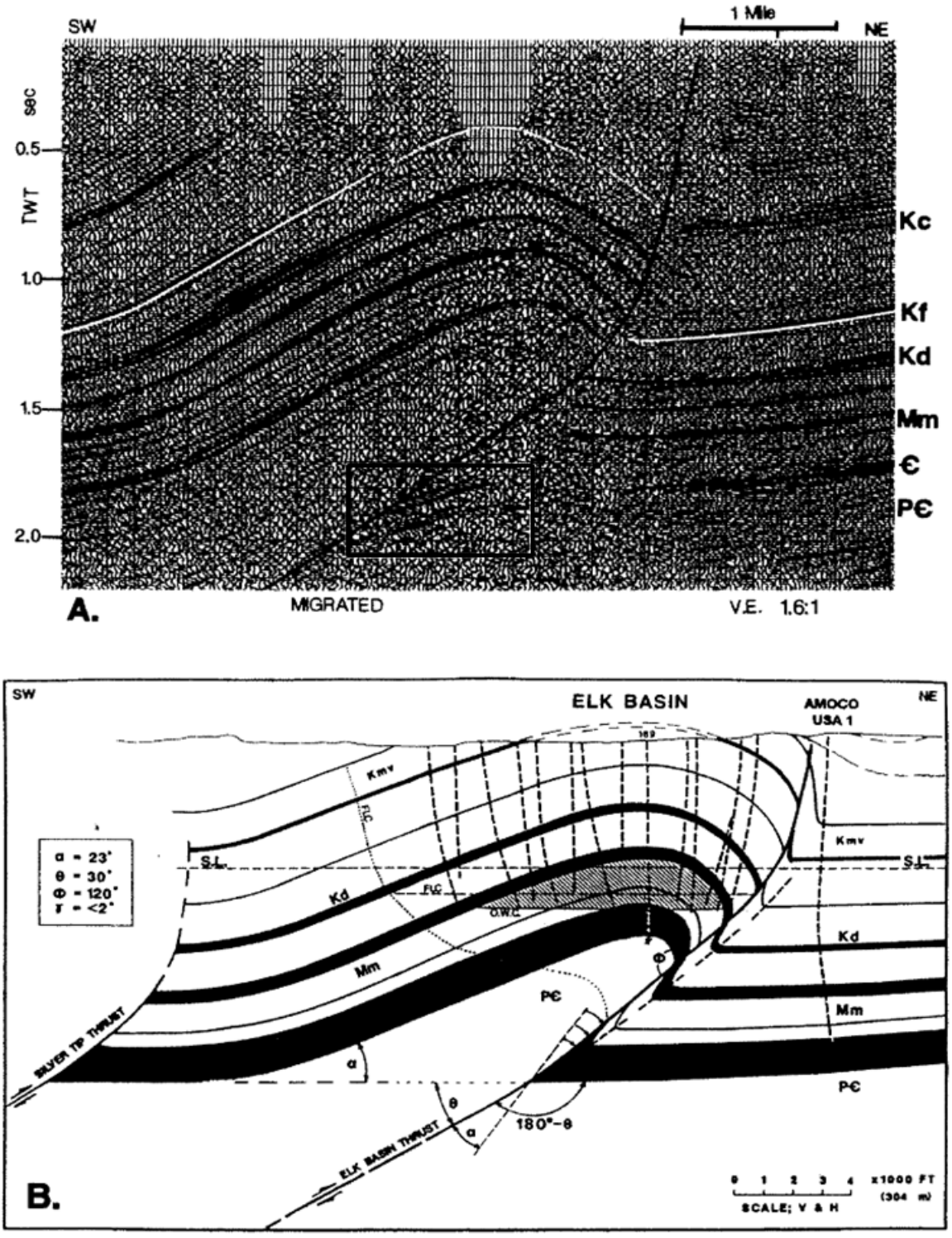

Figure 4: Interpretation of a typical Laramide structural uplift in Big Horn Basin creating an asymmetric anticline shown on a 2D seismic section (A) and in a corresponding cartoon (B) of the same cross section (Stone, 1993)

4.0 Anisotropic Time Migration

4.1 Theory

Traditional isotropic time processing truncates the Taylor series expansion of the ray-traced two-way travel time at the second order term to estimate the hyperbolic P-wave normal-moveout (NMO) given by Taner and Koehler (1969) as

$$t_x = \sqrt{t_0^2 + \frac{x^2}{v_{nmo}^2}} \qquad (1)$$

where x is offset, t_x is two-way time, t_o is the zero-offset travel time and v_{nmo} is the moveout velocity. Although useful, this hyperbolic moveout equation (1) is valid only for short offsets of a homogeneous isotropic plane layer with zero dip (Tsvankin and Thomsen, 1994).

This approximation has been very successfully applied on many vintage datasets with limited offsets since on short spreads the P-wave moveout is close to hyperbolic even if there is anisotropy present (Tsvankin and Thomsen, 1994). However, new acquisition designs providing better offset and azimuth sampling are making it increasing important to correct for the fourth order moveout to optimize the data. The data in this study, which was acquired to be a high resolution survey with good offsets (Appendix A), was corrected to the fourth order moveout term. Alkhalifah and Tsvankin (1995) show that by expanding the NMO equation applied from a second order to a fourth order approximation (2), we can more accurately account for long offsets recorded in the dataset, this is often referred to as the Long Offset NMO (LNMO):

$$t_x = \sqrt{t_0^2 + \frac{x^2}{v_{nmo}^2} - \frac{2\eta x^4}{v_{nmo}^2[t_0^2 v_{nmo}^2 + (1+2\eta)x^2]}} \quad (2)$$

where η is the amount of deviation from hyperbolic moveout. The smaller the η value the closer the moveout is to being purely hyperbolic and properly being described by the second order NMO equation (1). Alkhalifah and Tsvankin (1995) also provide a definition of the anisotropic coefficient η in terms of the Thomsen parameters:

$$\eta = \frac{\varepsilon - \delta}{1+2\delta} \quad (3)$$

where ε and δ are defined by Thomsen (1986).

The fourth order term is correcting for two different long offset effects: anisotropy and the truncation of the Taylor series expansion described above. These effects can only be separated by the introduction of the sixth order term (Starr and Pandey, 2006), which was not performed on this dataset. This creates an unavoidable ambiguity in the anisotropic analysis of the fourth order η term within this study.

One of the limitations of the LNMO equation, applied to this dataset, is that it does not take into account any azimuthal variation present in the data. When azimuthal variations are taken into account, the long offset fourth order correction (Equation 2) becomes more complex,

$$t_{x,\alpha} = \sqrt{t_0^2 + \frac{x^2}{v_{nmo}^2(\alpha)} - \frac{2\eta(\alpha)x^4}{v_{nmo}^2(\alpha)\{t_0^2 v_{nmo}^2(\alpha) + [1+2\eta(\alpha)]x^2\}}} \quad (4)$$

where $v_{nmo}(\alpha)$ is given by Grechka et al. (1999) in equation 5:

$$\frac{1}{v_{nmo}^2(\alpha)} = \frac{cos^2(\alpha)}{v_{fast}^2} + \frac{sin^2(\alpha)}{v_{slow}^2} \quad (5)$$

and $\eta(\alpha)$ is the azimuthally varying aneslasticity parameter given by Pech and Tsvankin (2004) in equation 6:

$$\eta(\alpha) = \eta^1 sin^2(\alpha) + \eta^2 cos^2(\alpha) - \eta^3 sin^2(\alpha) cos^2(\alpha) \qquad (6)$$

where α is the azimuth. This additional variation causes the migration to run slower and thus cost more. A larger roadblock for applying the azimuthally varying moveout correction, however, is often the difficulty in correctly determining all of the required parameters.

4.2 Expected Anisotropy

Thin beds and shales are expected to be major contributors to the amount of vertical transverse isotropy (VTI) layer anisotropy (Figure 5) observed in seismic data. As shown in Figure 3, the Big Horn Basin consists of mostly thin beds with has a high percentage of shales present in the stratigraphic column, especially in the upper section. These thin beds and shales suggest that we should expect to have anisotropy present in the basin due to stratigraphy alone. Also influencing anisotropy of the basin is the present day regional stress and the presence of both vertical and horizontal fractures influencing both layer and azimuthal anisotropy. With geologic bed dips greater than 15 degrees, it is clear that if the axis of isotropy is related to lithology, a tilted transverse isotropy (TTI) should be used rather than VTI. To properly account for both HTI and TTI, an orthorhombic pre-stack depth migration (PSDM) would be required (Figure 5). Since orthorhombic geometry is not practical for this project due to the difficulty and ambiguity in the parameter determination of the nine elastic parameters required for orthorhombic PSDM,

the current ideal solution would be a TTI PSDM which only requires five elastic parameters.

In the time domain, both the VTI and HTI corrections should be included in the migration. The methodology available for this project, however, solved for the η (VTI) and ω (HTI) terms separately instead of simultaneously with velocity. Solving for the anisotropic parameters separately is an issue in the Big Horn Basin due to the geologic dip present which breaks the assumption of VTI being purely perpendicular and HTI being purely parallel to the surface. The geologic dip results in the HTI, when solved independently, accounting for some of the VTI effect, thus over-correcting the VTI effect. To circumvent this issue, the data in this study had an HTI correction calculated and applied post η (VTI) migration.

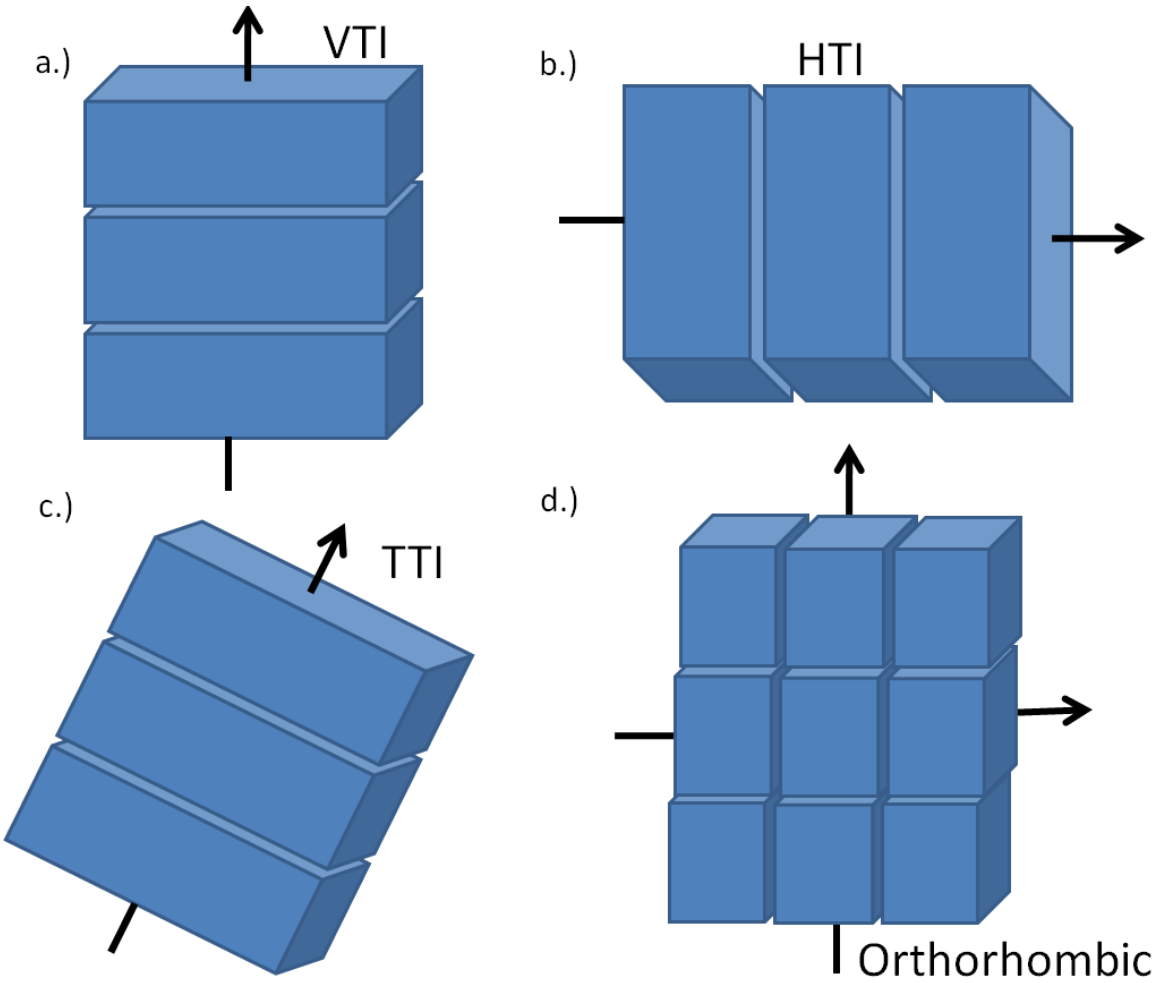

Figure 5: Representation of geometry and axis of isotropy for VTI (a), HTI (b), TTI (c), and Orthorhombic (d). The VTI, HTI, and TTI geometries are all based upon two equal axis and a third unequal axis, where the orthorhombic geometry is based upon three unequal axes perpendicular to each other.

The azimuthal anisotropy in the Rocky Mountains has been observed to be, on average, around three to four percent (Cooley, 2009). Prior to migration, there is also an apparent azimuthal anisotropy caused by the dip of the beds that must be corrected for prior to azimuthal anisotropy evaluation. In Figure 6, Cooley (2009) presents the relationship between equivalent azimuthal anisotropy and geologic dip. This relationship suggests that a geologic dip larger than 15 degrees will create a larger azimuthal variation than HTI effects, such as similarly orientated vertical fractures. In the Big Horn Basin it is common for the backlimb to have dips between 15 to 25 degrees and the forelimb to have 60 to

greater than 90 degree dips. In the field studied the backlimb dips at about 20 degrees and the forelimb at about 75 degrees. By using the relationship shown by Cooley (2009) this would equate to an equivalent azimuthal anisotropy due to geologic dip of around 6% on the backlimb (Figure 6). Due to the very high dip on the forelimb, the time migration will be unable to correct for the azimuthal variation caused by the dip and thus the azimuthal anisotropy analysis will be contaminated in this region of the survey.

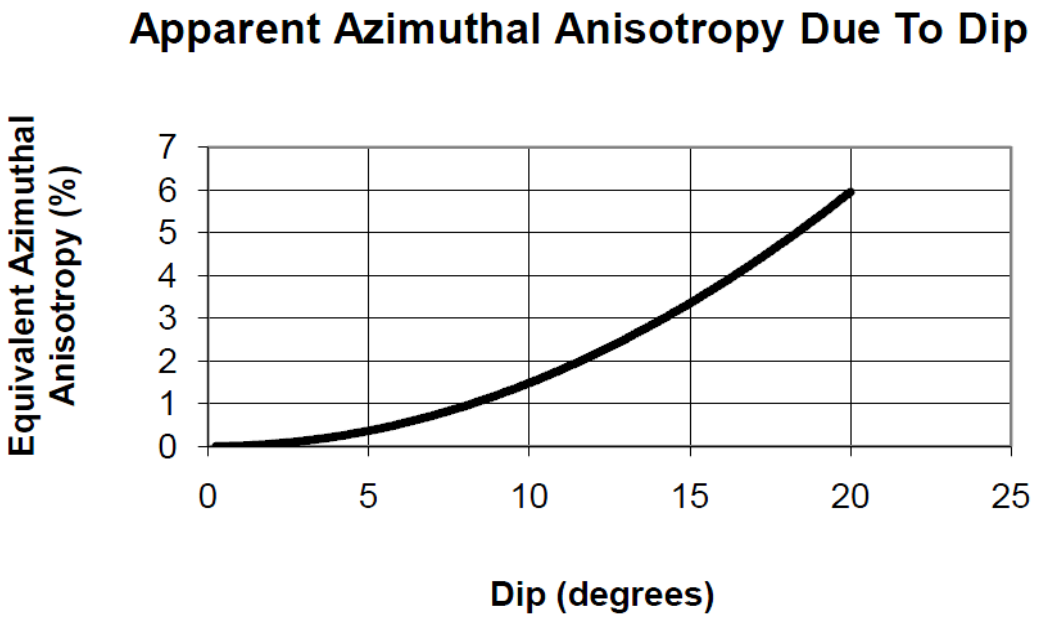

Figure 6: Apparent azimuthal anisotropy due to geologic dip for dips between 0 and 20 degrees prior to migration (Cooley, 2009)

5.0 Processing

Seismic interpretation begins during processing as decisions made during processing can influence the interpretation of the final seismic image. Proper seismic processing is thus a crucial precursor to performing a seismic interpretation that best represents the subsurface. One of the main objectives of processing, required to get a good image and meaningful amplitudes, is to produce flat gathers which will stack constructively to produce a clean final image (Gulunay et al., 2007). The correct isotropic velocity, or various combinations of incorrect velocities, can flatten the gathers at near offsets but are unable to properly flatten gathers at far offsets. Even if the all of the layers in the media are flat and isotropic the standard hyperbolic approximation (1) can't accurately represent the offsets with an offset-to-depth ratio of greater than one (Tsvankin and Thomsen, 1994). The presence of anisotropy in the media will cause the moveout to further separate from hyperbolic significantly increasing the error resulting from the hyperbolic approximation (Tsvankin and Thomsen, 1994). Figure 7 shows a synthetic example of the potential increase in gather flatness at far offsets which can be obtained by taking into account fourth order anisotropic corrections (2). The same non-hyperbolic residual moveout at large offsets (commonly called hockey sticks) shown in the synthetic example in Figure 7 is observed in the real data gathers (Figure 8).

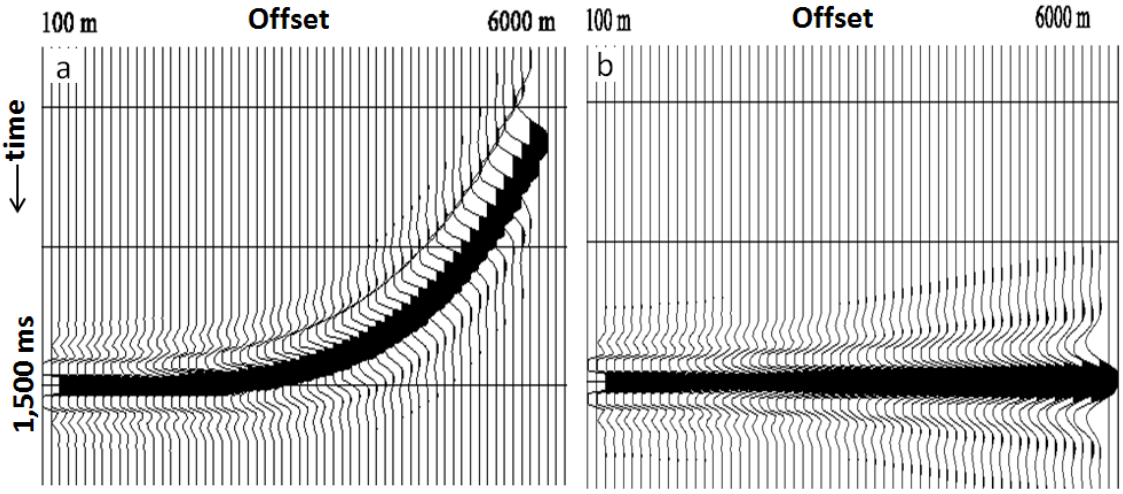

Figure 7: A synthetic dataset with a single anisotropic event at one and a half seconds was created to demonstrate the impact of applying the correct fourth order moveout. The figure on the left (a) was NMO corrected with the known isotropic velocity flattening the near offsets but leaving the 'hockey stick effect' at far offsets. The figure on the right (b) takes into account the fourth order moveout (moveout coefficient of $-5*10^{-16}$) which properly flattens the gathers across all offsets (Leggott et al., 2000).

The processing flow (Appendix B) for the isotropic PSTM and the anisotropic PSTM, incorporating η and residual post-migration HTI, were processed identically as far as feasible. This allows for a fair comparison between the isotropic and anisotropic final migrations to judge the observed uplift in data quality and accuracy. Early on in processing long offset 'hockey stick effects' were observed, suggesting the need for the fourth order moveout equation (Figure 8).

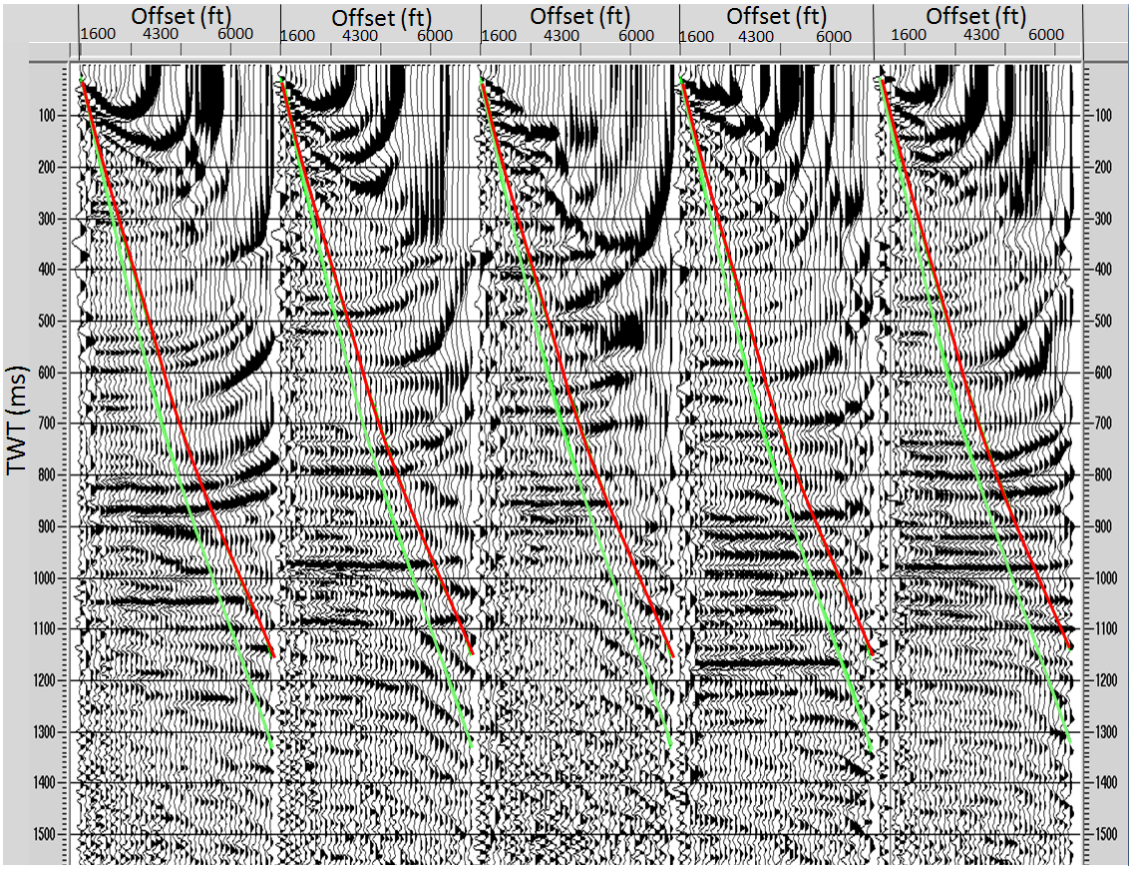

Figure 8: The above NMO corrected gathers shows non-hyperbolic moveout at offsets with an offset-to-depth ratio of greater than 1.2 (represented by red line, offset-to-depth ratio of 1.0 shown for reference in green).

Stacking of gathers with different values of constant η was performed to test the effects of the η field upon the final stacked image. Figure 9 through 14 show how using a larger η value can better collapse a previously uncollapsed diffraction, circled in yellow. It is apparent, however, that although a value of η exceeding a certain value, 10% in this case, collapsing the diffraction, the improvement comes at the cost of introducing noise into other portions of the section. The solution to the issue of the section requiring different η values at various depths and in different portions of section is a variable η field. The variable η field was selected instead of a constant η field for the final anisotropic migration since it properly collapsed diffractions without introducing additional noise into the section (Figure 15-18).

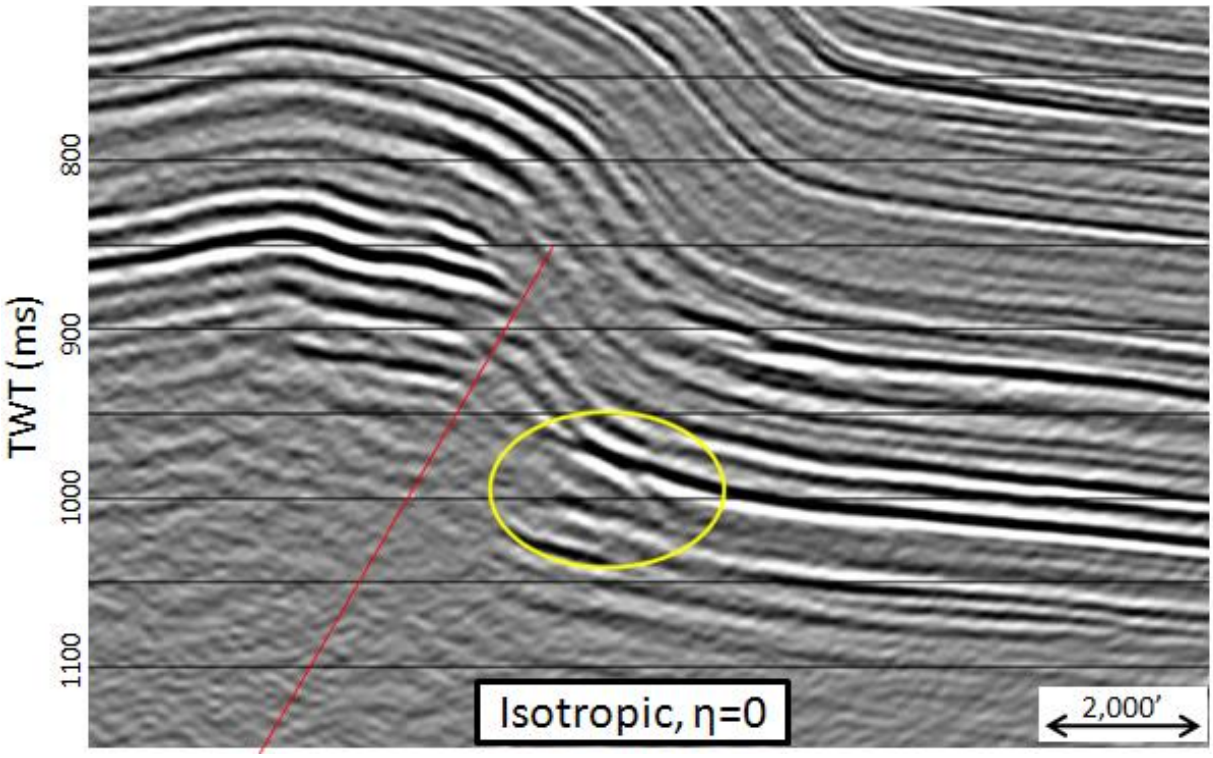

Figure 9: The isotropic migration, η=0, does not properly collapse the diffraction circled in yellow

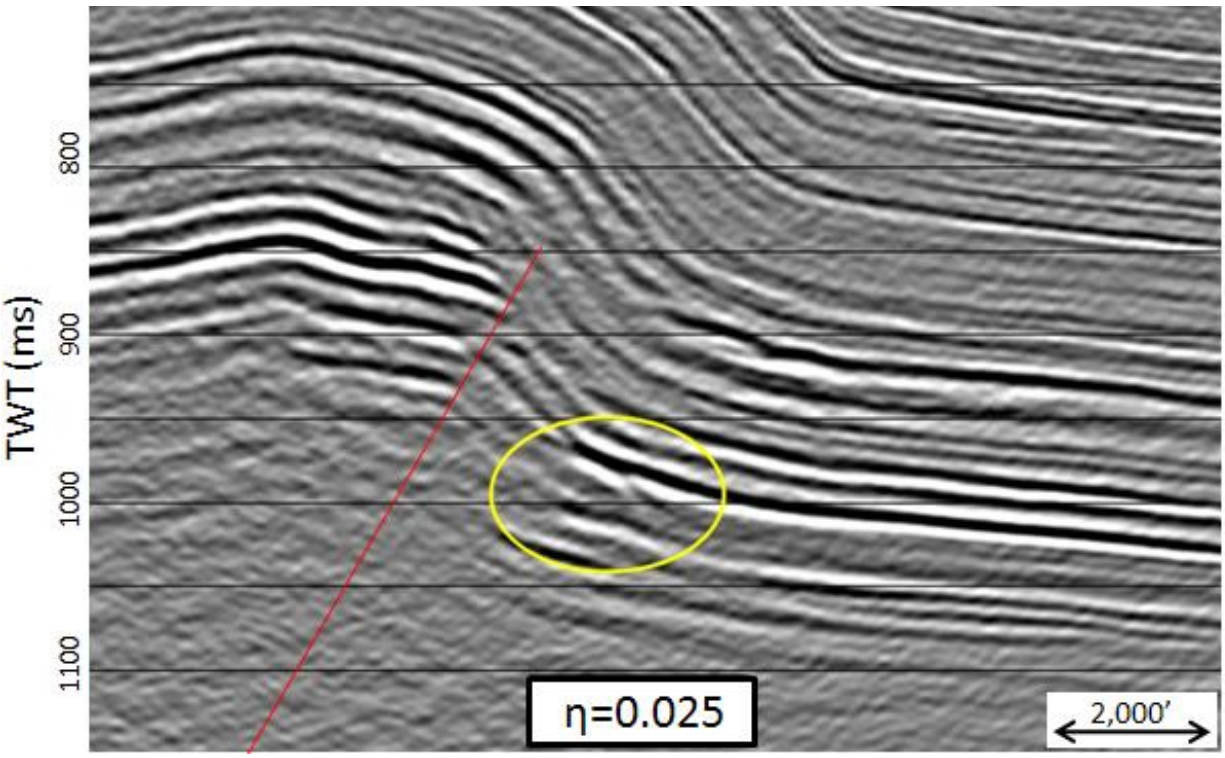

Figure 10: Using a 2.5% η, the diffraction circled in yellow is better collapsed than the isotropic case shown in Figure 9 but is still not fully collapsed suggesting a higher value of η is required.

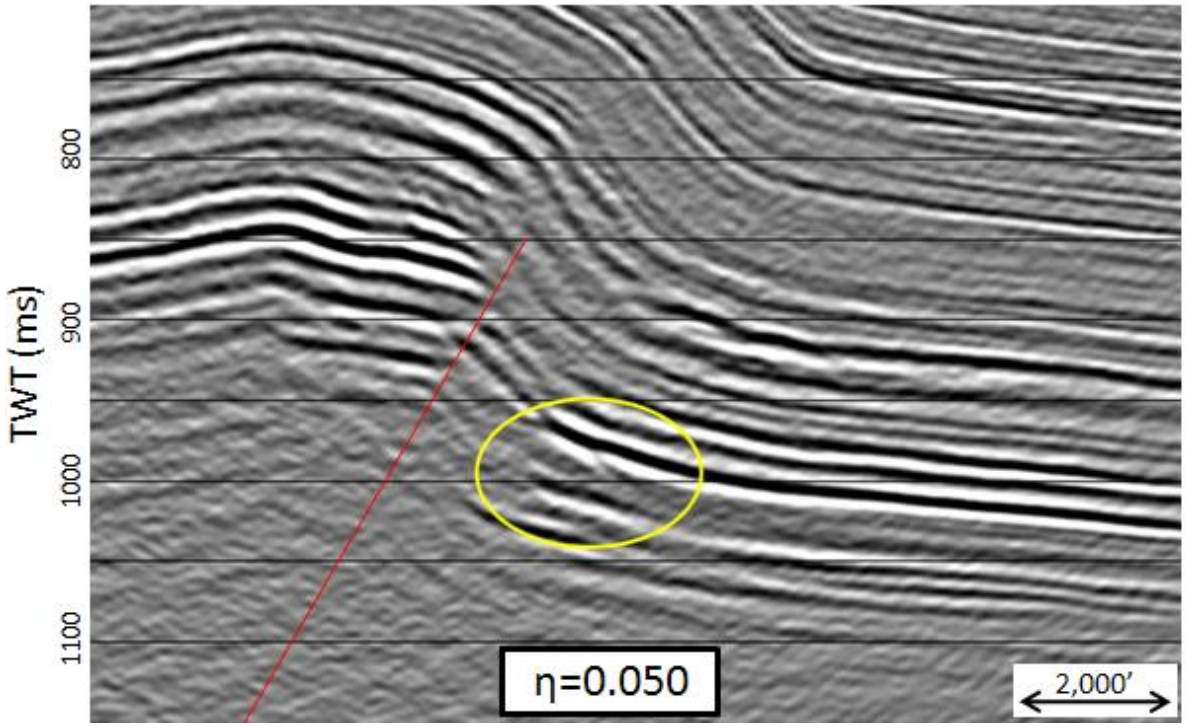

Figure 11: Using a 5% η the diffraction circled in yellow is getting closer to being fully collapsed than observed in the isotropic or 2.5% η case shown in Figure 9 and 10 but is still not fully collapsed suggesting a higher value of η is still required.

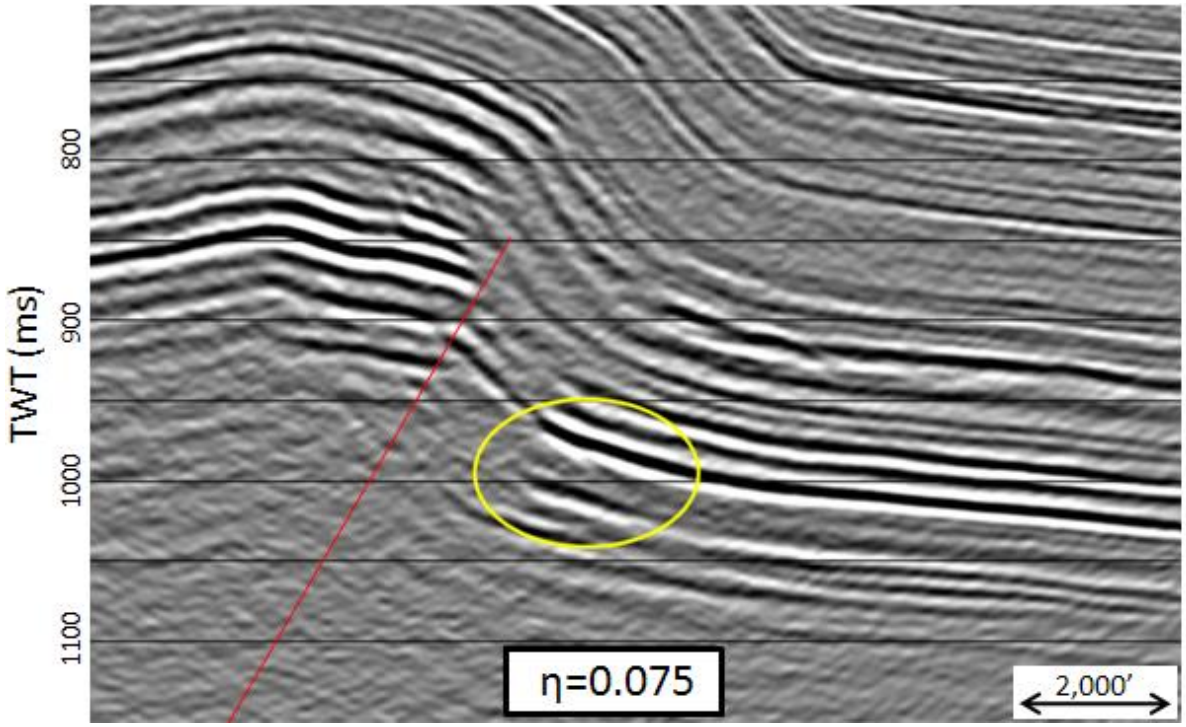

Figure 12: Using a 7.5% η the diffraction circled in yellow is very close to being fully collapsed. It is observed, however, that the diffraction is still not fully collapsed suggesting a slightly higher value of η is required.

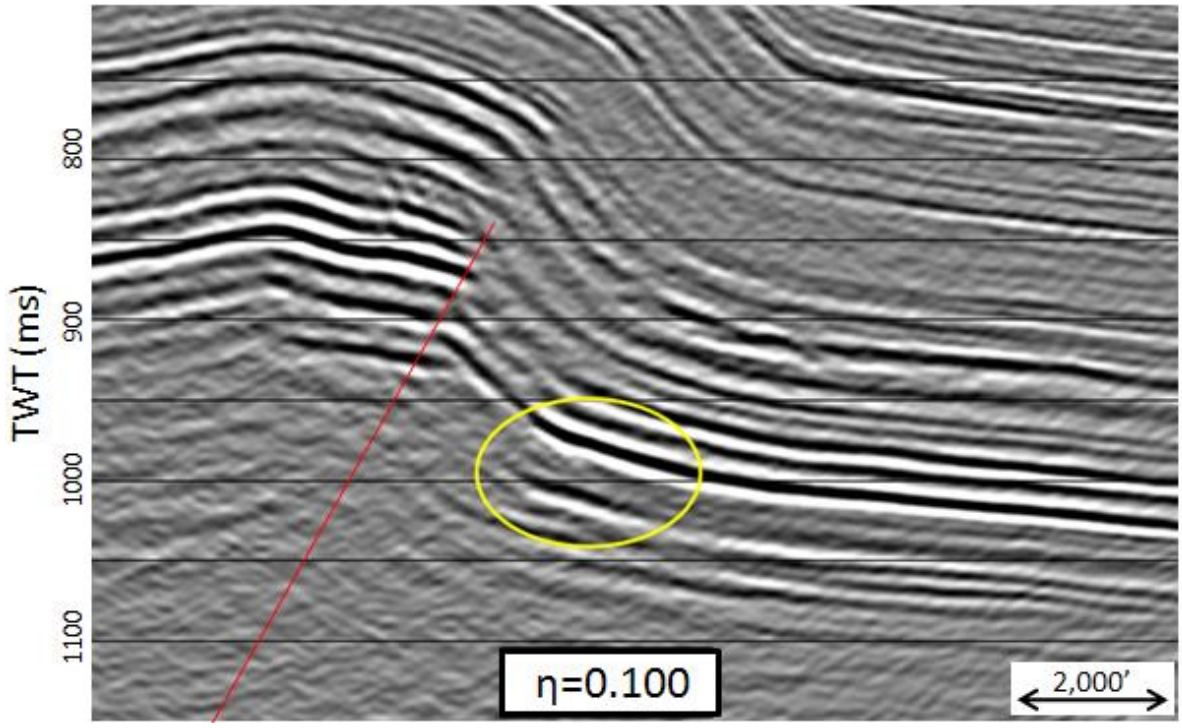

Figure 13: Using a 10% η the diffraction circled in yellow is fully collapsed suggesting that this is the correct η volume for this section.

.

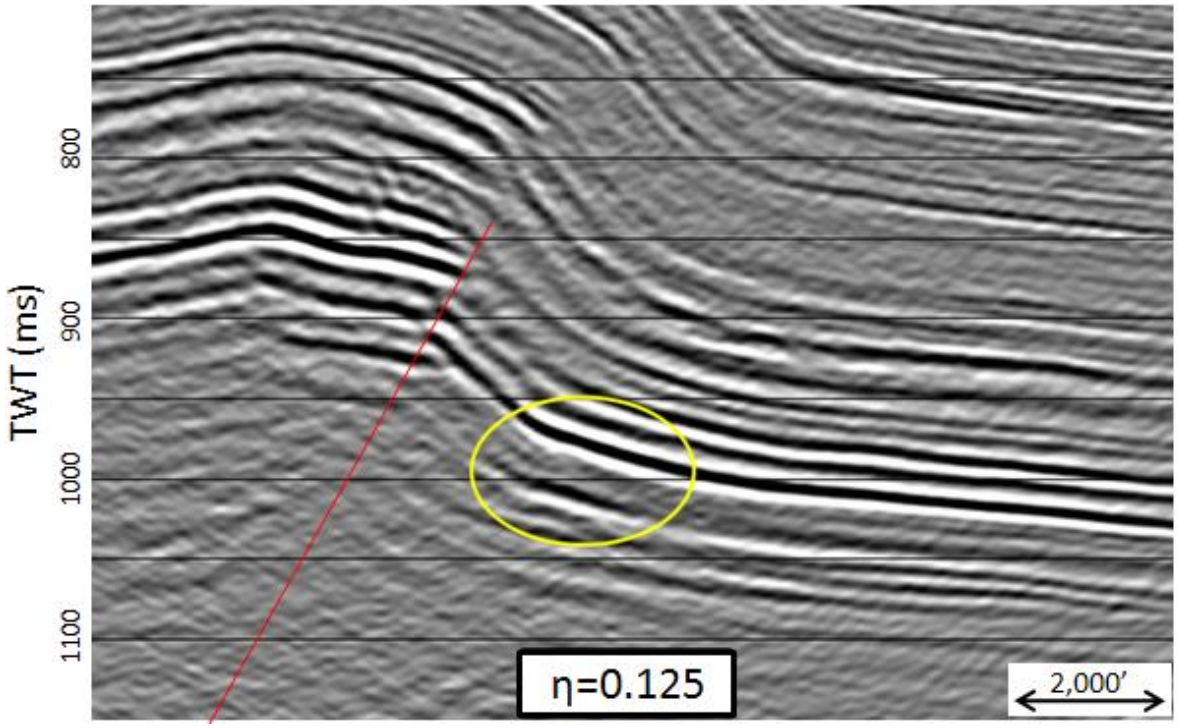

Figure 14: Using a 12.5% η the diffraction circled in yellow is still fully collapsed but introduces overmigration chatter to the section.

By using a variable η value, shown in Figure 15, instead of the constant η volume, shown in Figure 9-14, the higher η value required for the deeper section can be applied while maintaining a lower, more appropriate, η value can be applied to the upper portion of the data. This results in collapsing the deeper diffraction while reducing the noise introduced by any over-migration of the data (Figure 18). The variation of η in Figure 15 appears to be following geology in some localized portions of the section, but does not correlate across the entire section. One region demonstrating this non-geologic variation could be attributed to anisotropic effects due to the localized increase in the stress field from tectonic compression or the η term attempting to correct for the rapid lateral velocity changes which the PSTM cannot properly account for. The crest of the structure also shows a different η value than the same geologic unit off the crest of the structure on the flank, outlined in yellow on Figure 18. This could be attributed to the differing overburden geology with some of the units present off structure which have been eroded above the crest of the structure (Figure 4) or the ray-bending effect which is comingled with the anisotropy effect within the η value.

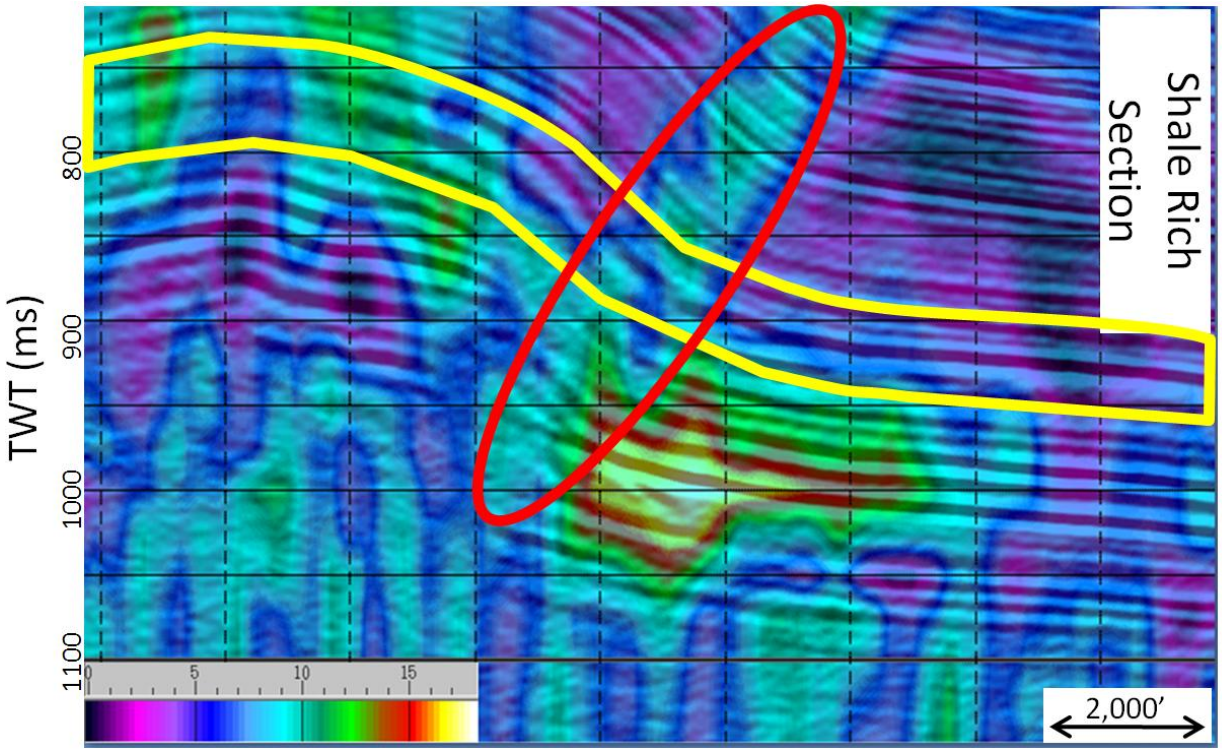

Figure 15: Isotropic stack with variable η field overlaid. Note the localized high value of η required to collapse the diffraction shown in Figure 9 through 14. The rapid lateral velocity variations contamination of the η term is highlighted in the region circled in red. The region outlined in yellow has a different η value on the crest of the structure than the same geology off structure.

In theory, we would expect a positive correlation between anisotropy and shale content and the anisotropy being consistent within the same geologic unit. In Figure 15, however, we do not observe a convincing correlation between the calculated variable η field and shale content and observe large changes in η within the same geologic unit. This is most likely due to η being heavily affected by ray bending instead of by anisotropy alone. The η correction is a combination of both ray bending and anisotropy which cannot be separated with the fourth order moveout correction used in study as discussed in the theory section (section 4). Therefore, the η value not having a positive correlation with the shale rich portion of the section or following geology is not a quality concern.

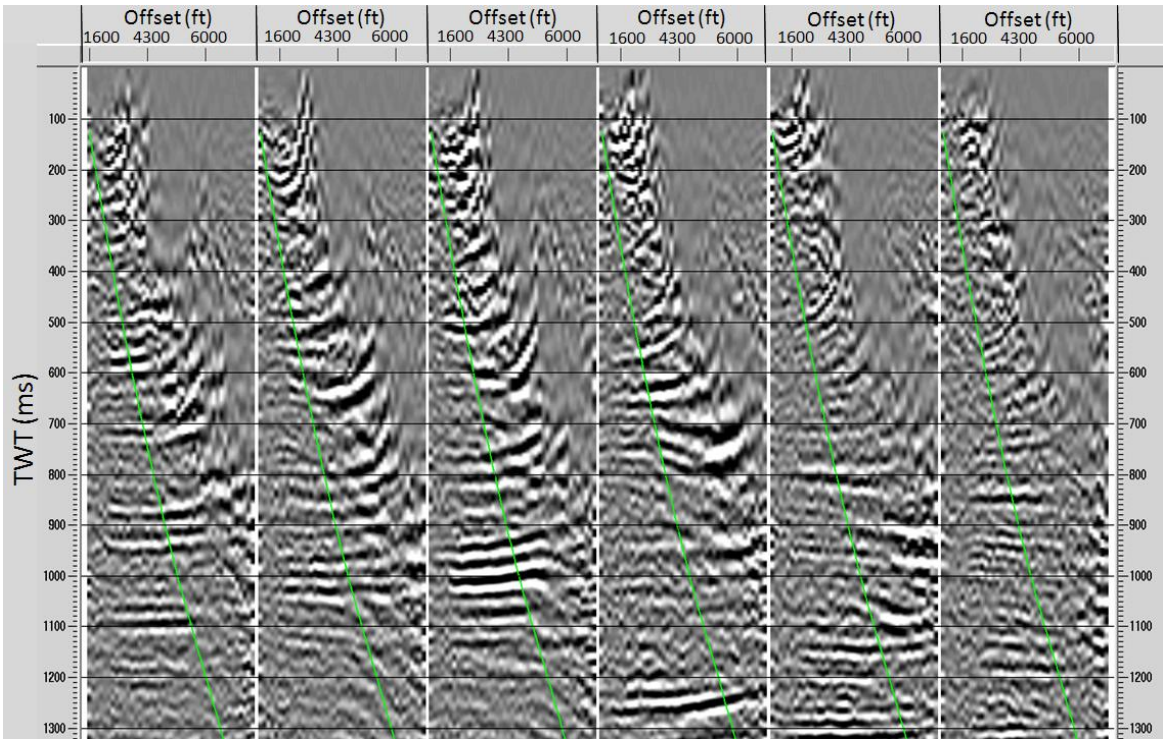

Figure 16: Isotropic PSTM gathers exhibiting the hockey stick effect suggesting non-hyperbolic moveout beyond offsets with an offset-to-depth ratio of greater than 1.0, represented by the green line.

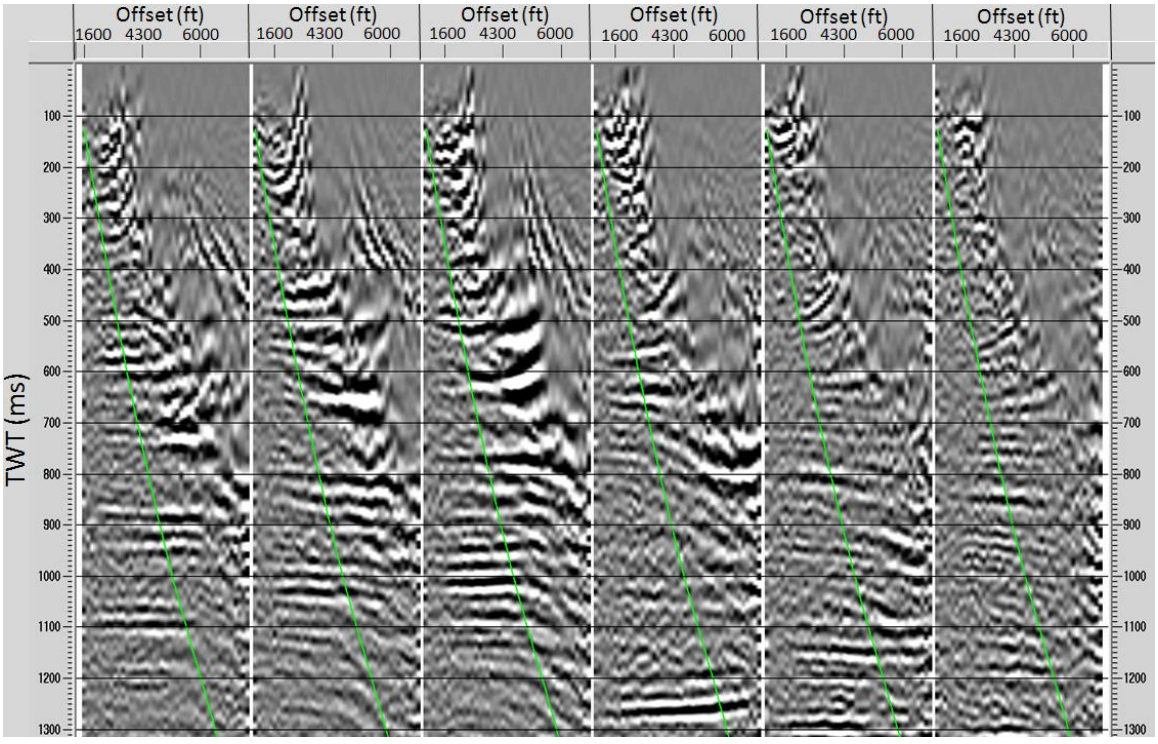

Figure 17: Anisotropic PSTM gathers with flatter gathers than the isotropic PSTM gathers shown in Figure 16 beyond offsets with an offset-to-depth ratio of greater than 1.0, represented by the green line.

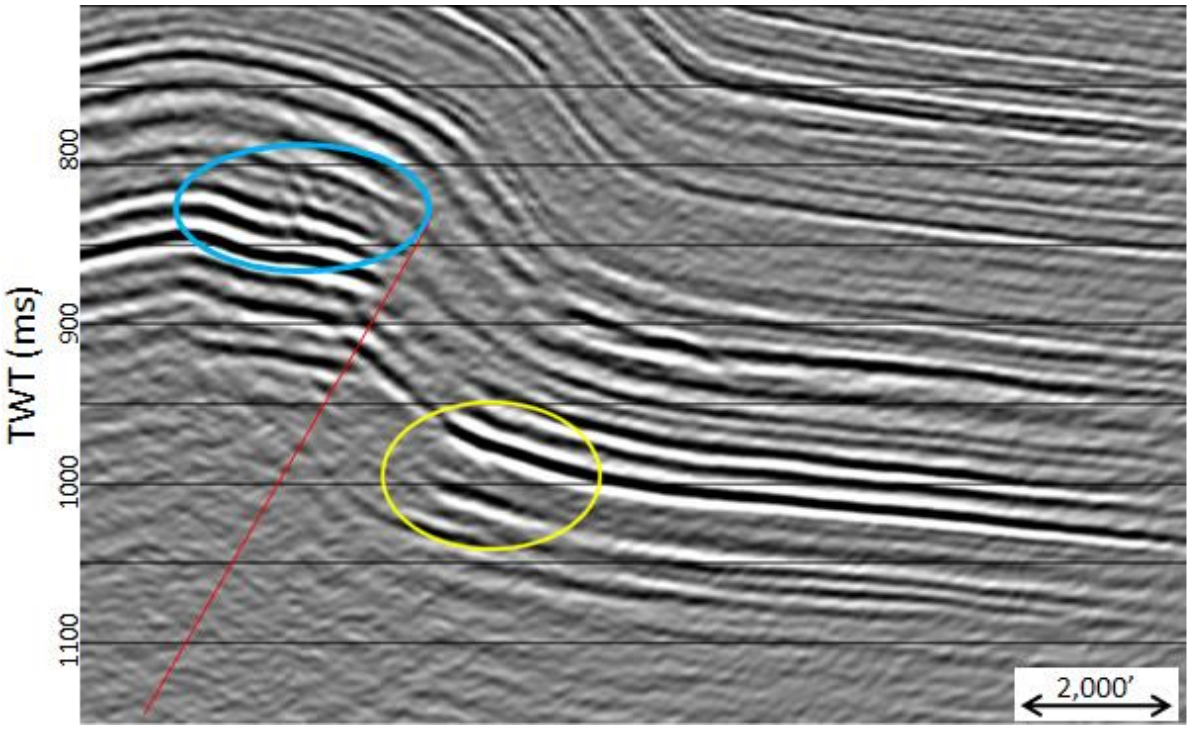

Figure 18: Image resulting from using a variable η field. Notice the collapsed diffraction and reduced chatter in the section. There is still some noise present, circled in blue, in the variable η migration which may be contributed to the rapid change of η value.

Many anisotropic studies are chosen in areas with relatively flat geology to avoid the complication that structural variations have on the interpretation and estimation of the anisotropic parameters (Kuhnel and Li, 2001). In these flat geology areas, it is possible to estimate the azimuthal anisotropy on un-migrated gathers. The complication of properly accounting for anisotropy in the presence of geologic dip was first discussed by Hood and Schoenberg (1989). In regions with steep dips, such as this project area, the dipping geology expresses the same sinusoidal signature as the anisotropy masking the azimuthal anisotropy variation (Figure 20). This makes it necessary to migrate the data prior to performing a proper anisotropic evaluation. Traditional CMP migration, however, blends all of the azimuths and offsets together eliminating the anisotropic information present prior to migration. Thus it was critical that the data was migrated with offset vector tiles

(OVT) which groups traces from different source and receivers over limited offset and azimuth ranges instead of by CMP (Figure 21), thereby preserving both the offset information required for η and the azimuthal information required for HTI corrections (Figure 21).

The signal to noise ratio and flatness of the gathers both greatly contribute to the quality of the final stacked seismic image. The gathers which have been migrated with η and had a post migration HTI correction applied are flatter than gathers which have had only isotropic processing applied (Figure 19).

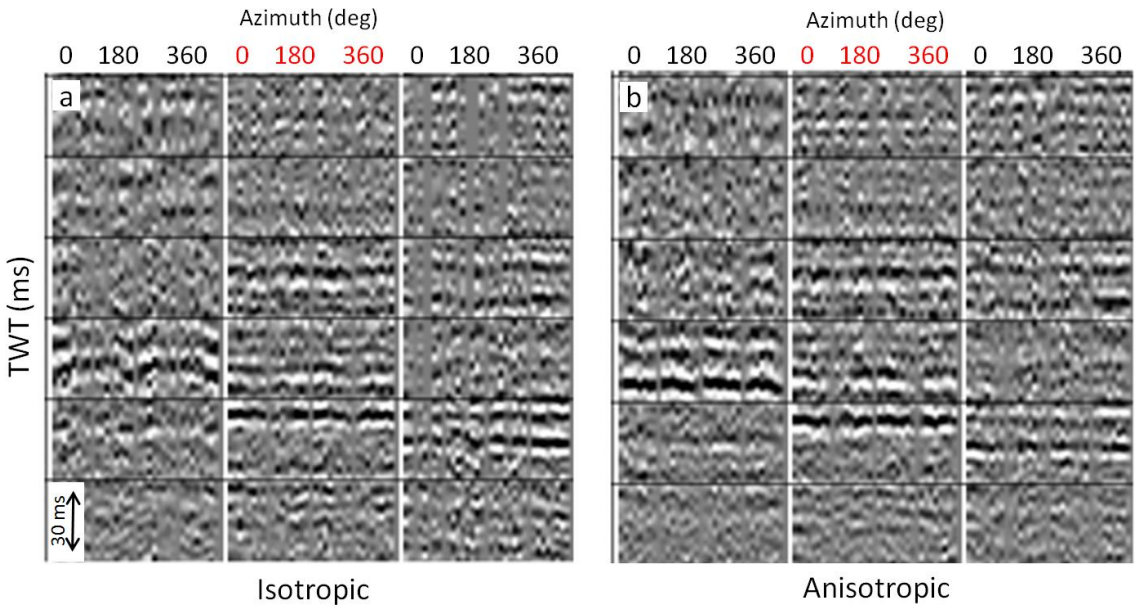

Figure 19: The anisotropic processing (b) produces flatter gathers with a better signal-to-noise ratio than isotropic processing (a).

By analyzing azimuth sorted OVT PSTM gathers, the proper HTI anisotropic corrections were able to be applied. Figure 20 shows the large sinusoids being removed from the gathers after migration, highlighting the HTI effect present in the data represented by smaller sinusoids on the PSTM gathers. By applying the post-migration HTI correction, it is clear that the gathers become flatter which will result in a better stacked image.

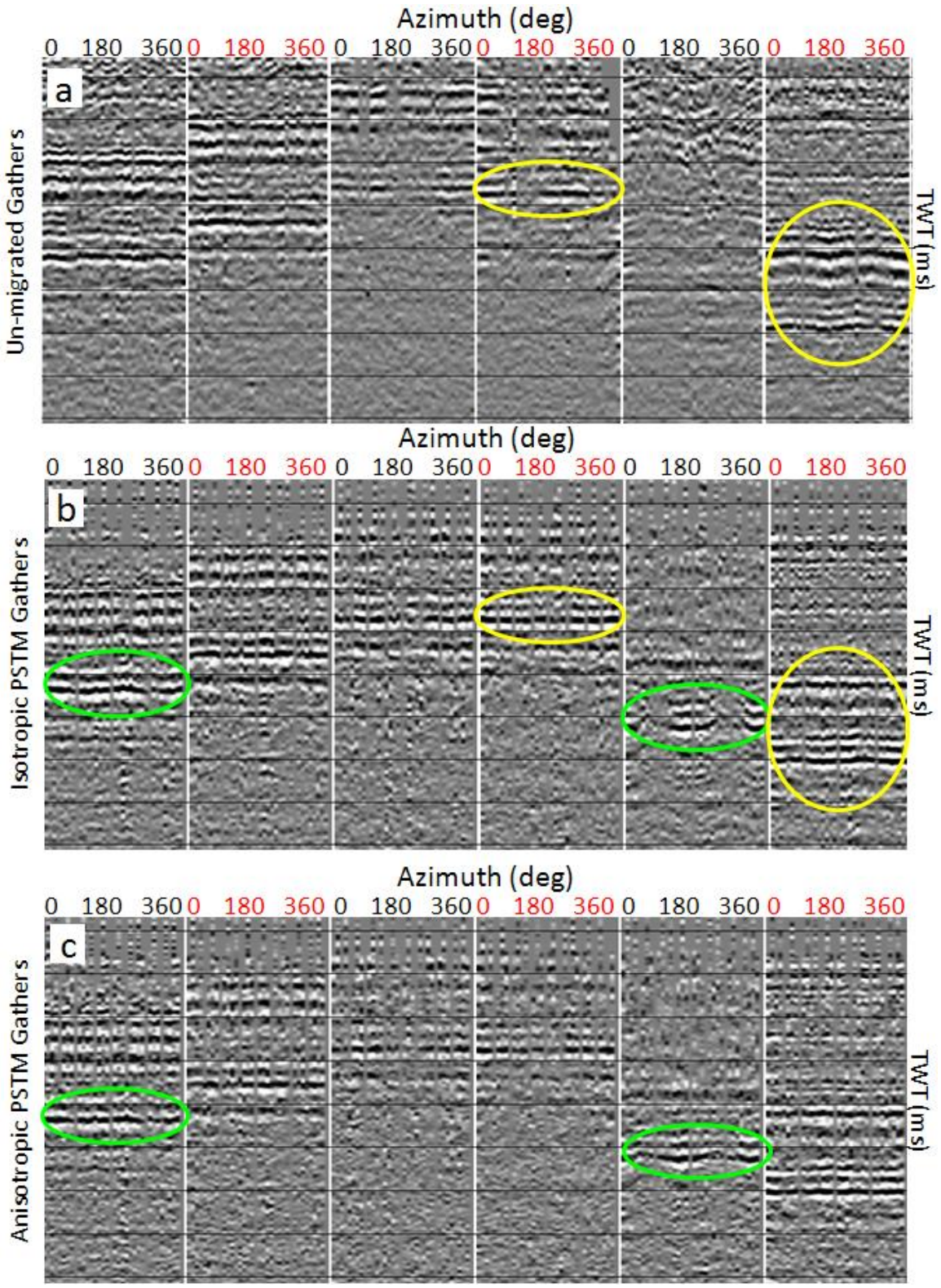

Figure 20: The sinusoids related to azimuthal anisotropic effects, circled in green, (b)/(c) can properly be corrected for after the azimuthal effect due to geologic dip, circled in yellow, have been removed by migration (a)/(b).

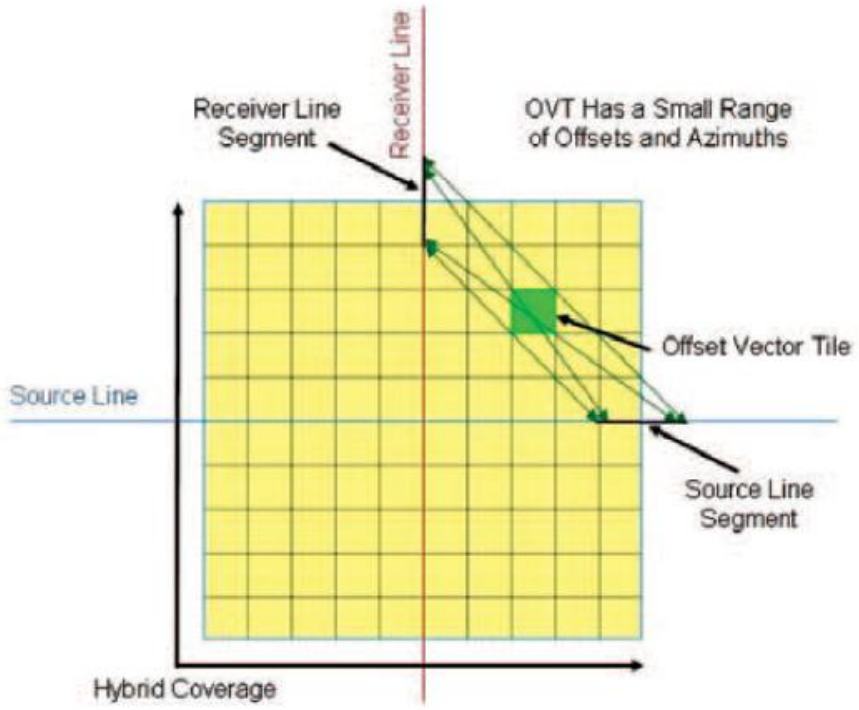

Figure 21: The figure above provides a visual representation of data selection which goes into each OVT allowing the bin to retain its azimuthal information (Stein et al, 2010)

6.0 Interpretation

To best evaluate the differences between the isotropic and anisotropic volume it is necessary to first create seismic trace synthetics from well logs and tie them to each seismic volume. Once the seismic synthetic is tied to the observed seismic a base interpretation of faults and three key horizons was performed.

6.1 Well A: Synthetic and Horizons

Well A is very close to a fault which cuts the lower section of the well. The well is also not ideal for creating a synthetic since it only has a recorded density measurement in the upper half of the well, which may explain a few of the small mis-ties with the seismic in the lower section. Despite these issues the synthetic seismic trace created from the well logs is observed to correlate well with the recorded seismic data (Figure 22). The anisotropic volume does not provide a substantial improvement in the seismic correlation of the upper portion of the section. In the region circled in Figure 22, however, there is a clear improvement in continuity of the reflector on the anisotropic volume which correlates well with a predicted peak on the synthetic.

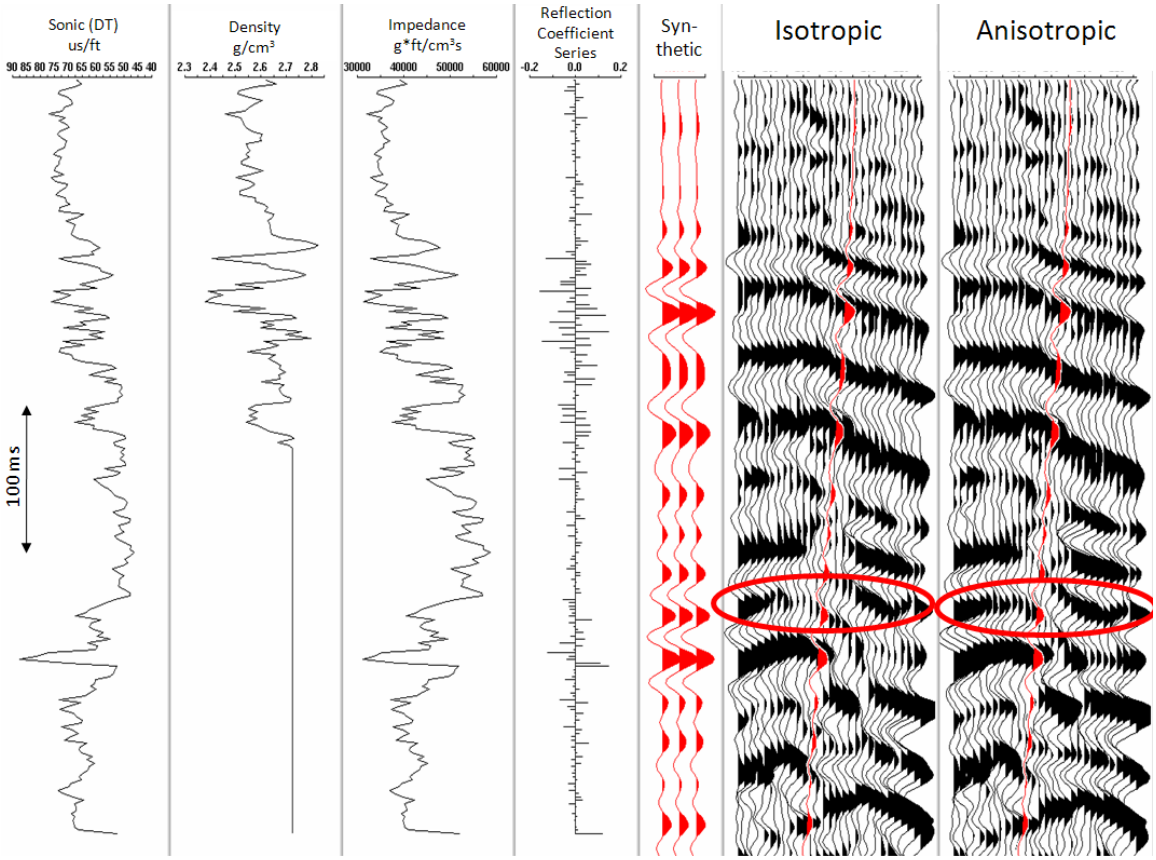

Figure 22: Synthetic for Well A overlaid on seismic extracted from the isotropic and anisotropic seismic volumes. The increased continuity of the reflector in the anisotropic volume, circled in red, as it approaches the fault creates a better tie with the synthetic than the same section on the isotropic section.

The synthetic seismic trace is based upon the convolution of two items; the reflection coefficient (RC) series, derived from the sonic and density logs, and a chosen wavelet (Figure 23). Outside of performing log editing, the RC series will remain constant, thus leaving the variability of the synthetic seismic to the chosen wavelet. There are two methods most commonly used to determine the correct wavelet to be used. One is deterministic and the other probabilistic. The deterministic method extracts a wavelet from the recorded seismic data to convolve with the RC series. This wavelet should properly represent the phase and frequency bandwidth of the observed seismic. The extracted wavelet is rarely close to an ideal wavelet, however, so a probabilistic ideal

Ricker wavelet is often used instead. When using a probabilistic synthetic wavelet it is important to ensure that the phase and frequency bandwidth selected is realistic and representative of the observed seismic data. To support the wavelet choice used to create the seismic synthetic for Well A, shown in Figure 23, the frequency spectrum in the region surronding the well was extracted from the seismic data (Figure 24). The seismic data was processed to be zero phased and was confirmed by well tie analysis as shown in Figure 23.

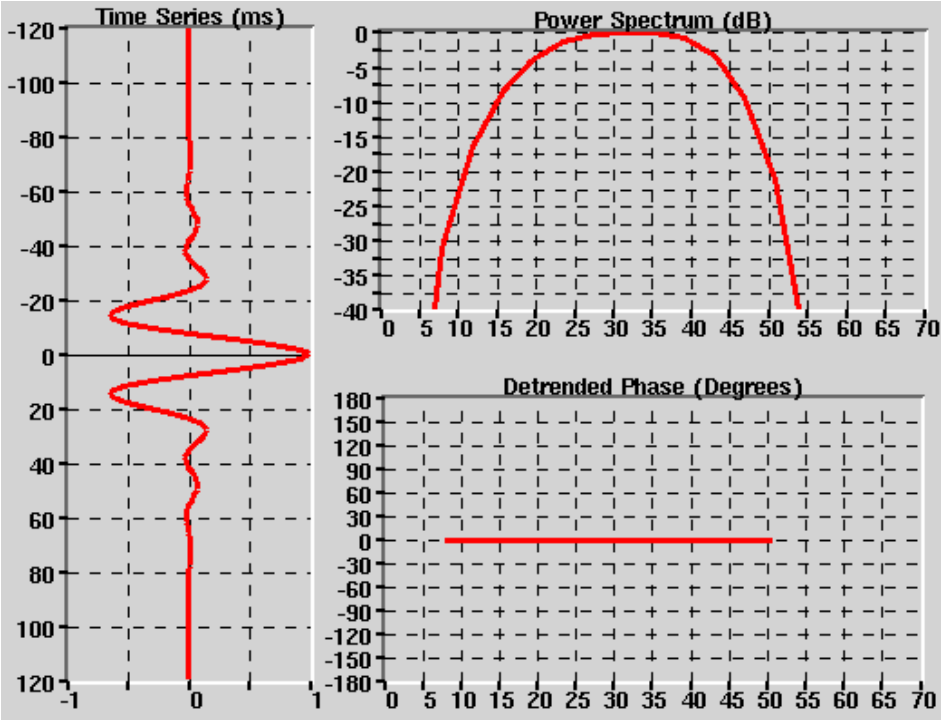

Figure 23: The wavelet (left) used to convolve with the reflection coefficient series to create the seismic synthetic for well A. The power spectrum in the upper right shows the trapezoid filter of 10-20-45-56 which was applied to the wavelet.

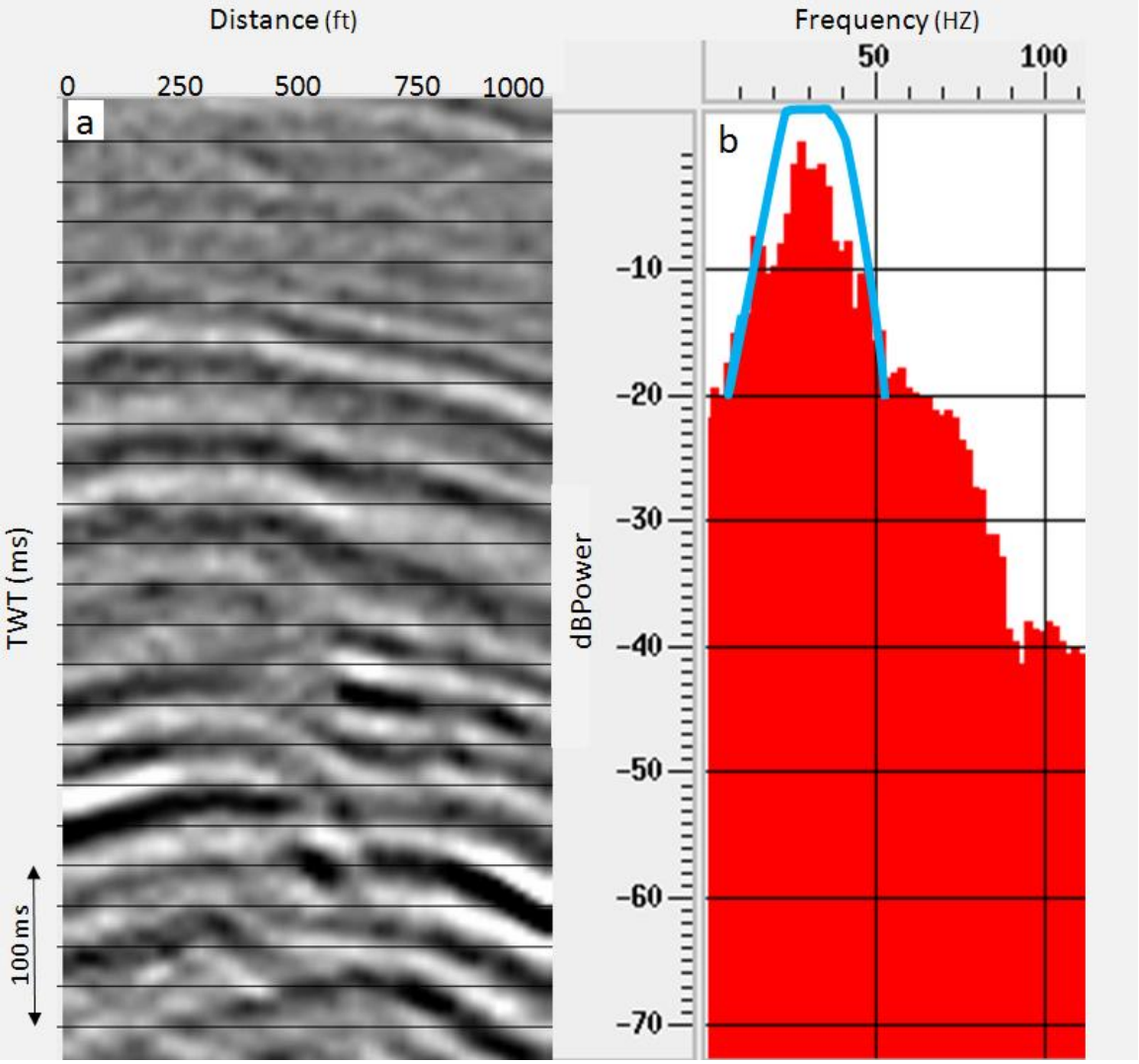

Figure 24: The extracted frequency spectrum (b) was extracted from the anisotropic seismic section around Well A (a). The extracted spectrum suggests the presence of 10-50HZ at -20 db down which matches the trend of the synthetic wavelet spectrum, represented by the teal line on the right, very well.

The seismic synthetic that correlates the well information to the seismic information also provides a time-to-depth (T-D) function to convert the well information in depth to the same domain as the seismic (time). The well information and synthetic can then be overlaid on the time seismic data allowing for the identification and interpretation of geologically meaningful seismic horizons (Figure 25 and Figure 26).

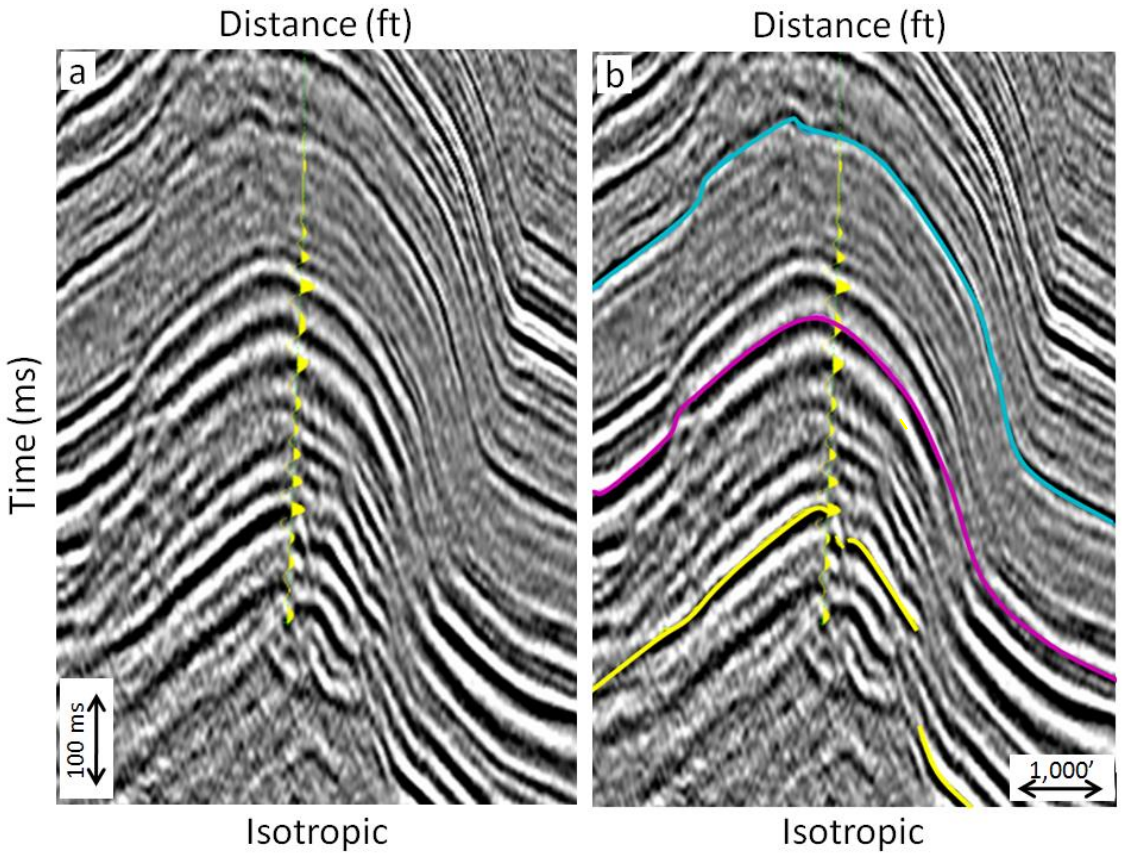

Figure 25: The synthetic for Well A is overlaid on the isotropic seismic section with (b) and without (a) the three key horizons used in this analysis. Notice that the well synthetic only covers the lower two horizons (#2 and #3), the top shallow horizon (#1) was picked based upon Well B (Figure 30 and Figure 31).

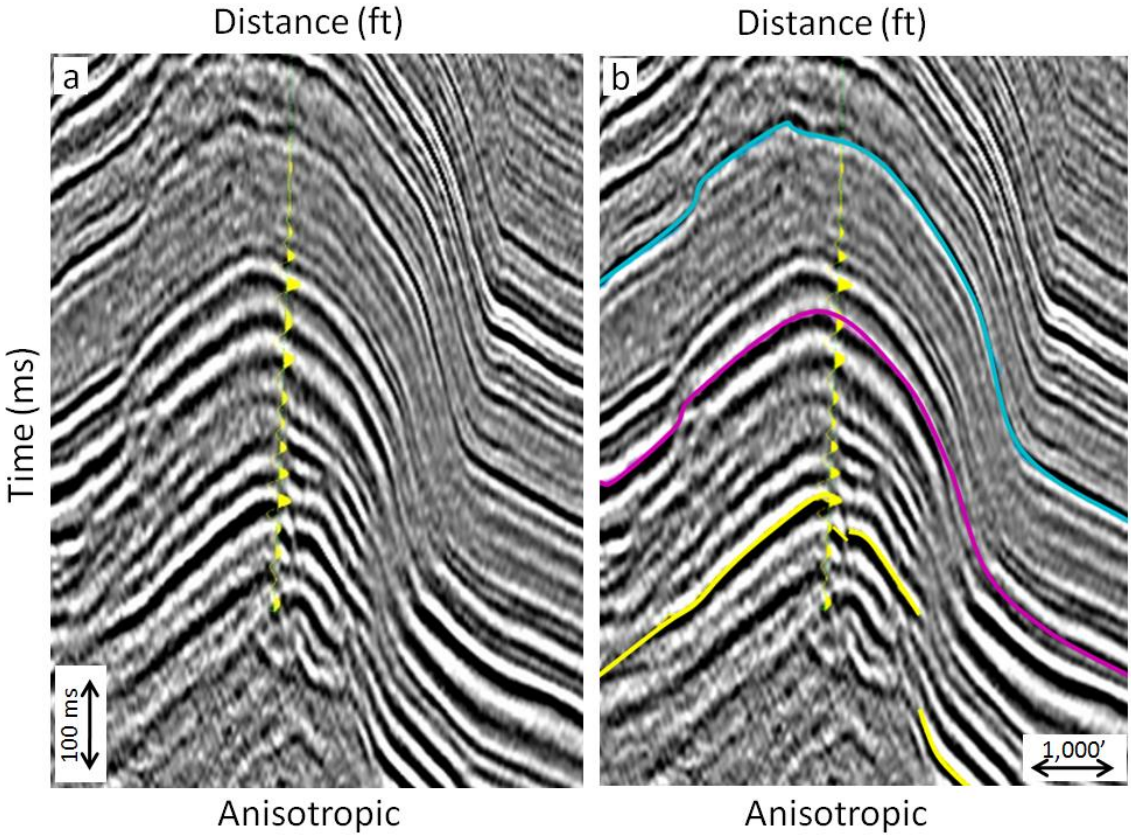

Figure 26: The synthetic for Well A is overlaid on the anisotropic seismic section with (b) and without (a) the three key horizons used in this analysis. The same horizons interpreted on the isotropic are shown to be valid for the anisotropic volume as well.

For horizon based analysis three key geologic horizons were selected and shall be referred to as shallow horizon (#1), mid-depth horizon (#2), and deep horizon (#3). The seismic synthetic generated from Well A, Figure 22, was tied to the surface seismic, Figure 26, to select the mid-depth horizon (#2) and deep horizon (#3). The correlation between Well B and the shallow horizon (#1) will be shown in the next section. Figure 25 and Figure 26 show that the difference in selection and base interpretation of the horizons near between the well are minimal between the isotropic and anisotropic volume.

6.2 Well B: Synthetic and Horizons

The synthetic for Well B (Figure 27) ties both the isotropic and anisotropic volumes well despite not being ideal due to the lack of a density log. The overall trend should not be affected by the lack of density log, some of the details may, however, be affected. The acoustic impedance (product of density and P-wave velocity) curve which the reflection coefficient series is based upon requires a density value so to create the seismic synthetic. It was elected to use a constant density value of 2.6 g/cc instead of creating a synthetic density log from the sonic log using Gardner's Equation. This decision was based on personal experience with several other wells across multiple Big Horn Basin fields. The deepest portion of the synthetic shows a strong reflection which is not present in either of the seismic volumes. There is no change in the diameter of the hole according to the caliper so a washout creating the error seems unlikely. It is proposed that there is an error in the sonic log, a depth error in logging, or a counter kick in the density which is not represented.

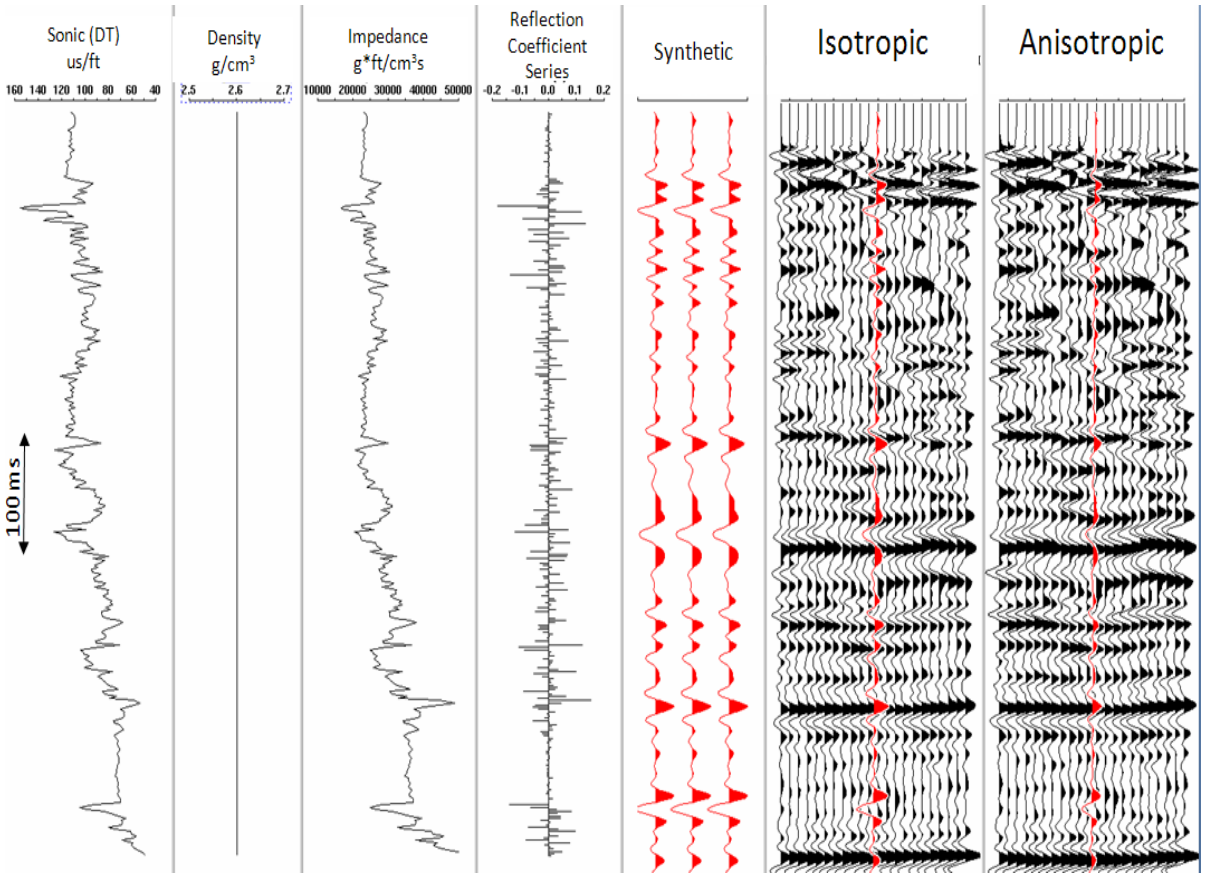

Figure 27: Synthetic for Well B overlaid on seismic extracted from the isotropic and anisotropic seismic volumes. There doesn't appear to be much meaningful difference between the isotropic and anisotropic sections in this case.

The difference between the synthetic tie with the isotropic and anisotropic volumes is very minor compared to the other sources of error, such as the lack of density log. The similarity of the isotropic and anisotropic volume around the well may be contributed to Well B being in a region with much flatter geologic dip than Well A (Figure 32 and 33).

To evaluate the wavelets chosen to create the synthetic, shown in Figure 28, the frequency spectrum in the region of the well was extracted from the seismic data (Figure 29). Due to the large depth range - 300' to 4,000' - represented by the Well B seismic synthetic a time variant filter was applied. The upper portion - 300' to 1,200'- of the well

used a higher frequency wavelet to convolve with the reflection coefficient series than the wavelet representing the lower portion – 1,400’ to 4,000’- of the well (Figure 28). A 200’ transition zone between the two filters -1,200’ to 1,400’- was used to reduce any artifacts which could result from sharp variations in frequency of wavelet. The frequency attenuation in the earth is more continuous than represented by the seismic synthetic which squeezes all of the attenuation into a 200’ interval. This assumption, however, has very little effect upon the final synthetic correlation, confirmed by testing.

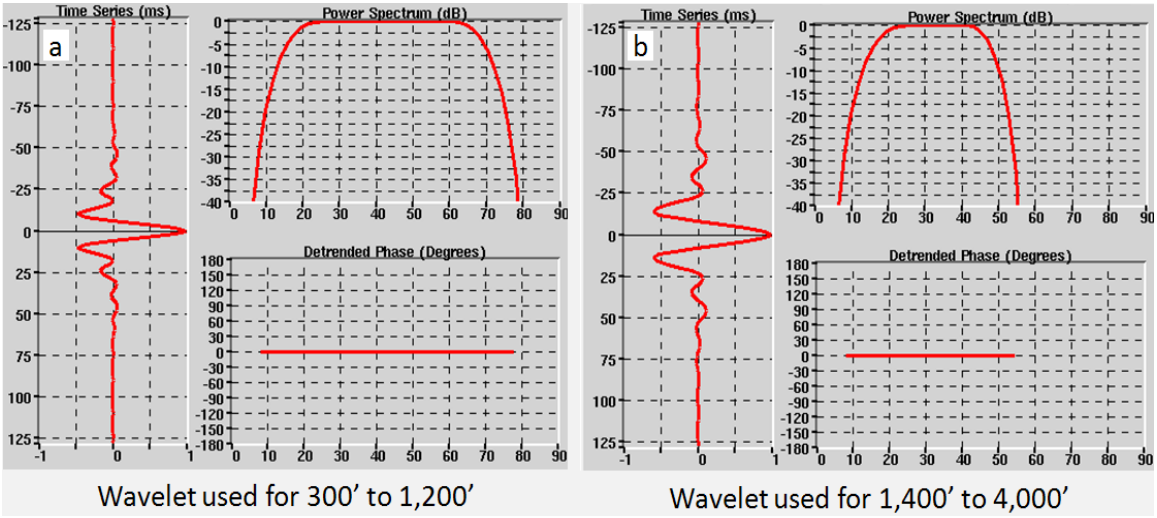

Figure 28: The trapezoid frequency filter (10-20-65-75) was applied to the wavelet used to convolve with the reflection coefficient series in the shallow section to best match the observed seismic data at Well B (a). Due to frequency attenuation, a wavelet with a narrower bandwidth trapezoid frequency filter (10-20-46-55) was applied to the deeper section (b).

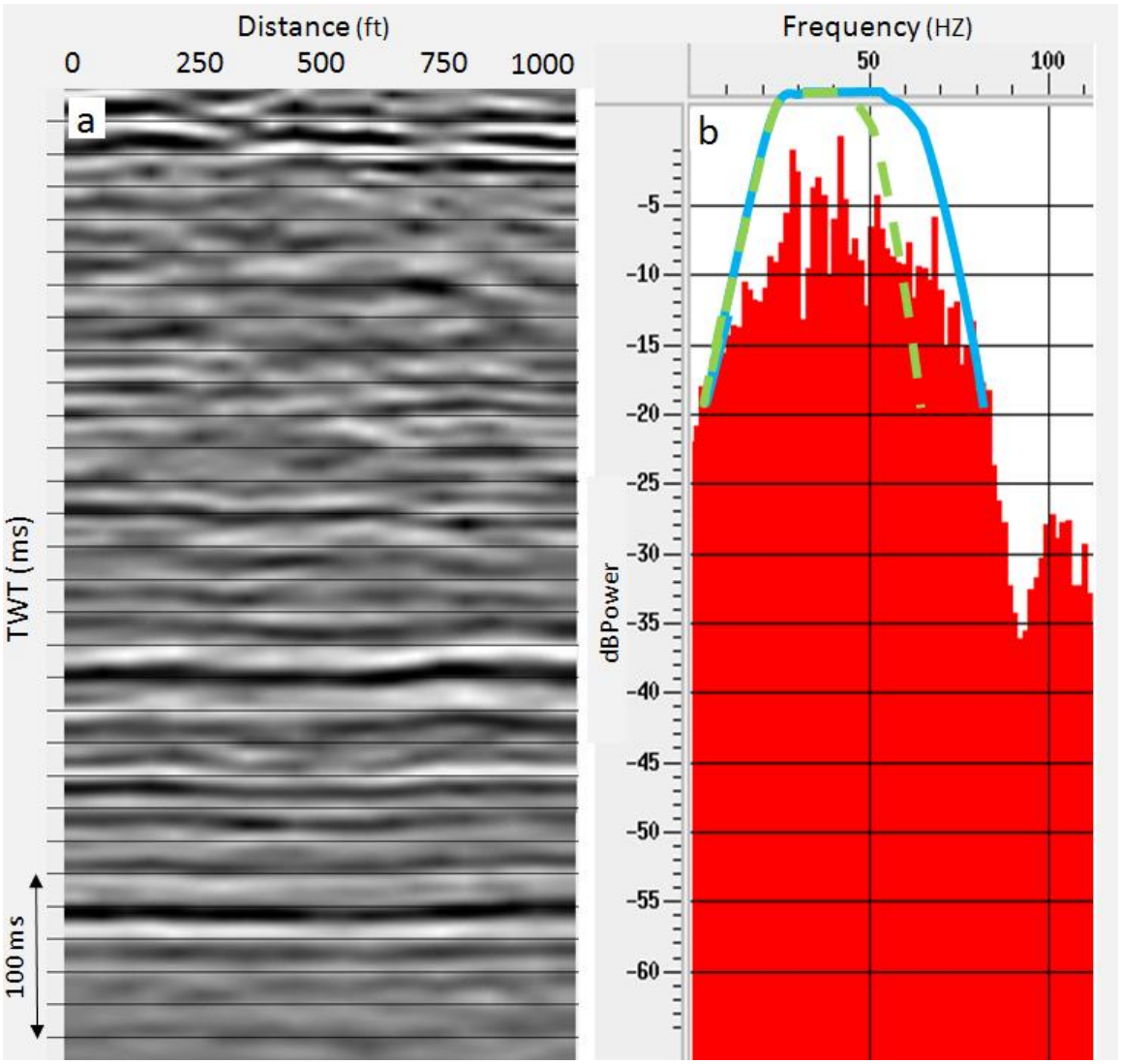

Figure 29: The frequency spectrum (b) was extracted from the anisotropic seismic section around Well B (a). The extracted spectrum suggests the presence of 5-70HZ at -20 db down which matches the synthetic wavelet spectrum in the shallow section, represented by the teal line, but is too broad for the wavelet spectrum of the deeper section, represented by the dotted green line (b).

Once the seismic synthetic and time-depth relationship was built for Well B it was overlaid onto the seismic data to interpret the key shallow horizon (#1) as shown in Figure 30 and 31. As observed with the two deeper horizons on Well A, the same shallow horizon pick honors both the isotropic (Figure 30) and anisotropic (Figure 31) volume.

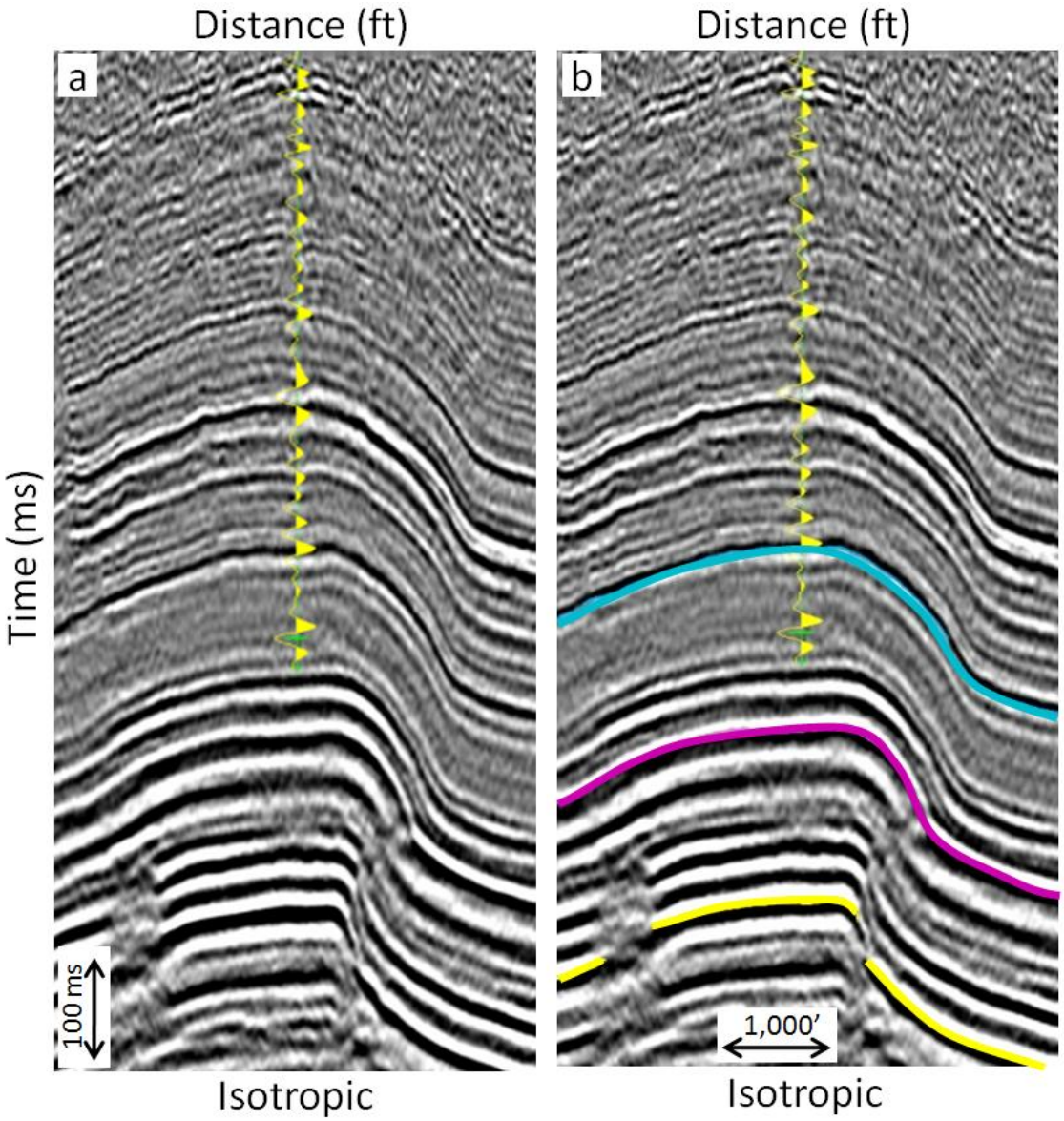

Figure 30: The synthetic for Well B is overlaid on the isotropic seismic section with (b) and without (a) the three key horizons used in this analysis. The seismic section with horizons (b) displays the same well and seismic section with three key horizons interpreted. Notice that the Well B seismic synthetic is used for picking only the key shallow horizon (#1).

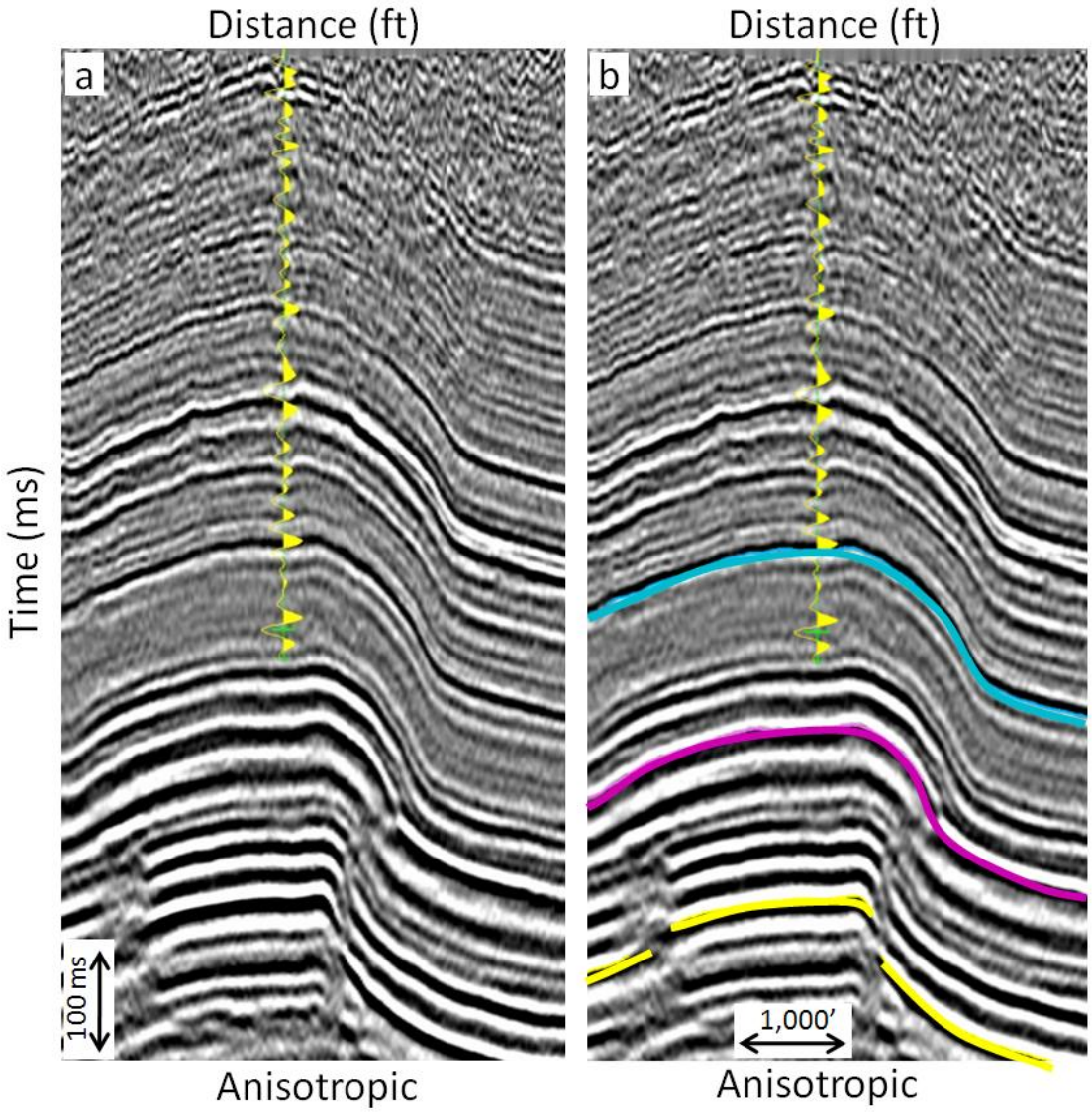

Figure 31: The synthetic for Well B is overlaid on the anisotropic seismic section with (b) and without (a) the three key horizons used in this analysis.

An arbitrary line intersecting both Well A and Well B was used to QC and better understand the relationship between the two wells (Figure 32and 33). This arbitrary line shows that Well A is on the crest of the structure in the deeper section, while Well B is off the main structure in the shallower section.

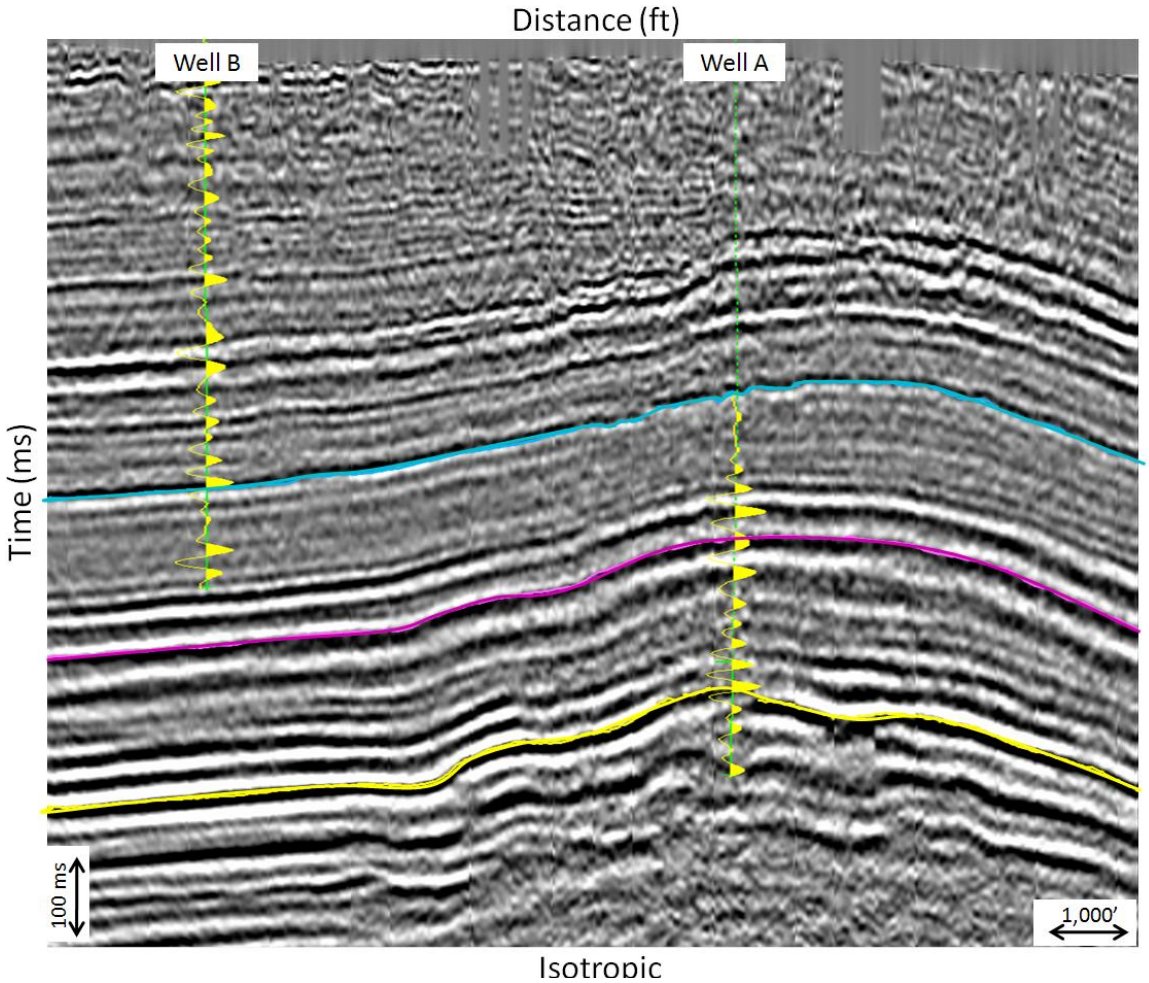

Figure 32: Wells A and B's seismic synthetics overlaid on the isotropic seismic section. Both wells are required to properly correlate the three key horizons between the well data and the seismic cross section. It also highlights the relationship between the wells and the geologic structure. Well A in the deeper section is on the crest of the structure and Well B is off the main structure in the shallower section.

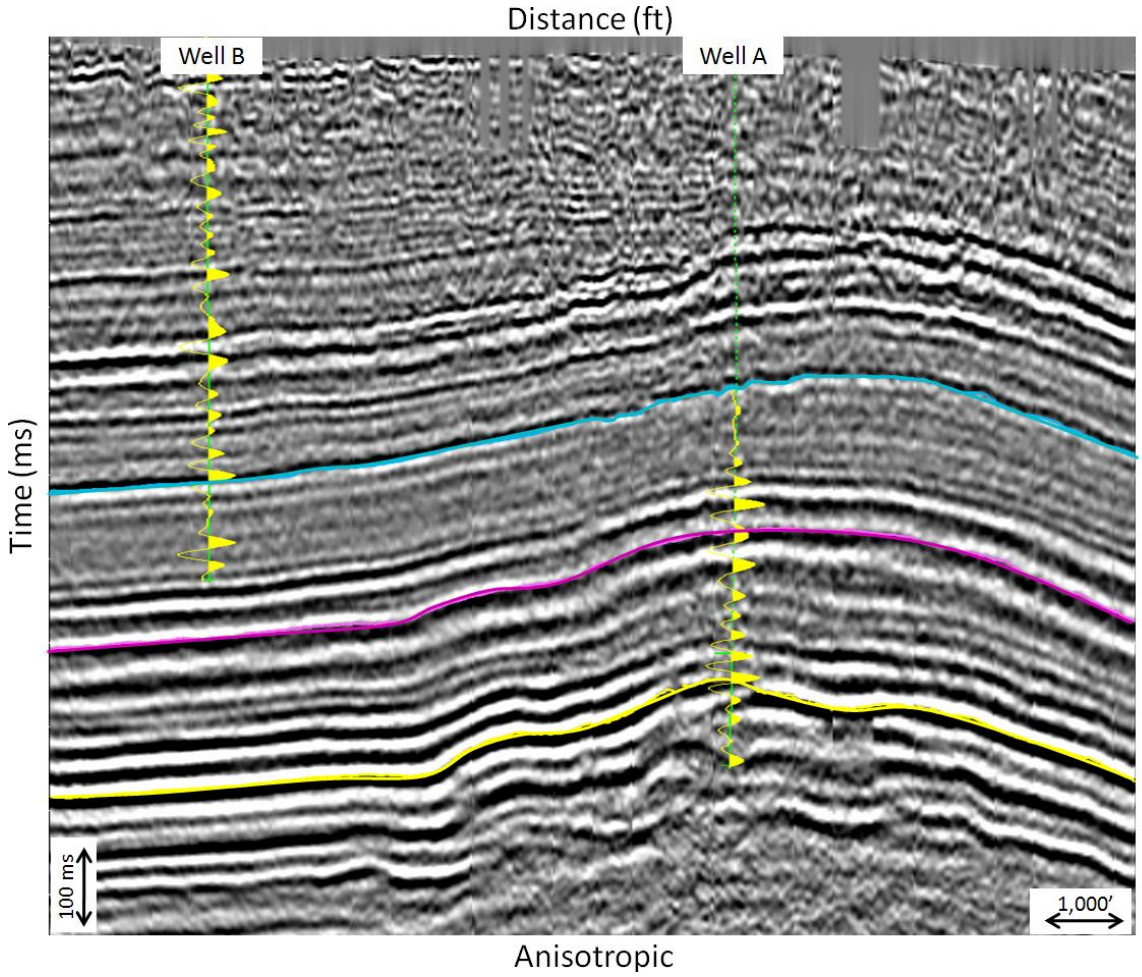

Figure 33: Wells A and B's seismic synthetics overlaid on the anisotropic seismic section. Notice the increased seismic continuity in the anisotropic image near Well A on the anisotropic image compared the isotropic volume shown in Figure 32. No substantial difference is observed in the region of Well B.

7.0 Data Evaluation

In the Big Horn Basin the sharpness of the seismic image to better define large faults locations, the ability to infer smaller faults and use of reliable seismic derived attributes are necessary to properly represent the subsurface. Any possible improvements in these interpretation efforts are critical for more aggressive infill drilling near faults, optimizing horizontal wells, and the determination of matrix versus fractured dominated regions to aid in the design of waterflood and enhanced oil recovery (EOR) programs.

7.1 Fault Clarity

The clarity of faults is very critical for yielding a high resolution interpretation capable of horizontal well planning and field development.

Some thin reservoirs in the Big Horn Basin are not economic with vertical wells but are a prime candidate for horizontal well development. Two of the largest risks in drilling these wells are the thickness of the reservoir and the presence of faults which can cause the well to go out of zone. Acquisition of 3D seismic reduces the risk of encountering an unknown fault while drilling horizontally. Seismic in the Big Horn Basin has been successful in reducing this risk with traditional isotropic migration usually performed in the basin. By utilizing anisotropic migration instead of isotropic migration, this risk is shown to be even further reduced, increasing the value of the seismic acquired. The anisotropic volume, shown in Figure 34 and 35, illustrates the increase in the sharpness of

the fault over the isotropic volume. These figures also show increased data continuity in the regions surrounding the fault. This increased continuity and clarity of faults helps determine the remaining potential for infill drilling next to faults which in some areas has been avoided due to the fault uncertainties.

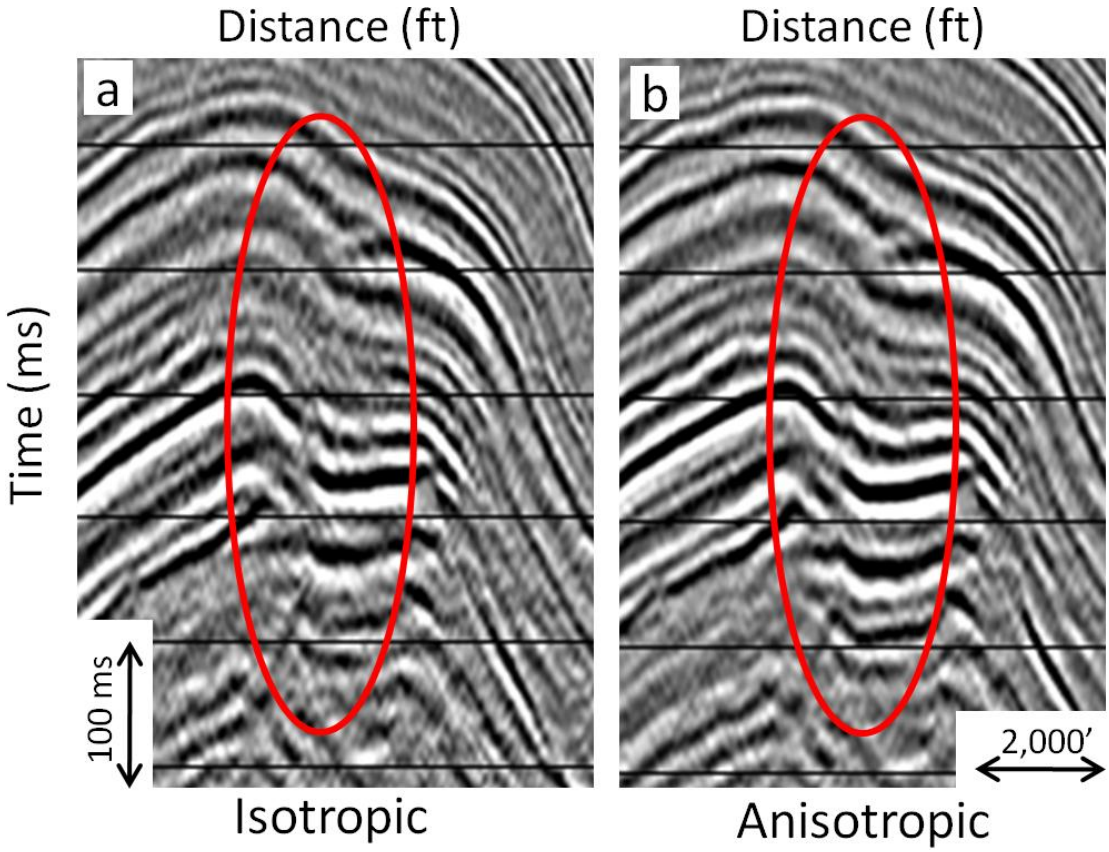

Figure 34: Fault clarity, circled in red, is much clearer on the anisotropic (b) than the isotropic (a) volume.

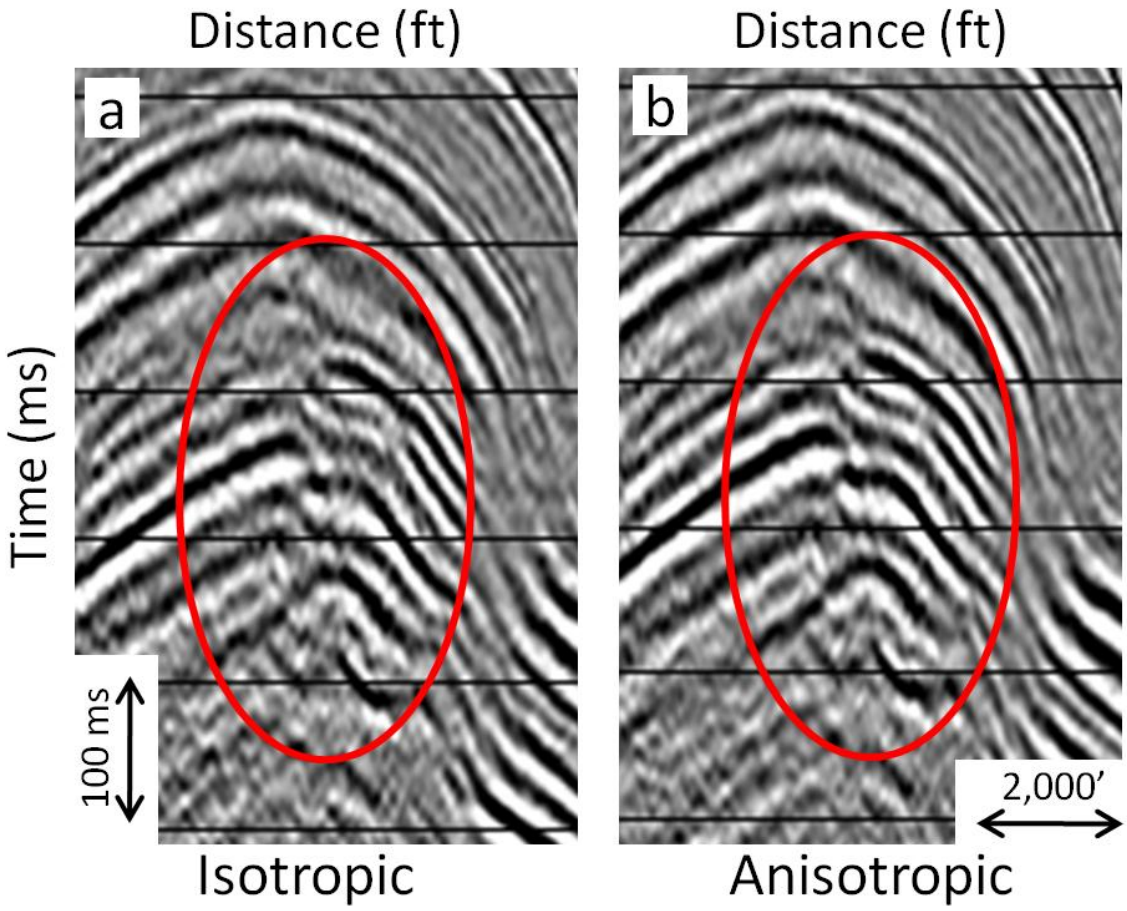

Figure 35: Fault clarity, circled in red, is much clearer on the anisotropic (b) than the isotropic (a) volume.

In areas with two faults in close proximity (within 1,000') the imaging of the seismic is greatly improved on the anisotropic seismic volume (Figure 36). On the isotropic volume, the region between the faults, circled in red on Figure 36, is very unclear and creates a high level of uncertainty in defining the size of the compartment and fault extent to the left of the compartment. The anisotropic volume, however, clearly defines the main fault to the left of the compartment as well as confirms the presence of the reservoir within the fault block with the clear white-black-white reflection series (Figure 36). This improvement is important both for the structural understanding of the reservoir as well as for the evaluation of potential drilling locations to drain the undrilled compartment.

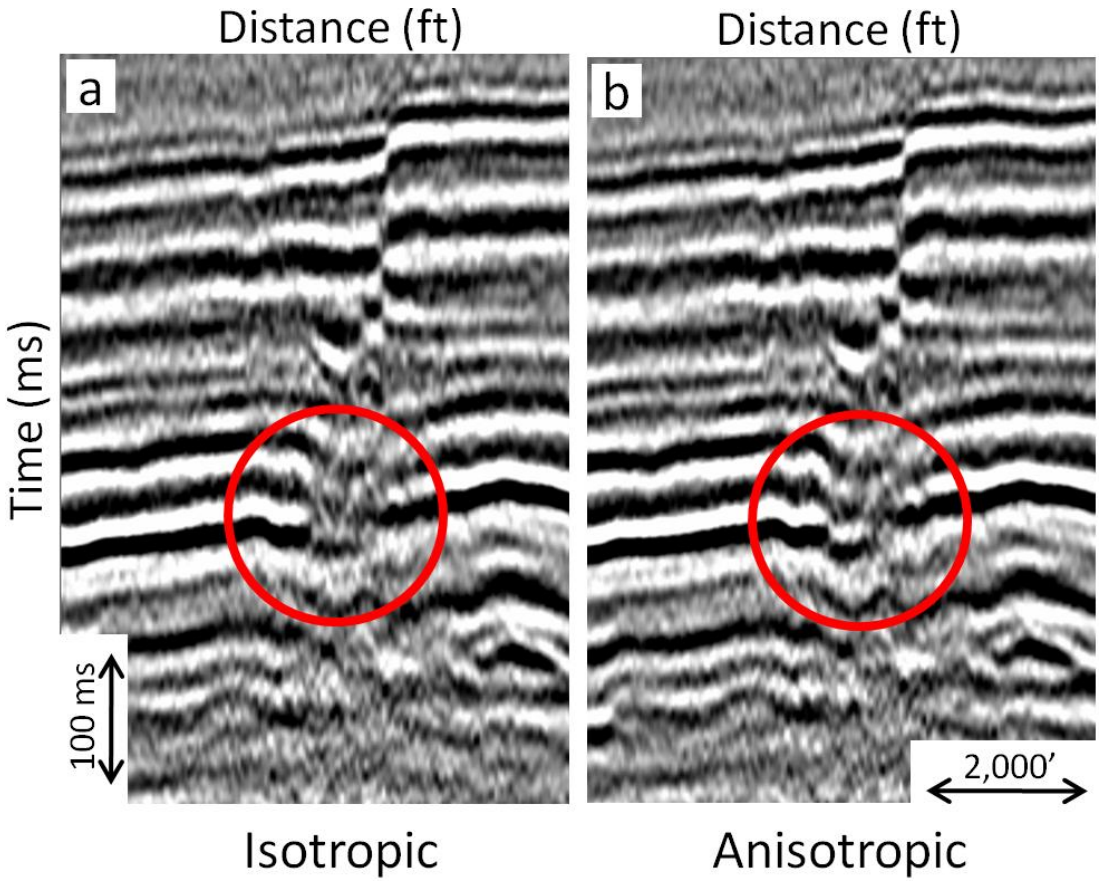

Figure 36: The data continuity within the fallen fault block, circled in red, is much clearer on the anisotropic volume (b) than the isotropic volume (a). The clarity of the deep reflector below the region circled are also much improved on the anisotropic image (b).

7.2 Data Continuity

Data continuity and the signal-to-noise ratio are very important in the study field for mapping and understanding the geologic horizons. Improved data continuity in unfaulted regions increases the effectiveness of the semblance calculation for fault detection of near sub-seismic faulting (Figure 46 and 44). Figure 37 and Figure 38 show a very clear improvement in the data quality, horizon continuity, and the signal-to-noise ratio in the anisotropic volume compared to the isotropic volume. Figure 37 shows a seismic cross section in which the zero amplitude crossing is very choppy and is poorly defined on the

isotropic volume compared to anisotropic volume. The seismic amplitude of the strong reflectors in this region, circled in red on Figure 37, are observed to dim on the isotropic volume, while maintaining amplitude consistency with the rest of the section on the anisotropic volume.

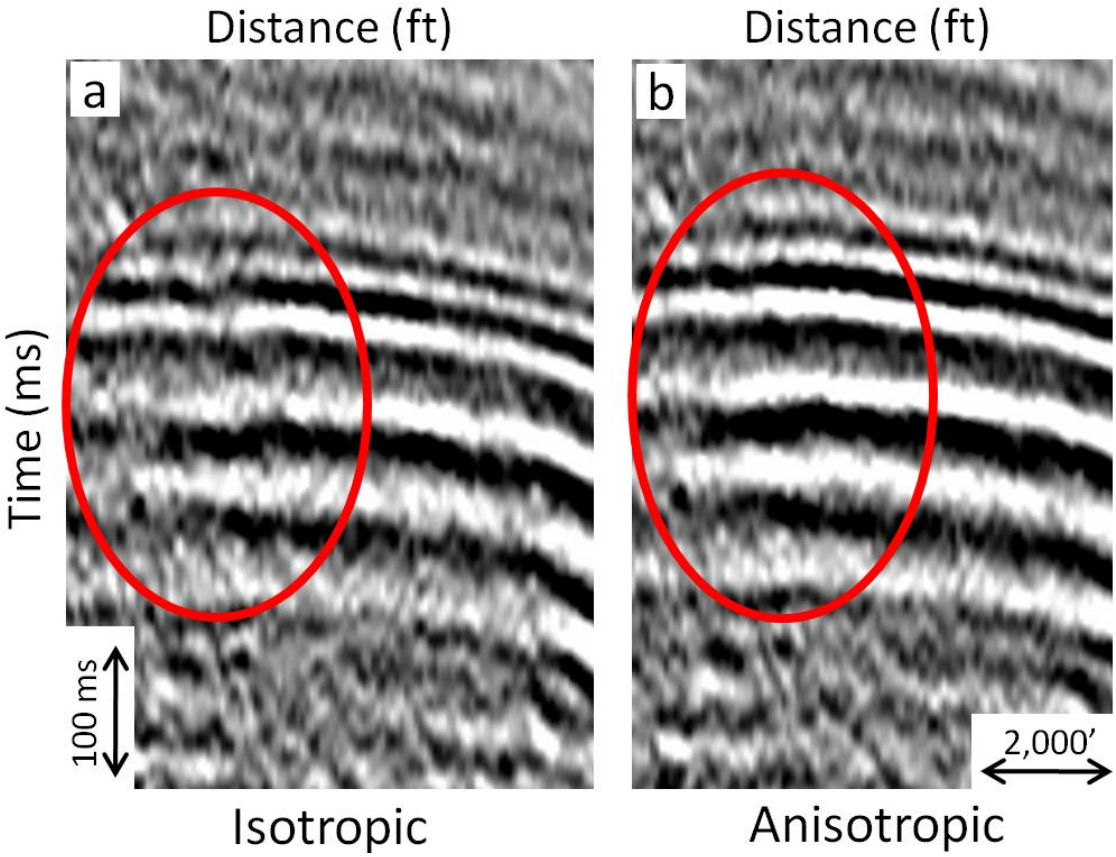

Figure 37: The anisotropic seismic section (b) has much better data continuity and clarity in the region circled in red than the isotropic seismic section (a).

Figure 38 shows a similar observation in another region of the field on a time slice with a strong reflector properly imaged on the anisotropic volume dimming to near background amplitude magnitude on the isotropic volume.

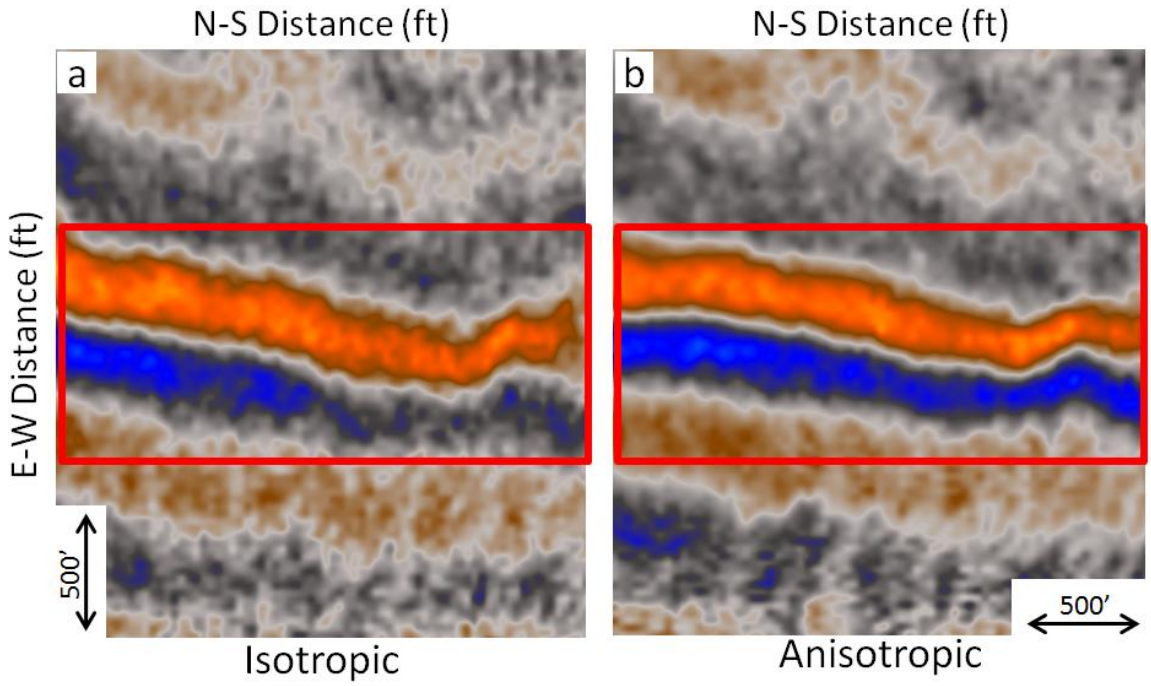

Figure 38: A time slice though the isotropic (a) and anisotropic (b) volumes highlights the improved amplitude continuity and signal-to-noise ratio of the middle key horizon (#2), outlined by the red box. A clearer and more defined zero amplitude crossing between the reflections is observed on the anisotropic data (b) compared to the isotropic data (a).

7.3 Seismic Resolution

As discussed in previous sections, a large percentage of the remaining undrilled potential in the Big Horn Basin is contained within thin target zones. Better focusing of seismic energy on the anisotropic volume should result in improved reflector resolution and clarity of thin bed events, which is essential for optimizing future field development.

The majority of the increased vertical and horizontal clarity and resolution on the anisotropic volume is believed to be due to the better focusing of the energy, with the additional benefit of a slight increase in bandwidth on the anisotropic volume (Figure 39). At -10dbs, the anisotropic migration improves the upper limit of the frequency bandwidth from 77 to 84 HZ. Assuming a velocity of 14,000 ft/s, this expanded frequency band on the high end improves the minimum wavelength of the seismic data from 182 to 166 feet.

This is almost a 10% improvement in the minimum wavelength of the data by performing anisotropic processing compared to isotropic. This improvement in the minimum wavelength could be beneficial in the evaluation of some of the thinner reservoirs in the basin. Although not performed, it is hypothesized that the increased bandwidth and increased signal-to-noise will improve the results of a seismic inversion for reservoir characterization and identification of thin beds.

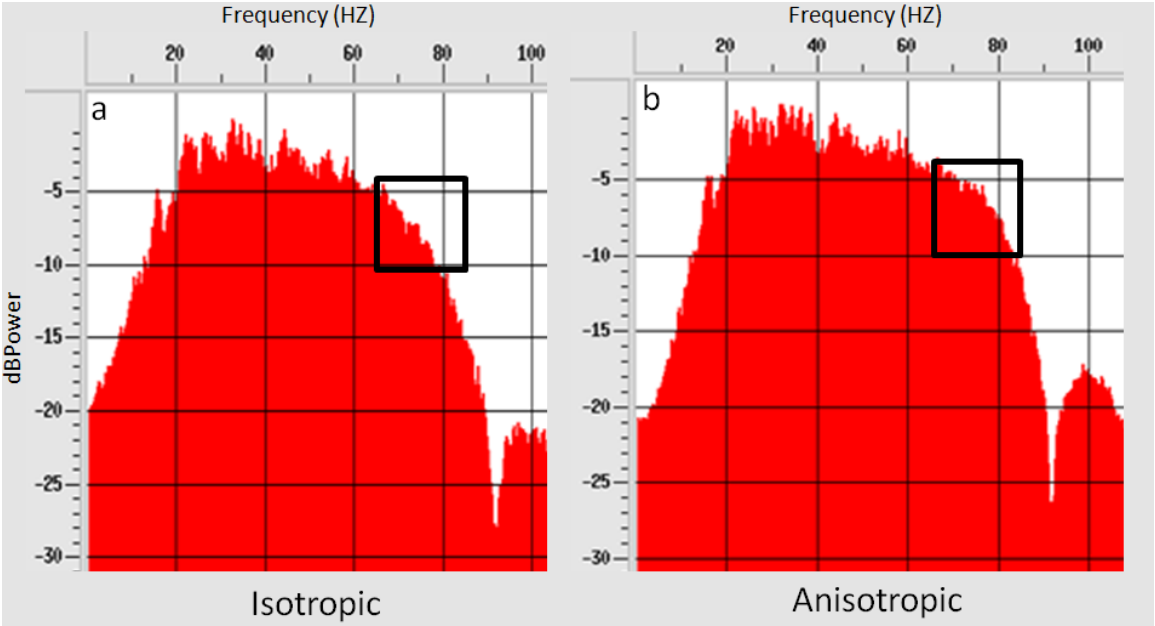

Figure 39: Anisotropic migration results (b) in a higher frequency dataset than the isotropic migration (a). The region within the black box shown, 75 to 80HZ, highlights the largest difference between the two spectrums.

This increase in vertical resolution resulting from the improved focusing of the seismic energy is observed on the anisotropic volume at the crest of the structure (Figure 40). In Figure 40 the individual thin bed events wash together on the isotropic volume which could lead to the incorrect interpretation of the zones as being partially eroded or having higher fracture density than other areas. The increased uncertainty of the thin zones in the isotropic volume equate to increased risk for a horizontal well in one of these thin reservoirs. The anisotropic volume, however, clearly defines the thin reflections allowing

for a higher confidence interpretation of the section (Figure 40). It is also observed in this seismic cross section that the amplitude of the thin bed reflectors maintains the character and relative magnitude of the same reflectors off the crest of the structure on the anisotropic volume.

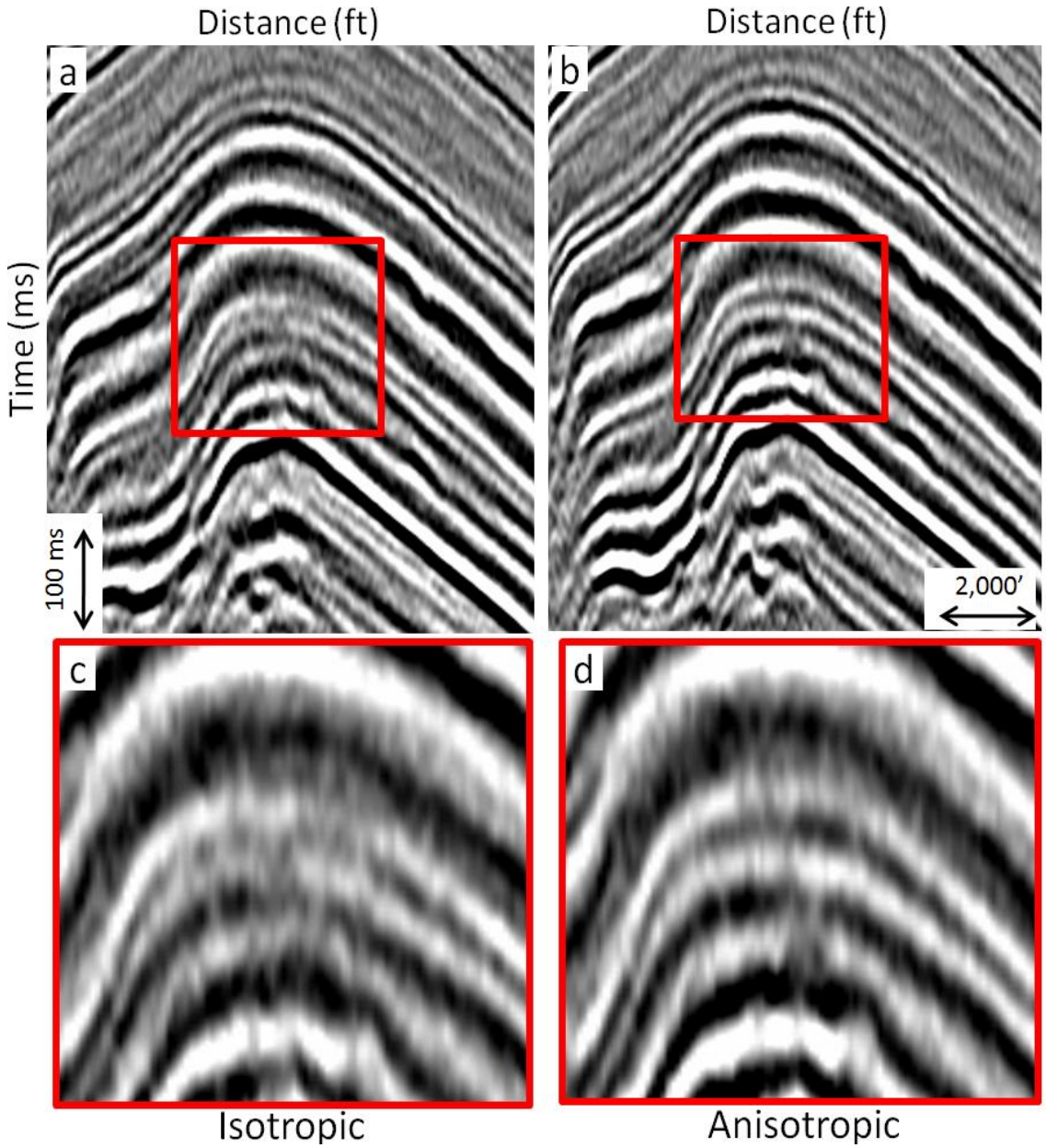

Figure 40: The seismic cross section of the isotropic (a) and anisotropic (b) data highlights the increased continuity on crest of structure within the red box. Zooming in on the region outlined by the red box shows the reflectors blending together without definition on the isotropic volume (c) compared with the clearly defined reflectors shown on the anisotropic migration (d).

7.4 Amplitude Extraction

Seismic derived attributes are a critical portion of seismic interpretation in reservoir characterization efforts. Theoretically, by better stacking the traces anisotropic processing should provide more reliable attributes. In the Big Horn Basin amplitude extractions must be performed around a horizon instead of evaluating time slices due to steep geologic dips present in the area. Root mean squared (RMS) amplitudes were extracted along the three key horizons with a centered window size of 10 samples or 40 ms (Figure 41-43). The RMS amplitude extraction along the shallow surface highlights an acquisition artifact on the left of both of the volumes. The anisotropic volume provides a slight improvement in amplitude strength and consistency, but overall the anisotropic volume extraction is very similar to the isotropic volume extraction (Figure 41).

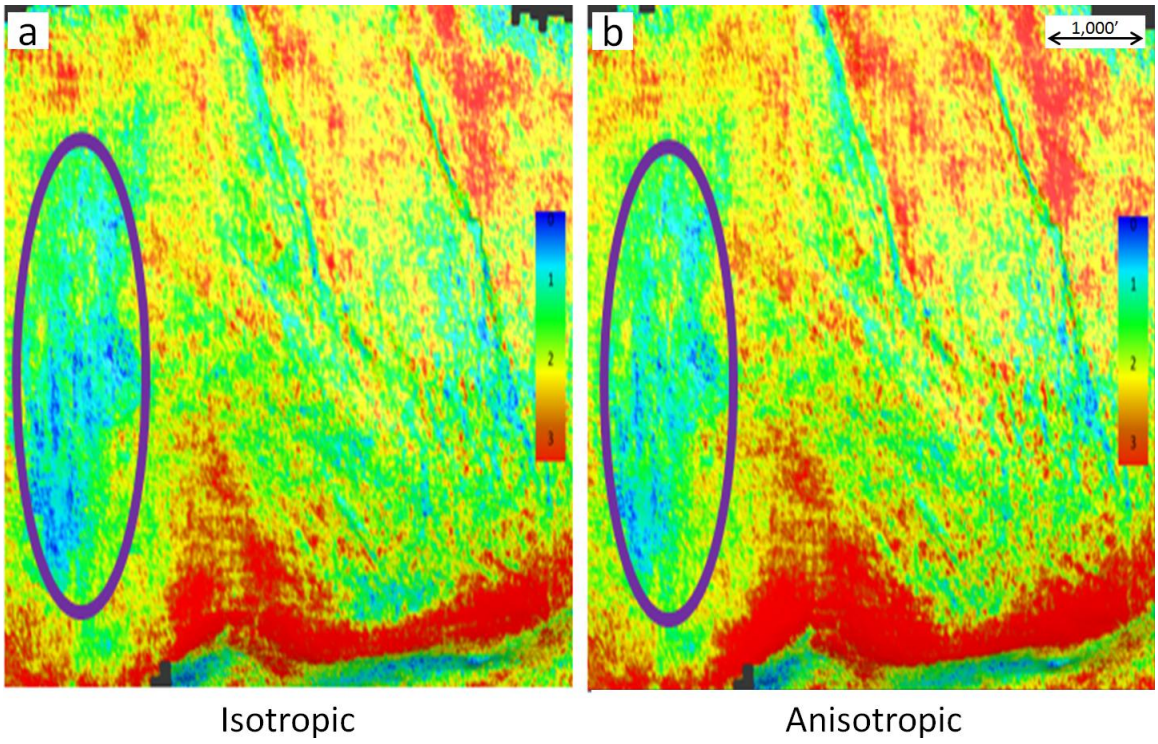

Figure 41: Map view of a windowed RMS amplitude extraction centered on the shallow horizon (#1). The anisotropic volume (b) shows a slightly stronger and more consistent amplitude

response than the amplitude extraction from the isotropic volume (b) but is very similar. The region circled in purple, which has anomalously low RMS amplitude, is an acquisition artifact.

The extracted RMS amplitude of the mid-depth horizon (#2) also shows an improvement in amplitude strength and consistency on the anisotropic versus isotropic volume. The relative improvement of the mid-depth horizon (#2) is greater than the improvement observed on the shallow horizon (#1), especially in the lower region of the Figure 42, corresponding to the crest of the structure. There is also a region in the upper portion of Figure 42, circled in purple, which is anomalously high; this is hypothesized to be due to a large karst. This interpretation is supported by the presence of a fault above and possibly within the suspected karst which could have supplied the water required for dissolution. The bright amplitude response of the karst and the washed out amplitudes below the mid-depth horizon amplitude anomaly is shown in cross section in Figure 43.

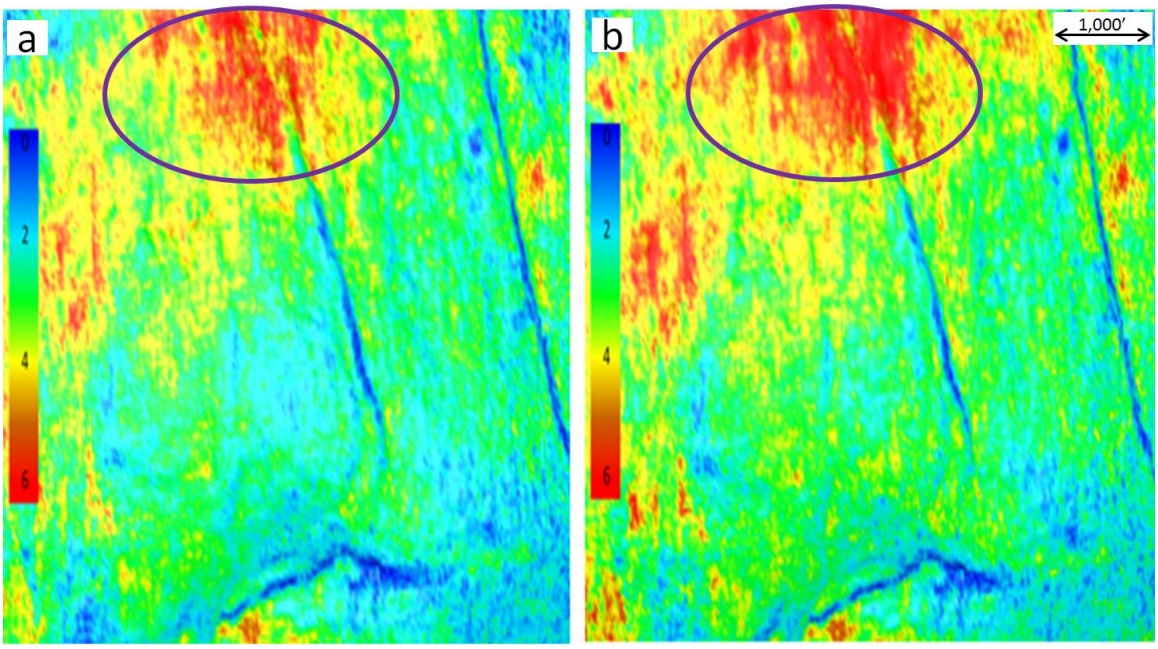

Figure 42: Map view of a windowed RMS amplitude extraction of the mid-depth horizon (#2). The anisotropic volume (b) shows a stronger and more consistent amplitude response than the amplitude extraction from the isotropic volume (b). The bright amplitude anomaly circled in purple is due to a karst within the mid-depth horizon (#2).

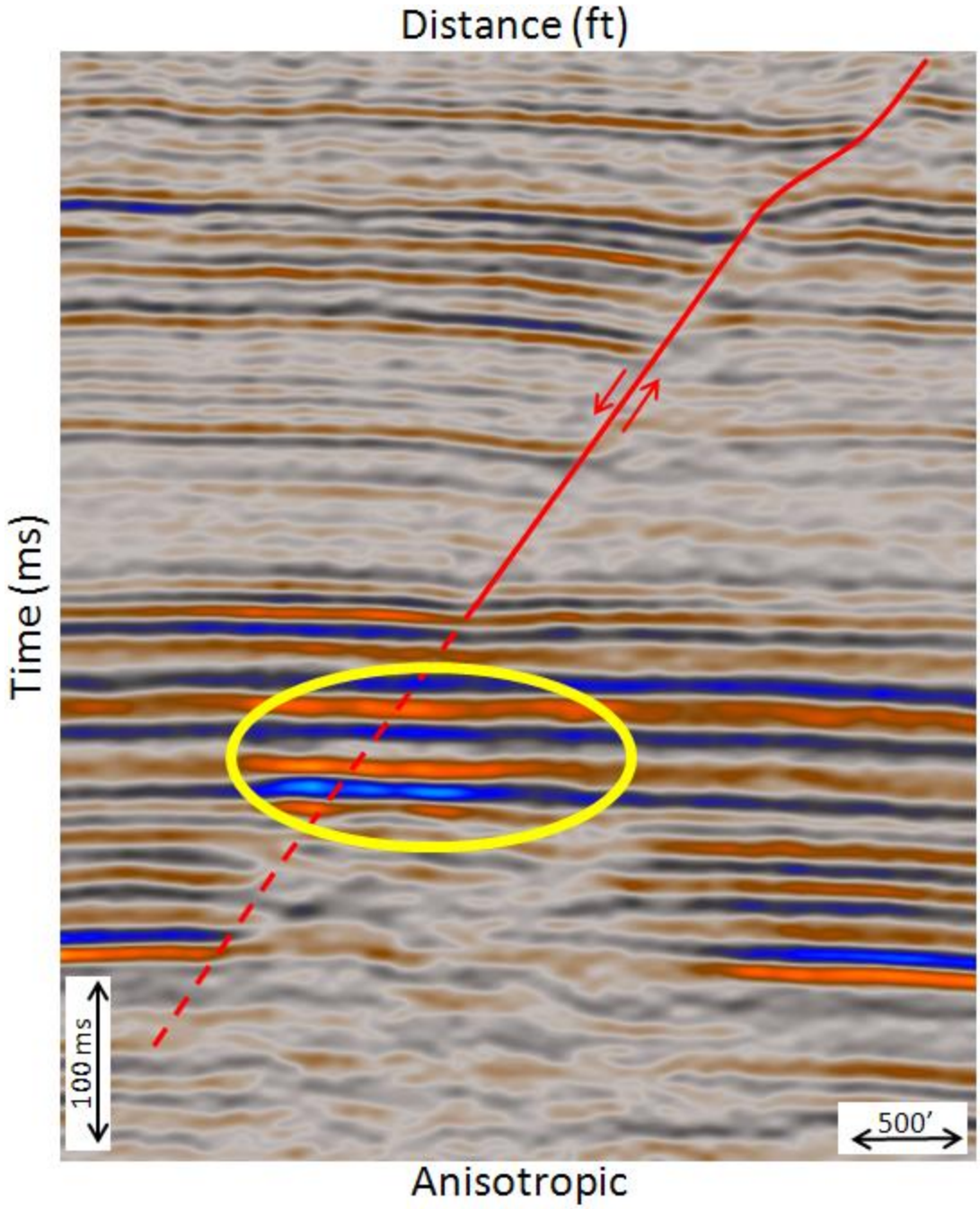

Figure 43: A seismic line from the anisotropic volume through the high amplitude anomaly (Figure 42) in the mid-depth horizon (#2), circled in yellow. The region underneath the amplitude anomaly shows very washed out amplitudes which affect the amplitude extraction of the deep horizon (#3), shown in Figure 44.

The RMS amplitude extraction of the deep horizon (#3) shows a significant improvement from the isotropic to anisotropic volume (Figure 44). This increasing improvement of the

amplitude strength and consistency with depth can be explained by anisotropy being an additive effect becoming a cumulatively larger correction with depth.

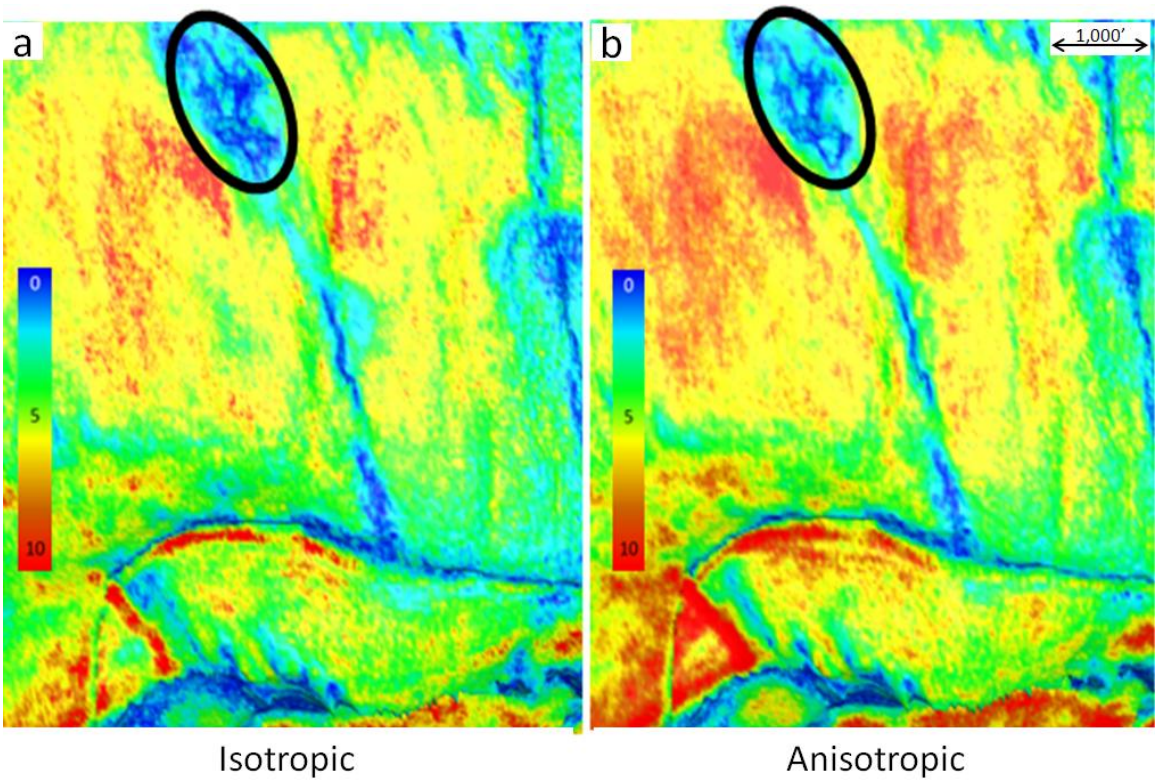

Figure 44: Map view of an RMS amplitude extraction of the deep horizon (#3). The anisotropic volume (b) shows a significantly stronger and more consistent amplitude response than the amplitude extraction from the isotropic volume (b). The amplitude anomaly, circled in black, is due to the amplitude attenuation at the level of the mid-depth horizon (#2) and is not attributed to a change at the deep horizon (#3) level.

To further evaluate the amplitude improvement at the deep horizon level an instantaneous amplitude was extracted from the isotropic and anisotropic volume. The anisotropic volume provides an overall improvement in the strength and consistency of the extracted amplitude. The most substantial, and beneficial, improvement in the amplitude extraction of the anisotropic volume is observed in the middle and right portion of Figure 45 near the crest of the structure.

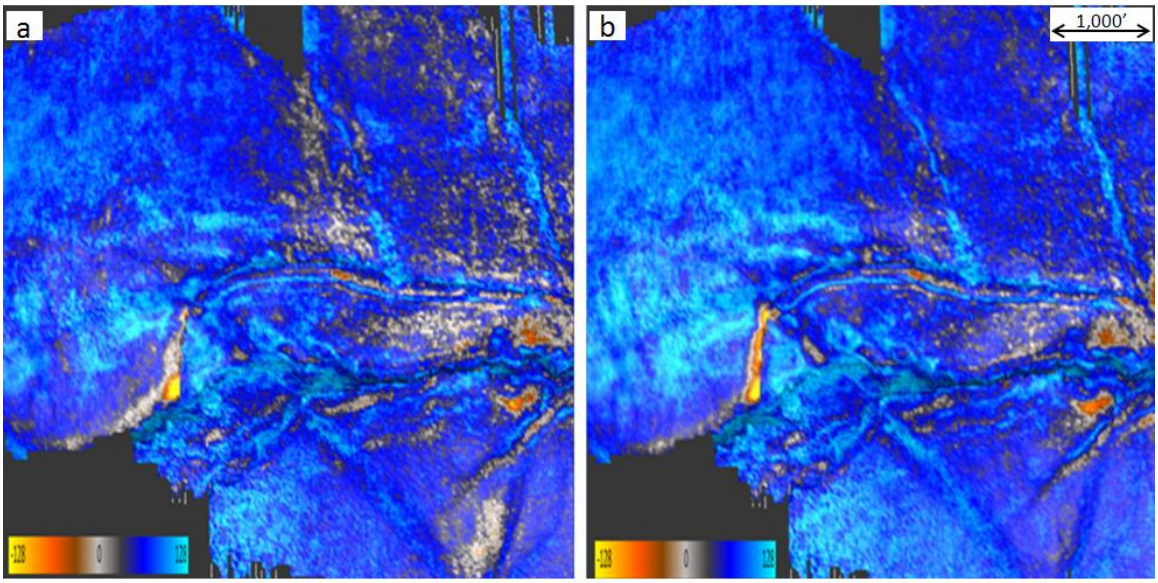

Figure 45: Map view of an instantaneous amplitude extraction of the deep horizon (#3). The anisotropic volume (b) shows a stronger and more consistent amplitude response than the amplitude extraction from the isotropic volume (a).

7.5 Near 'Sub-Seismic' Fault Interpretation

A substantial amount of the remaining potential in the mature oil fields of the Big Horn Basin is in horizontally drilling of thin zones, waterflooding, and EOR techniques. To optimize EOR efforts it is crucial to understand the reservoir faulting and fracturing as best as possible. To maximize the success rate of drilling thin reservoirs with non-

consistent thickness anisotropic migration is essential. The increased amplitude reliability of thin reservoirs, as seen in Figure 40, can improve the correlation between seismic amplitude and reservoir thickness. The horizontal drilling required to make these zones economic is very susceptible to small faults in the reservoir. The larger faults in the region, which were already known from well data, are not substantially different in the isotropic and anisotropic volumes other than clarity (Figure 34, 35, and 37). The increased reflector continuity in the anisotropic data, however, helps to identify the smaller discontinuities present in the data due to small faults. A horizontal well drilled prior to the acquisition of the seismic data encountered two unexpected small faults resulting in the well being out of zone for a large percentage of the horizontal portion of the well. Both of the encountered faults are considered to be near sub-seismic resolution but capable of being identified using seismic attributes, such as semblance. Using semblance to interpret small faults often requires some art in distinguishing noise from discontinuities which have geologic geometries. The anisotropic volume reducing the amount of noise and increasing the continuity of the discontinuities over the isotropic volume may be very beneficial (Figure 46 and 47). The benefits could include increased avoidance of faults, optimized well planning, and increased horizon well performance resulting from a larger portion of the well staying within the targeted reservoir zone.

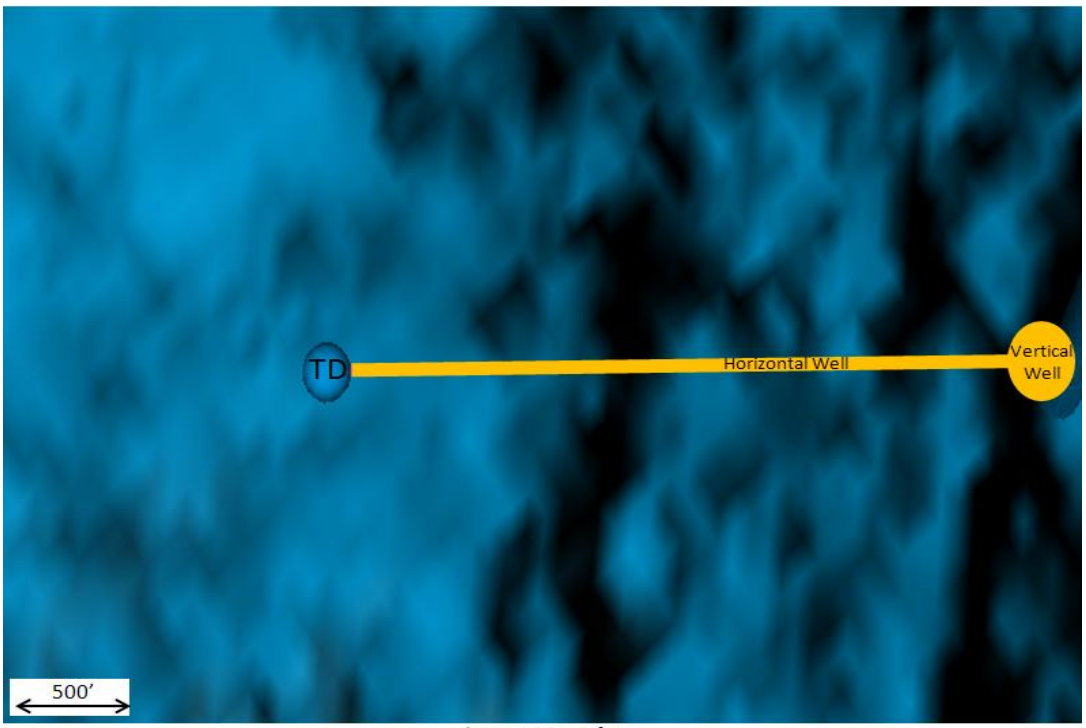

Isotropic

Figure 46: Map view of the semblance attribute calculated from the isotropic volume projected on the middle key surface (#2). Shows possibility of faulting across the well path, however, the faults are not very convincing since they are barely above the background noise.

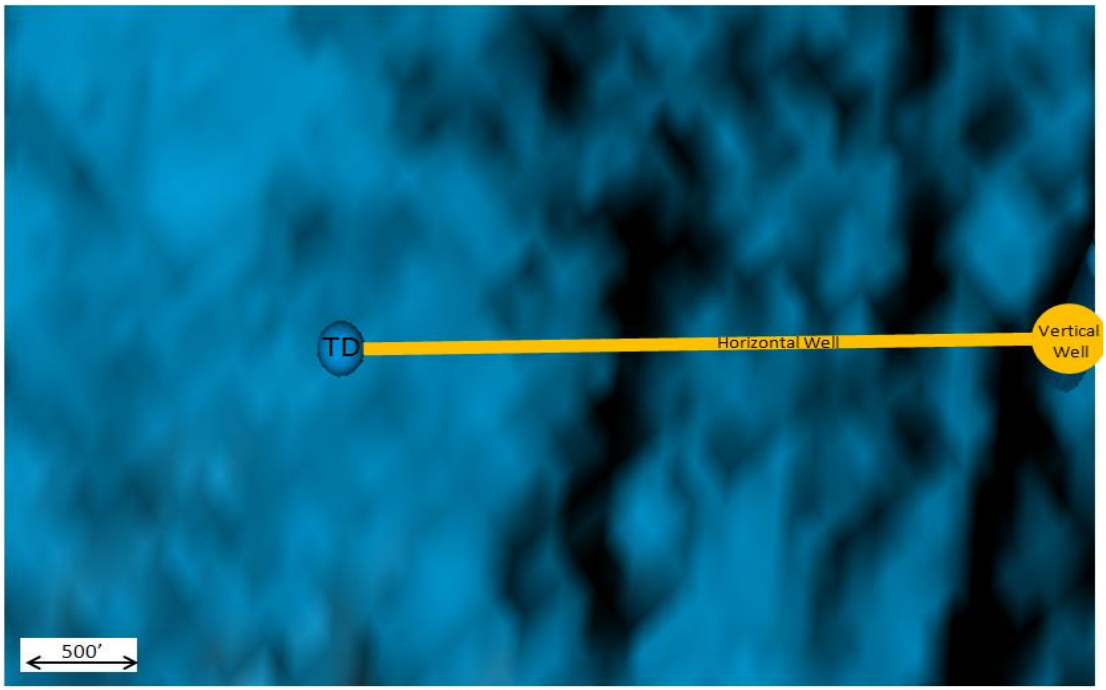

Anisotropic

Figure 47: A map view of the semblance attribute calculated from the anisotropic volume projected onto the middle key surface (#2) shows the possibility of faulting across the well path. The suggested faults still require some interpretation but now become clearer than the isotropic semblance extraction (Figure 46) and follow the same trend as the main fault increasing the confidence in the interpretation.

It is important to validate the interpretation of the semblance volume extraction along the middle key surface (#2) of the anisotropic migration to confirm that the apparent increased continuity on the anisotropic volume is real. The semblance calculation using the anisotropic volume, Figure 47, was used to interpret the previously known large main fault and two smaller near sub-seismic faults that could be drilling hazards. A very good correlation between the two previously unmapped near sub-seismic interpreted faults and the two locations in which the horizontal well encountered faults is shown in Figure 48. The improved fault signature to background noise by using the semblance from the anisotropic volume, Figure 47, instead of from the isotropic volume, Figure 46, provides an increased confidence in fault prediction for future well development.

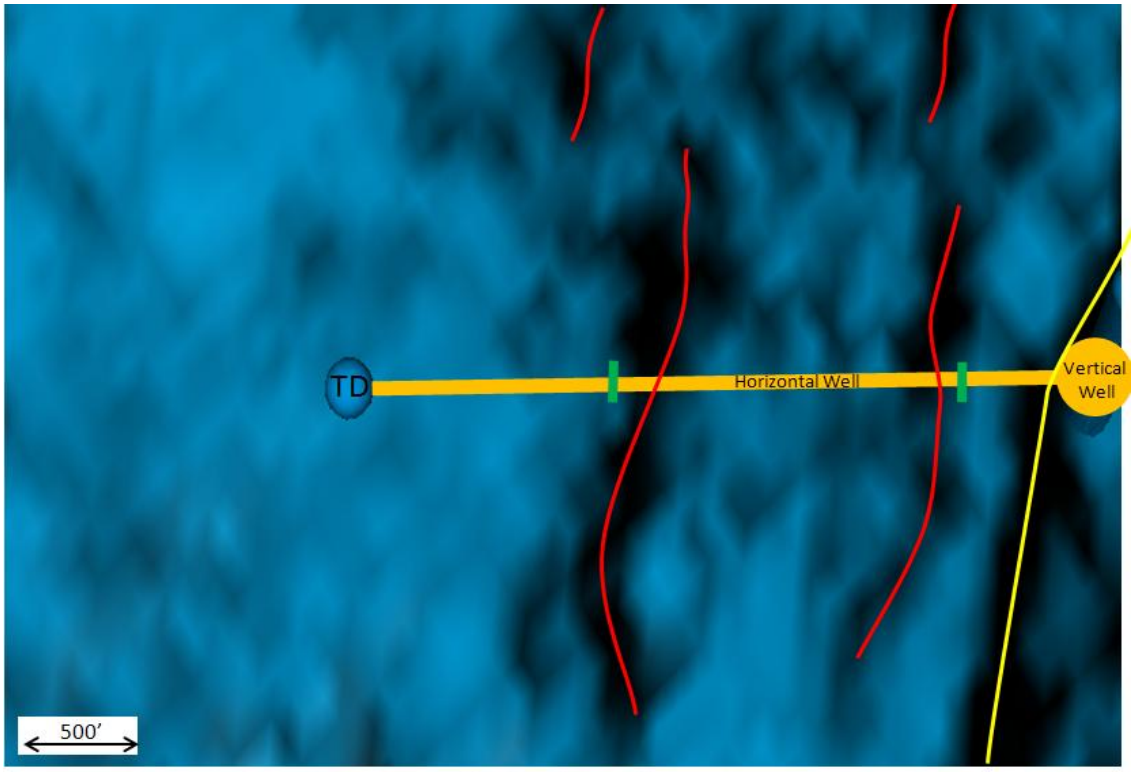

Anisotropic

Figure 48: The semblance calculated from the anisotropic volume, shown in Figure 47, with the main fault, drawn in yellow, and suspected faults based upon the semblance, drawn in red. The green markers on the horizontal portion of the well show the two points in which the well encountered faults causing the well to become out of the target zone. The two suspected faults from the semblance correlate very well with the encountered faults.

7.6 Anisotropic Velocity Attributes

The anisotropic velocity analysis provides a suite of anisotropic attributes such as V_{fast}, V_{slow}, and V_{fast}-V_{slow}. Azimuthal velocity variations are often utilized for fracture characterization. Many interpretations over-simplify the complex relationship between azimuthal velocities and subsurface fractures. The classical assumption is that fractures are represented by a large V_{fast} -V_{slow} value with vertical fractures perpendicular to the V_{fast} azimuth (Figure 49). Although this assumption can be valid, as shown in Figure 50 by Haijun et al., (2001), in many cases it will be very misleading and can result in an incorrect interpretation. In fact, if the rock has conjugate sheer fractures (Figure 51), instead of vertical fractures, heavily fractured regions will have a small V_{fast} -V_{slow} value. A rock with the conjugate sheer fractures can be detected instead by its anomalously low V_{fast} and V_{slow} values.

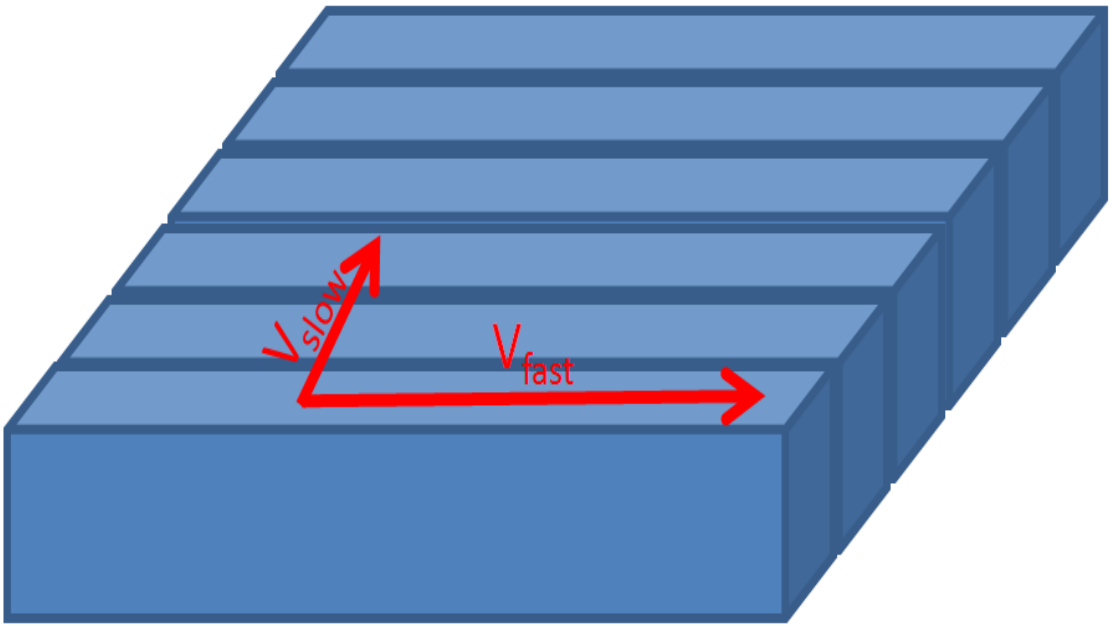

Figure 49: Representation of Vfast and Vslow in the presence of vertical fractures. In this scenario V_{fast} - V_{slow} would be a good indicator of fractures and the azimuth of V_{slow} would suggest the azimuth normal to the fracture direction.

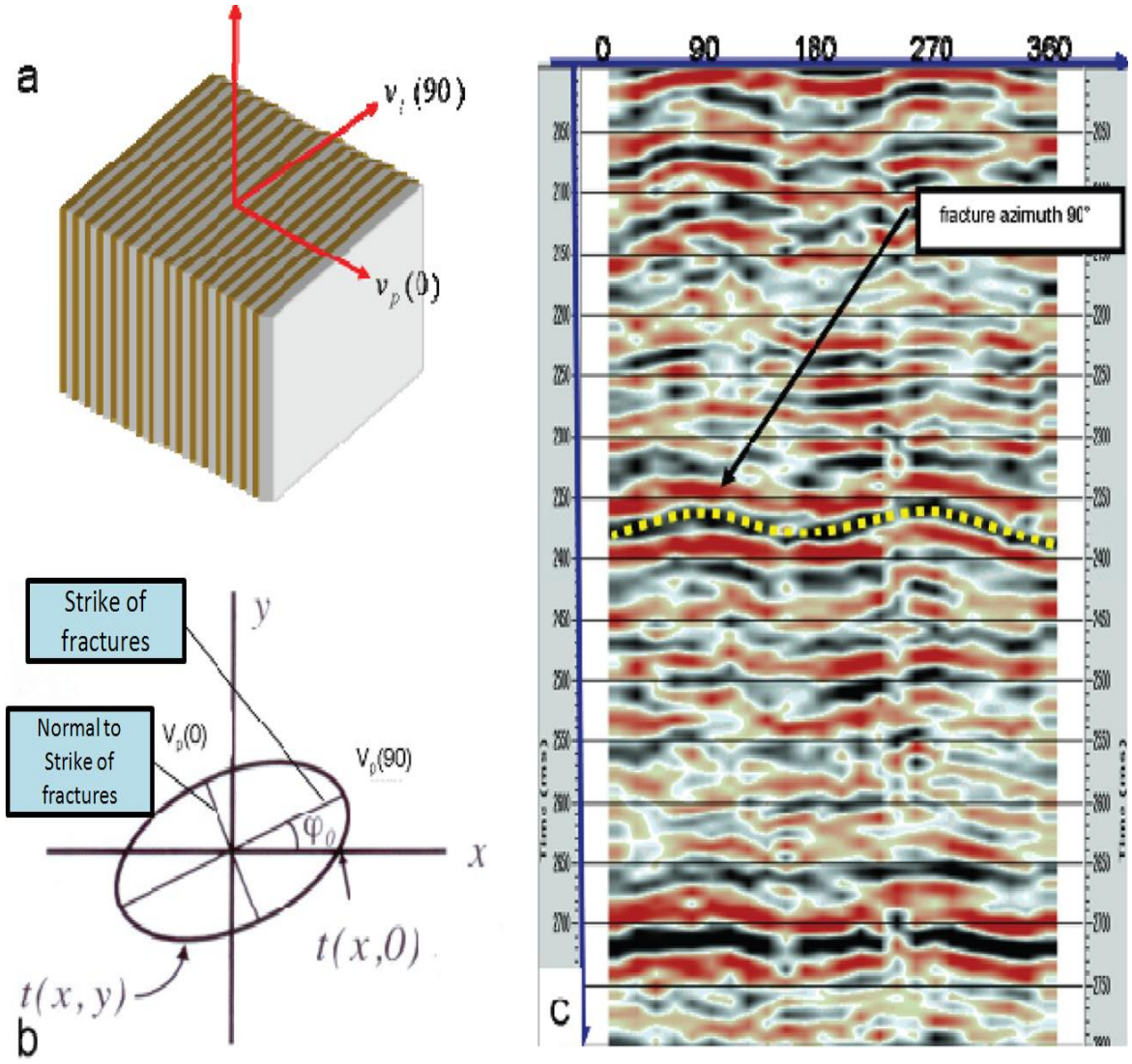

Figure 50: Assuming the presence of vertical fractures (a) the V_{fast} direction is expected to be along the strike of the fractures and V_{slow} in the direction normal to the strike of the fractures (b). The azimuth sorted seismic gather (c) shows the sinusoidal geometry of the reflector with the peak of the sinusoid corresponding to the azimuth of the fractures (Haijun et al., 2011).

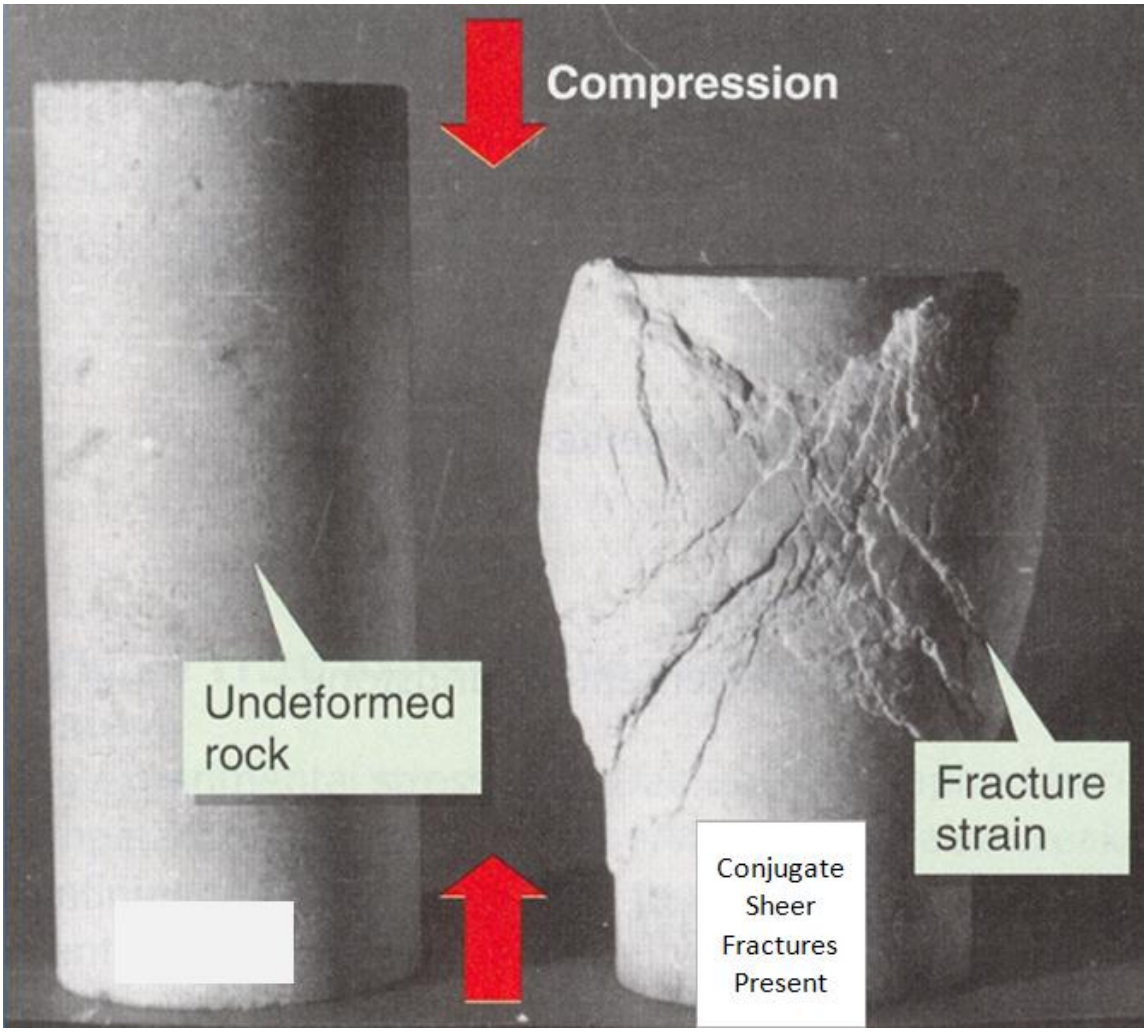

Figure 51: Conjugate sheers fractures resulting from compressional stress in laboratory (Smith and Pun, 2009). These fractures would have a low V_{fast} and V_{slow} values resulting in a low V_{fast} - V_{slow} value.

This ambiguity in the meaning of the anisotropic velocity attributes requires that other information is combined with the attributes to yield a meaningful interpretation of the sub-surface. The additional information which can be used to better understand the anisotropic velocity attributes is very broad including FMI, core fracture analysis, outcrops, geologic history, present day stress region and other seismic attributes. The best interpretation incorporates and is compatible with as many independent sources of information as possible. The faulted region which the horizontal well, discussed in

Section 7.5, was drilled in what is believed to be highly fractured due to the high density of faulting in the region. The anomalously low values of V_{fast} (Figure 52) and V_{slow} (Figure 53) support this interpretation and suggest that the rock is fractured or faulted in multiple azimuths instead of a singular direction. This corresponds well to the expected fracture orientations caused by the formation of the anticline and large faults present in the field near the well with orientations roughly parallel and perpendicular to the well direction.

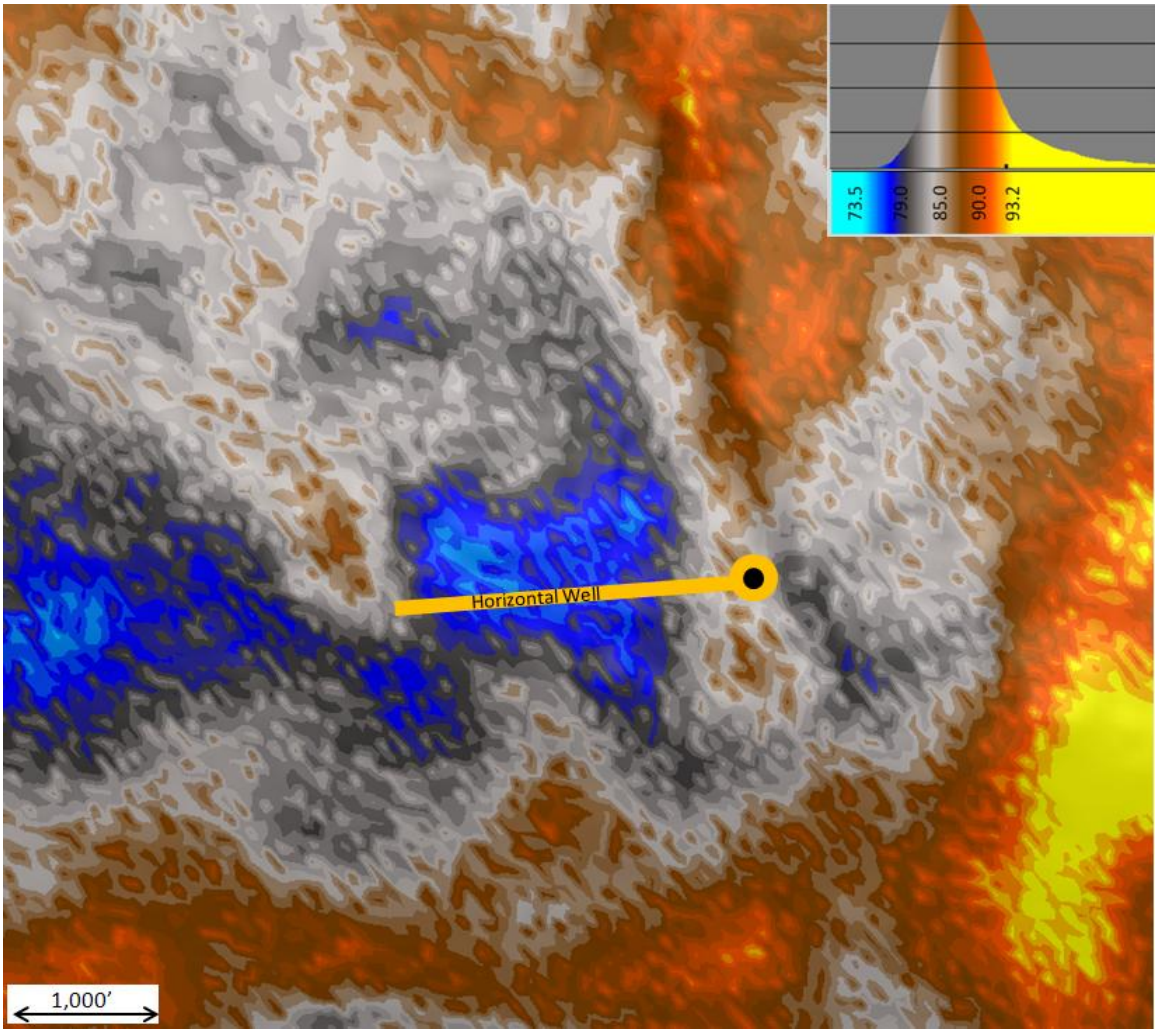

Figure 52: Map view of the anomalously low V_{fast} value over the region of the horizontal which is faulted, shown in Figure 48, helps support the semblance interpretation. The V_{fast} information would not be reliable enough to make this interpretation alone, but does show compatibility with the interpretation which is important.

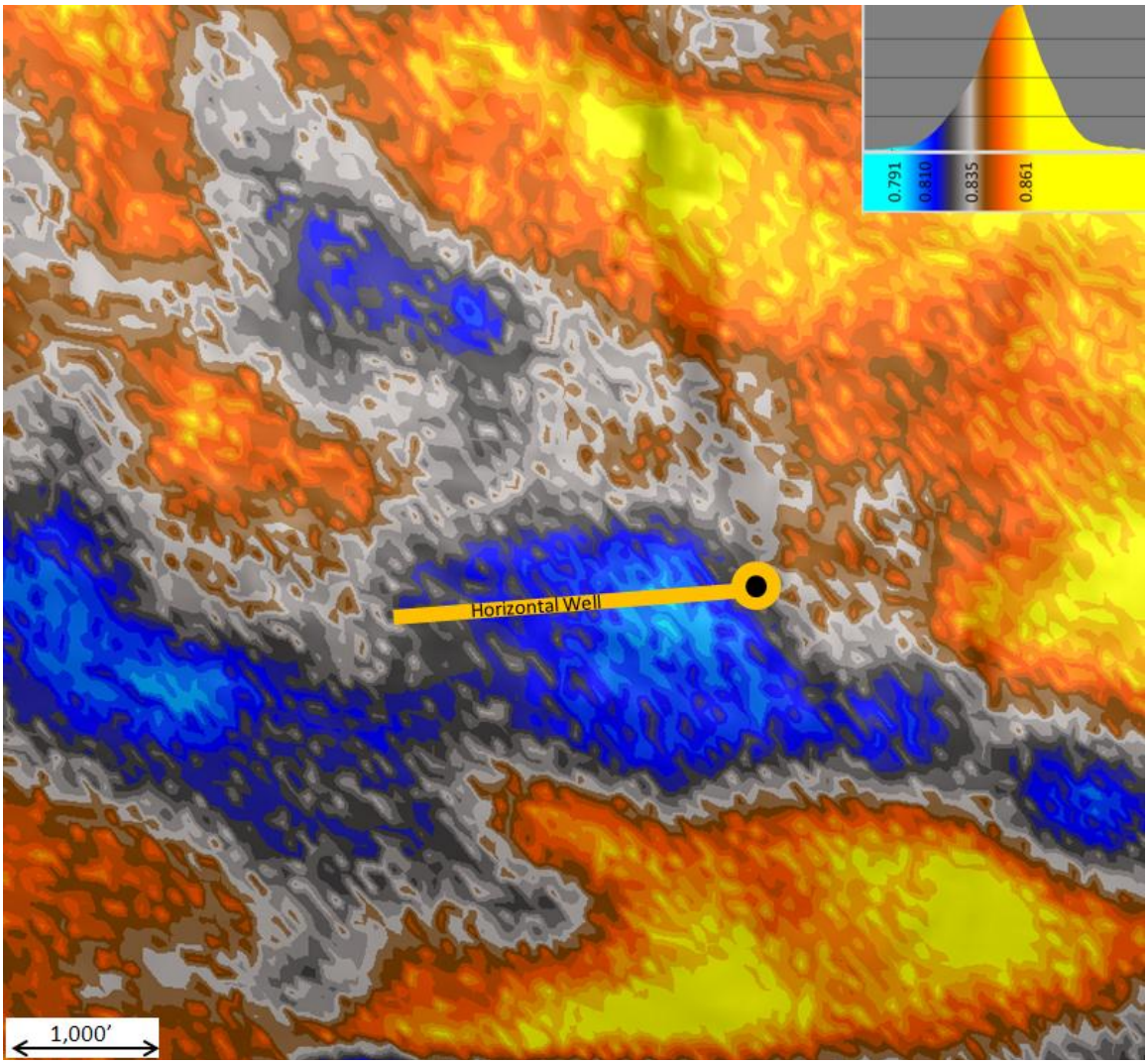

Figure 53: Map view of the anomalously low V_{slow} value also supports the semblance interpretation shown in Figure 48. Since the low V_{slow} value corresponds to the low V_{fast} value in Figure 52 we would not expect a V_{fast} - V_{slow} anomaly in this region.

7.7 Fracture versus Matrix Dominated Analysis

There is a significant amount of remaining potential in fields within the Big Horn Basin which can be captured with waterflood and EOR programs. The success of these programs can be greatly improved with the enhanced identification of faults and determination of matrix versus fracture dominated regions. Having a good understanding

of the major, as well as near sub-seismic, faults is often the largest value seismic can provide for these projects. The improved fault identification from performing anisotropic instead of isotropic processing is discussed in Sections 7.1 and 7.5. It is also very beneficial to have a good understanding of the fracture network present in the reservoir. One popular methodology which has been applied for fracture estimation is geometrical attributes such as curvature (Chopra and Marfurt, 2007). This methodology has been successful in many areas and been demonstrated to correlated to both field outcrops (Lisle, 1994) and production data (Hart et al., 2002). Geometrical attributes can benefit from the synergy of their combination with azimuthal velocity attributes. Geometrical attributes infer faults and fractures based upon the geometry of the geology where azimuthal velocity attributes infer fractures based upon the assumption that the seismic velocity will decrease in at least one azimuth in the presence of fractures. Having two independent methodologies for fracture detection greatly increases the confidence of the interpretation.

As discussed in section 7.6, the anisotropic velocity attributes can sometimes be difficult to interpret. One attribute which is hypothesized by the author to have a more consistent correlation to fractures is the V_{slow} attribute. In the presence of open fractures, whether aligned in one direction or multiple, will result in one or more azimuths being slowed down; thus reducing V_{slow}. One exception to this would be horizontal fractures which may not provide an azimuthal velocity variation. To test this hypothesis for this basin V_{slow} was compared to a seismic section co-rendered with semblance through a known faulted and fractured region (Figure 54). There appears to be a good correlation between

faulted and fractured regions and a low V_{slow} as hypothesized. This relationship can then be used to evaluate which portions of the field may be more fracture or more matrix dominated (Figure 55).

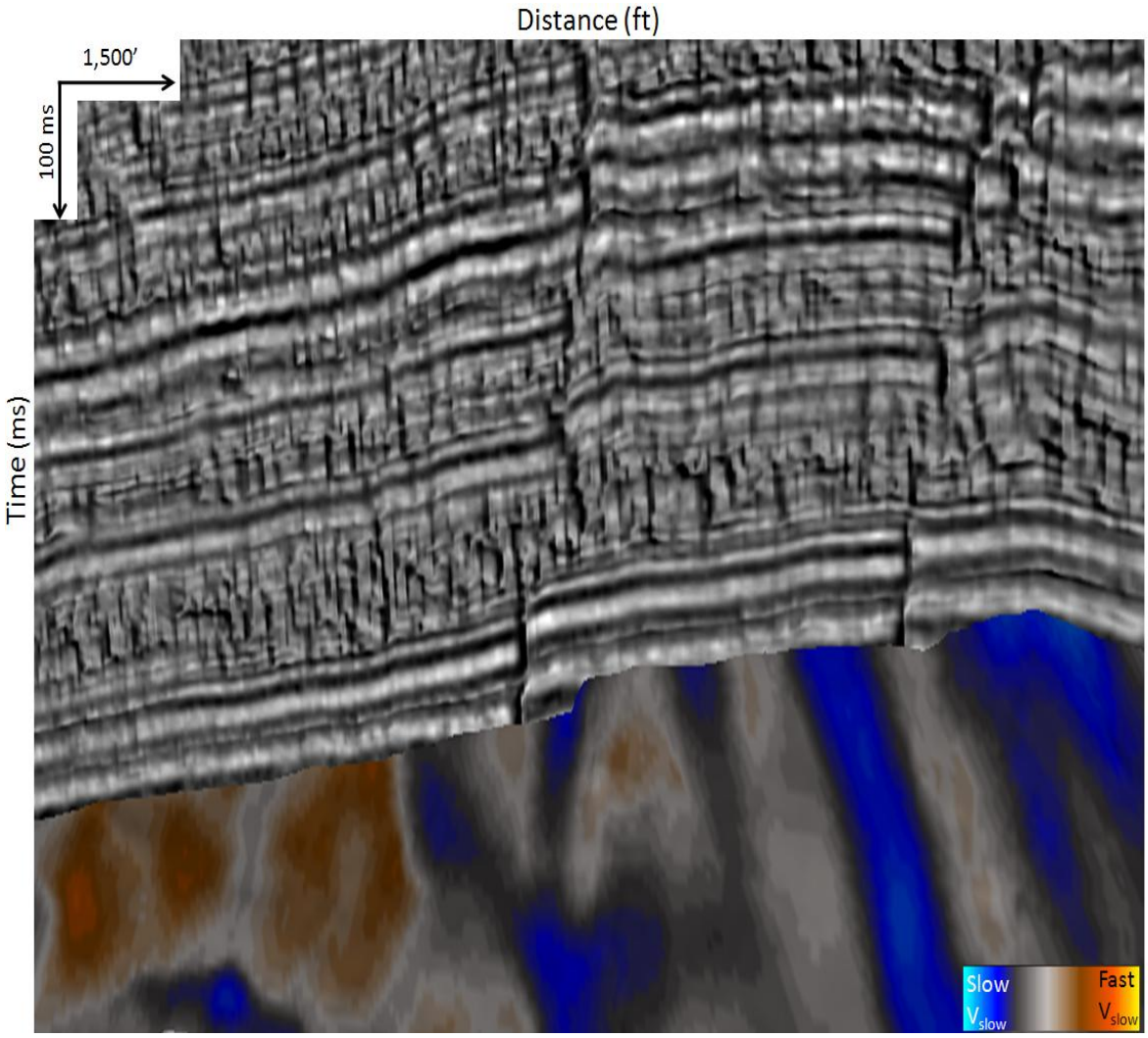

Figure 54: A side view of the V_{slow} attribute overlaid on the mid-depth horizon (#2) and the seismic amplitude co-rendered with semblance in cross section view. There is an apparent inverse relationship between the discontinuities in the seismic and the V_{slow} value. The two clear faults correspond to regions with a low V_{slow} value (blue) where the region on the left which appears to be unfaulted has a higher V_{slow} value (red).

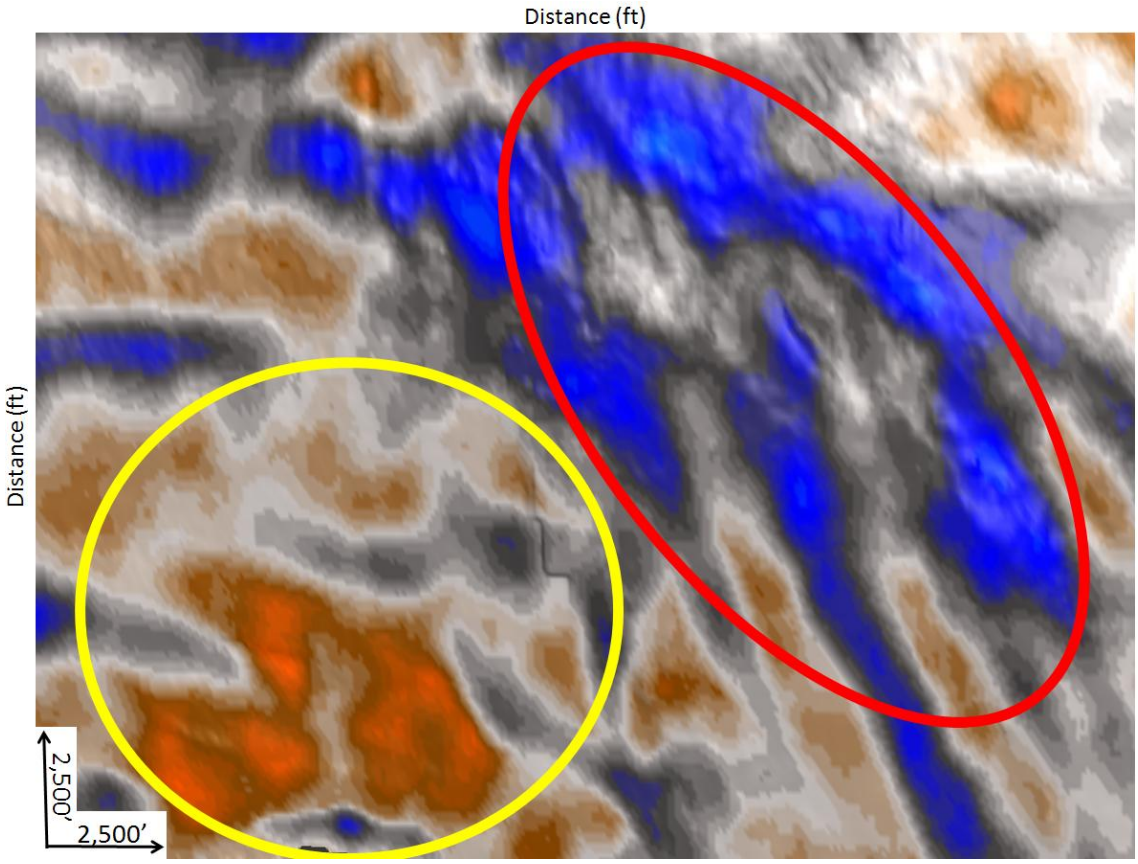

Figure 55: Map view of V_{slow} attribute overlaid on the mid-depth horizon (#2) surface. The region circled in yellow is suspected to be more matrix supported while the region circled in red appears to be more fracture dominated.

Another benefit seismic can provide with the application of seismic inversion is an improved estimation of the rock properties for the evaluation and planning of waterflood and EOR programs. A good inversion result can improve the reservoir model used to model the waterflood and EOR programs. Seismic inversion is most successful when the input gathers used have a good offset range, signal-to-noise (S:N) ratio, and as flat as possible. The anisotropic migration has been shown to provide flatter gathers with a better S:N ratio to longer offsets than the isotropic migration. Although not tested in this study, this should mean the anisotropic volume will lead to improved inversion results and thus better reservoir characterization.

8.0 Conclusions

The value of performing anisotropic processing is determined by evaluating the incremental increase in fault resolution, near sub-seismic fault detection, reflector resolution, and seismic attribute reliability. The better positioning and focusing of the seismic energy near faults on the anisotropic volume may lead to additional infill wells of bypassed pay. The increase in seismic reflector continuity and increased signal-to-noise ratio allows for a more reliable interpretation of near sub-seismic faulting. A better understanding of the near sub-seismic faulting is critical in preventing future horizontal wells from being drilled out of zone decreasing their efficiency and increasing drilling cost. The more reliable attributes which can be extracted from the anisotropic volume results in better reservoir characterization. The better reservoir characterization will aid in both waterflood and EOR programs which are crucial for extending the life of mature fields and improving the ultimate recovery of the resources. The incremental cost and time of performing anisotropic migration compared to seismic acquisition cost, base processing cost, future drill wells, and water flood and EOR programs is extremely minimal. It has been demonstrated that this minimal additional investment is greatly outweighed by its benefits and should be considered in seismic processing projects in the Big Horn Basin where the data was recorded with adequate receiver offsets.

Future Work

This study was limited to the evaluation of isotropic PSTM and anisotropic PSTM and did not consider isotropic PSDM or anisotropic PSDM. Although the incremental

improvement from anisotropic PSTM is very valuable, it is important to recognize that anisotropic PSTM still has issues which can only be solved in the depth domain. The rapid lateral velocity changes and steep dips cannot be accounted for in time processing and can create positioning errors of faults and other geologic features. Time processing also puts limitations on the anisotropic analysis and corrections which can be applied to the data. In time the axis of isotropy must be assumed to be vertical (VTI) and/or horizontal (HTI) instead of the more likely case of being tilted (TTI). With these considerations, the processing flow with greatest value is hypothesized to be an anisotropic PSDM.

References

Alkhalifah, T. and Tsvankin, I., 1995. Velocity analysis for transversely isotropic media: Geophysics, **60**, 1550-1566

Alkhalifah, T., 1997, Velocity analysis using nonhyperbolic moveout in transversely isotropic media: Geophysics, **62**, 1839-1854

Chopra, S and Marfurt, K., 2007, Volumetric curvature-attribute applications for detection of fracture lineaments and their calibration: The Record, Denver Geophysical Society, June, 23-28

Cooley, R., 2009, Structural, lithological, and regional tectonic controls on P-wave azimuthal anisotropy: Casper Arch area, Wyoming: CSU Master's Thesis

Grechka, V., Tsvankin, I., and Cohen, J.K., 1999, Generalized Dix equation and analytic treatment of normal-moveout velocity for anisotropic media: Geophysical Prospecting, **47**, no. 2, 117-148

Gulunay, N., Magesan, M., and Roende, H., 2007, Gather flattening: The Leading Edge, **26**, 1538-1543

Haijun, L., Yun, L., Xiangyu, G., and Desheng, S., 2011, Fracture prediction based on stress analysis and seismic information: A case study: Society of Geophysicist Expanded Abstracts, **30**, no. 1, 1118-1123

Hart, B.S., R. Pearson, R. Pearson, and Rawling, G.C., 2002, 3-D seismic horizon-based approaches to fracture-swarm sweet spot definition in tight-gas reservoirs: The Leading Edge, 21, 28-35.

Hayes, K.H., 1976, A Discussion of the Geology of the Southeastern Canadian Cordillera and its comparison to the Idaho-Wyoming-Utah Fold and Thrust Belt: Rocky Mountain Association of Geologist (RMAG), Symposium on Geology of the Cordilleran Hingeline, 59-82.

Hood, J. and Schoenberg,M., 1989, Estimation of vertical fracturing from measured elastic moduli: Journal of Geophysical Research, **94**, no. 15, 611-618

Kuhnel, T. and Li, X., 2001, Advances in Anisotropy: Selected Theory, Modeling, and Case Studies, Tulsa, OK, 47-74.

Lageson, D.L. and Spearing, D.R., 1988, Roadside Geology of Wyoming, Missoula, MT, 2nd ed., 158

Leggott R., Cheadle S., Whiting P., and Williams R.G., 2000, Analysis of higher order moveout in terms of vertical velocity variation and VTI anisotropy: Exploration Geophysics, **31** , 455–459.

Lisle, R. J., 1994, Detection of zones of abnormal strains in structures using Gaussian curvature analysis: AAPG Bulletin, 78, 1811-1819.

Pech, A., and Tsvankin, I., 2004, Quartic moveout coefficient for a dipping azimuthally anisotropic layer: Geophysics, **69**, no. 3, 699-707.

Richter, H, 1981, Occurrence and Characteristics of Ground Water in the Wind River Basin, Wyoming: Wyoming State Geological Survey, **5,** 2.

Smith, G., and Pun, A., 2009, How Does Earth Work? Physical Geology and the Process of Science. 2nd ed. Prentice Hall, NM, 244.

Starr, J., and Pandey, A., 2008, NMO application in VTI media: Effective and Intrinsic Eta: 7th International Conference and Exposition on Petroleum Geophysics, Hyderabad, 356.

Stein, J., Wojslaw, R., Langston, T., Boyer, S., 2010, Fracture detection using offset vector tile technology: The Leading Edge, **29**, 1328-1337.

Stone, D.S., 1967, Theory of Paleozoic oil and gas accumulation in Big Horn Basin, WY: Association of Petroleum Geologist (AAPG), **51** No 10, 2056-2114.

Stone, D.S., 1993, Basement-involved thrust-generated folds as seismically imaged in the subsurface of the central Rocky Mountain foreland: Geological Society of America (GSA), Special Paper 280, 271-318.

Taner M. T. and Koehler F., 1969, Velocity spectra-digital computer derivation and application of velocity functions: Geophysics, **34**, 859-881.

Thomas, H., 1957, Geologic history and structure of Wyoming: Wyoming geological association (WGA), Wyoming oil and gas fields symposium, 15-23.

Thomsen, L, 1986, Weak elastic anisotropy: Geophysics, **51**, No. 10, 1954-1966.

Tsvankin, I., and Thomsen, L., 1994, Nonhyperbolic reflection moveout in anisotropic media: Geophysics, **59**, no. 8, 1290-1304

Tsvankin, I., 1996, P-wave signatures and notation for transversely isotropic media: An overview: Geophysics, **61**, no. 2, 467-483

Appendix A: Acquisition Parameters

Fold: 99

Energy Source: Vibroseis

Sweep: 6-128 HZ

Natural Bin: 55X55 ft

Shot Line Spacing: 660 ft

Shot Interval: 110 ft

Receiver Line Spacing: 660 ft

Receiver interval: 110 ft

Appendix B: Processing Flow

1) Geometry assignment and QC
    - 55x55ft bin
    - 270 Degree Azimuth
2) True amplitude recovery
3) Trace edits plus 60 Hz noise reduction
4) Air blast attenuation
5) Apply refraction statics => shift to floating datum
6) Surface consistent amplitude scaling
7) Surface consistent deconvolution
    - 160ms 0.01 prewht
    - Line, Shot and Receiver component
8) Spectral shaping: 10-90 Hz
9) Two passes of velocity analysis plus residual statics
10) High density isotropic velocity analysis
11) Noise attenuation on CDP gathers
12) Surface consistent amplitude scaling followed by residual amplitude correction
13) PSTM velocity analysis on sparse grid
14) OVT PSTM migration
15) Migration only trace edits
16) Isotropic RMO analysis
17) **ISOTROPIC VOLUME OUTPUT**
18) Time and spatially varying VTI analysis
19) HTI analysis
20) OVT PSTM migration with variable η
21) Migration only trace edits
22) Residual HTI correction
23) Mute
24) Robust Scaling
25) Stack
26) **ANISOTROPIC VOLUME OUTPUT**